

**A Chemical-Scale Study on the Ligand-Binding Site of  
a Serotonin-Gated Ion Channel**

Thesis by

**Tingwei Mu**

In Partial Fulfillment of the Requirements

For the Degree of

Doctor of Philosophy

California Institute of Technology

Pasadena, California

2006

(Defended August 8, 2005)

© 2006

Tingwei Mu

All Rights Reserved

## Acknowledgements

It is really the case that Caltech is the “crown of science.” This is similar to Pasadena, where Caltech is located, which means “crown of the valley” in the language of the Chippewa Indians. The scientific atmosphere at Caltech is wonderful, with highly talented faculties and students. I feel so lucky to have spent my five-year graduate student life here, and I appreciate having received all kinds of help, which is beyond any verbal or written expression of gratitude.

I want to thank my advisor, Professor Dennis A. Dougherty. He possesses all the characteristics of a good mentor, in my mind. Dennis’s scientific insights amaze me greatly. For my research, he can always grasp the key point and give me directions; under his guidance, I can also gain freedom to try different things. Dennis always encourages me on my research. His encouragement and optimism are precious, especially when some difficulties are met in the experiment. Without Dennis as the mentor, I doubt that I could have achieved this much both in research and in personal life.

I am also grateful to my mentor in Biology, Professor Henry A. Lester. Henry will always be there for you when you need any help. I cherish the chance to learn electrophysiology directly from Henry, and I appreciate his patience to explain every related detail. I thank Henry’s insights and advice in our “unnatural” meetings, which I

will miss a lot in the future. The way I learned to analyze experiments will definitely benefit my future research.

I thank all my other committee members, Professor Linda Hsieh-Wilson, William Goddard, and Douglas Rees, for their advice and help during these years. I appreciate having had the opportunity to have a joint group meeting with Linda's group, where I could learn carbohydrate chemistry. I thank Bill for his advice on the modeling study and for all the help from his group members. I thank Doug for writing a recommendation letter for my post-doc application.

My graduate life in the Dougherty group has been wonderful due to many smart, helpful, and friendly colleagues. I would like to thank Darren Beene. I learned molecular biology and electrophysiology from him. His patience helped me master the experimental techniques much quicker than my own expectation. He is also interested in ancient Chinese culture. Therefore, I enjoyed discussing Confucius with him. Josh Maurer is someone who you can always find in the lab and who you can ask for help no matter what you encounter. Gabriel Brandt is also a source of knowledge and has many scientific ideas. Playing soccer with him is fun. Lintong Li showed me how to do my synthesis and helped me in many other ways. I liked to talk with her in our native language. Niki Zacharias is always ready to help, even though she is now working at Neurion in Pasadena. Therefore, in case our HPLC does not work, we can still drive to Neurion. Donald Elmore gave me some knowledge on computational modeling including how to use SPARTAN. What impressed me most was his star performance in a movie. I

appreciate E. James Petersson's help on my synthesis. His enthusiasm for science amazes me. I enjoyed talking with Steve Spronk. He knows almost everything about sports except soccer. Sarah May (Monahan) is versatile and I am sure that her photography career will be successful. I would like to thank Dr. David Dahan for his help on molecular biology. It is amazing that David can speak both English and French fluently. I thank Dr. Vince Liptak for his helpful discussion. Amanda Cashin is warm-hearted and good at organization. I appreciate her help with troubleshooting OpusXpress as well as being an MC at my wedding reception. I thank Lori Lee for her advice on my synthesis. Talking with Lori about her trip to China is fun. Eric Rodriguez is making great progress in his research on four-base codons. Michael Torrice and Ariele Hanek are the new OpusXpress captains. They have huge responsibility to take care of this robot. Xinan Xiu is eager to try new experimental techniques, which can reward her with good results. I also thank her for being another MC at my wedding reception and for much other help. Amy Eastwood is a self-motivated runner in both life and research. Katie McMenimen works hard to unveil the magnesium blockage mechanism in the NMDA receptor. Kiowa Bower is continuing to study the hydrogen bonding pattern of serotonin in serotonin receptors. Jinti Wang and Kristin Rule are just starting their exciting journey in this group. It is amazing that Jinti can finish tons of mutations in just several days. The new group website provided by Kristin looks really great.

I also want to thank many members of the Lester group. I appreciate all the help and suggestions I have gotten from Purnima Deshpande, Pam Fong, Stephanie Huang, Dr.

Raad Nashmi, Dr. John Leite, Dr. Fraser Moss, Dr. Mohammed Dibas, Dr. Rigo Pantoja, Dr. Bruce Cohen, and Dr. Ping Li.

For the modeling study in Chapter 3, I want to thank Dr. Vaidehi Nagarajan, Wely Floriano, Victor Wai Tak Kam, and Huazhang Shen in the Goddard group for their help and suggestions.

I thank Professor Dennis Dougherty for proofreading the whole thesis. I thank Amanda Cashin for proofreading Chapter 1 and 5, Amy Eastwood for Chapter 2, Katie McMenimen for Chapter 3, and Lori Lee for Chapter 4. All remaining errors are my responsibility.

I reserve my final thanks for my family. I thank my parents and my elder brothers for their love. Finally, I want to thank my dear wife, Yajuan Wang, whom I love very much. She always accompanies me and supports my work. She did the proofreading and formatting for this thesis. Without her, life is unimaginable.

## Abstract

Signal transmission is a combination of electrical and chemical processes. Upon binding neurotransmitters, ligand-gated ion channels (LGICs) open to allow ion flux, which converts chemical signals to electrical signals. In this thesis, experiments in conjunction with computations are utilized to study the mechanism of the ligand-binding process. The powerful unnatural amino acid mutagenesis methodology provides a great tool to obtain a high-resolution image of the binding pocket at the chemical level.

The target protein is a serotonin-gated ion channel, MOD-1. In order to understand the binding mechanism, we need to identify the non-covalent interactions responsible for binding. In Chapter 2, as a starting point, we prove that cation- $\pi$  interactions between the agonist serotonin and Trp 226 in loop C of MOD-1 play a key role in binding the ligand. Surprisingly, this cation- $\pi$  site in MOD-1 is different from that in 5-HT<sub>3</sub>R, although these two receptors both bind serotonin and are highly homologous.

Next, efforts are made to obtain the entire orientation of the ligand inside the binding pocket. Upon binding, the agonist serotonin can potentially form hydrogen bonds with the MOD-1 receptor at three positions. If we can identify the hydrogen bonding pattern of serotonin inside the binding pocket, its orientation will be fixed at the chemical level.

No crystal structure data are available for MOD-1. Therefore, in Chapter 3, a homology model of MOD-1 is built by using the template of acetylcholine binding protein (AChBP). We continue to dock the agonist into the binding pocket. The binding pattern from the model shows that there exist three hydrogen bonds between serotonin and the MOD-1 receptor, providing guidance for the ensuing experimental studies.

In Chapter 4, a forward and reverse pharmacology strategy is applied to test the hydrogen bonding pattern of serotonin in MOD-1 experimentally. Both conventional and unnatural amino acid mutagenesis are used in conjunction with serotonin analogues. The results from these thorough structure-function studies confirm aspects of the hydrogen bond pattern described in the model.

In Chapter 5, we apply another strategy called the tethered agonist approach to further probe the agonist-binding site. The tethered agonists are incorporated into the receptor so that the channel will be in the spontaneously opening state even without the addition of the natural agonist. Results from the tethered agonist experiments can provide further information on the ligand-binding pocket. This is another elegant example of the effectiveness of the unnatural amino acid mutagenesis methodology.

## Table of Contents

<b>Acknowledgements .....</b>	<b>iii</b>
<b>Abstract.....</b>	<b>vii</b>
<b>List of Figures.....</b>	<b>xiii</b>
<b>List of Tables .....</b>	<b>xvii</b>
<b>List of Schemes.....</b>	<b>xix</b>
<b>Chapter1: Introduction .....</b>	<b>1</b>
1.1 Chemical Neurobiology .....	2
1.2 Incorporation of Unnatural Amino Acids into Proteins.....	5
1.3 The Cys-Loop Superfamily of Ligand-Gated Ion Channels and Insights from the Crystal Structure of Acetylcholine Binding Protein (AChBP) .....	14
1.4 Summary .....	21
1.5 References.....	23
<b>Chapter 2: Different Cation-<math>\pi</math> Sites at Two Homologous Serotonin Receptors, MOD-1 and 5-HT<sub>3</sub>R.....</b>	<b>30</b>
2.1 Introduction.....	31
2.1.1 Cation- $\pi$ Interactions .....	32
2.1.2 The MOD-1 Receptor .....	35
2.2 Electronic and Steric Effects on Ligand-Binding at Position 180 of MOD-1 .....	37
2.3 Cation- $\pi$ Interactions between Serotonin and Trp 226 of MOD-1 .....	40
2.4 Switch of Tyr 180 and Trp 226 in MOD-1 .....	43

2.5	Discussion.....	44
2.6	Methods .....	45
2.6.1	Electrophysiology.....	45
2.6.2	Incorporation of Unnatural Amino Acids by <i>in vivo</i> Nonsense Suppression Methods.....	46
2.6.3	Synthesis of Aminoacyl dCA (dCA-AA).....	47
2.7	References.....	49
<b>Chapter 3: Prediction of the Ligand-Binding Site of MOD-1: Implications for the Hydrogen Bonding Pattern of Serotonin.....</b>		<b>52</b>
3.1	Introduction.....	53
3.2	Methods .....	56
3.2.1	Sequence Alignment.....	56
3.2.2	3-D Model Building.....	56
3.2.3	Agonist Docking by HierDock .....	57
3.2.4	Side Chain Optimization by SCREAM .....	58
3.2.5	Serotonin Re-docking by HierDock.....	59
3.3	Results .....	59
3.3.1	Model of MOD-1 .....	59
3.3.2	The Binding Pocket of Serotonin in MOD-1 .....	61
3.3.3	Docking of Other Agonists .....	65
3.4	Conclusions and Discussion .....	68
3.5	References.....	70

<b>Chapter 4: Hydrogen Bonding Pattern of Serotonin in MOD-1 .....</b>	<b>73</b>
4.1 Introduction.....	74
4.2 Hydrogen Bond between Gln 228 and the Indolic Amine Group of Serotonin.....	76
4.2.1 Use of Serotonin Analogues and Conventional Mutations to Probe the Hydrogen Bond between Gln 228 and Serotonin .....	76
4.2.2 Use of Unnatural Amino Acid Mutations to Further Prove the Hydrogen Bond between Gln 228 and Serotonin .....	82
4.3 Hydrogen Bond between Asn 223 and the Hydroxyl Group of Serotonin.....	92
4.4 Hydrogen Bond between Main Chain Carbonyl Group of Tyr 180 and the Terminal Ammonium of Serotonin.....	94
4.5 Conclusions and Future Directions.....	96
4.6 Materials and Methods.....	98
4.6.1 Electrophysiology .....	98
4.6.2 Incorporation of Unnatural Amino Acids by <i>in vivo</i> Nonsense Suppression Methods.....	99
4.6.3 Synthesis of Amino Acids, dCA-Amino Acid and Others .....	99
4.6.4 Computational Methods.....	109
4.7 References.....	110
 <b>Chapter 5: Tethered Agonist Approach to Map the Ligand-Binding Site of MOD-1 .....</b>	 <b>113</b>
5.1 Introduction.....	114
5.2 Effect of the Channel Blocker Picrotoxin on MOD-1 .....	116

5.3	Tethered Agonist Experiments in MOD-1.....	119
5.4	Conclusions.....	123
5.5	Methods .....	124
5.5.1	Electrophysiology.....	124
5.5.2	Incorporation of Unnatural Amino Acids by <i>in vivo</i> Nonsense Suppression Methods.....	125
5.6	References.....	126

## List of Figures

<b>Figure 1.1</b> Neurons and signal transmission through synapses .....	3
<b>Figure 1.2</b> The nonsense suppression methods <i>in vitro</i> and <i>in vivo</i> .....	7
<b>Figure 1.3</b> Chemical acylation of an unnatural amino acid to an <i>in vitro</i> transcribed suppressor tRNA .....	8
<b>Figure 1.4</b> Codons used in response to the aminoacylated suppressor tRNAs to incorporate unnatural amino acids into proteins .....	9
<b>Figure 1.5</b> Four-base codons assigned to unnatural amino acids.....	11
<b>Figure 1.6</b> Structures of unnatural amino acids incorporated into proteins using nonsense suppression method .....	13
<b>Figure 1.7</b> Structural features of nAChR .....	16
<b>Figure 1.8</b> Ligand-binding sites of nAChR.....	17
<b>Figure 1.9</b> Crystal structure of AChBP .....	18
<b>Figure 1.10</b> Structure of the whole receptor of nAChR.....	21
<b>Figure 2.1</b> Molecular structures of serotonin and acetylcholine .....	31
<b>Figure 2.2</b> The cation- $\pi$ interaction.....	32
<b>Figure 2.3</b> <i>Ab initio</i> electrostatic potential surfaces (EPS) of fluorinated Trp side chains.....	34
<b>Figure 2.4</b> Sequence alignments for the key regions of the agonist binding sites .....	35
<b>Figure 2.5</b> AM1 electrostatic potential surfaces of the side chains of phenylalanine derivatives .....	39

<b>Figure 2.6</b> Electrophysiology recording of fluorinated tryptophans at position 226 of MOD-1 .....	41
<b>Figure 2.7</b> Fluorination effects versus cation- $\pi$ binding energies.....	42
<b>Figure 2.8</b> Dose-response curves for the switch between Tyr 180 and Trp 226 of MOD-1 .....	43
<b>Figure 3.1</b> Potential hydrogen bonding positions of serotonin in the MOD-1 receptor ..	53
<b>Figure 3.2</b> Sequence alignment of the amino-terminal domain of MOD-1 ( <i>C. elegans</i> ), 5-HT <sub>3A</sub> R (mouse), and AChBP (snail) .....	59
<b>Figure 3.3</b> Model of MOD-1 after minimization .....	60
<b>Figure 3.4</b> Docking result of serotonin in MOD-1.....	63
<b>Figure 3.5</b> The structures of agonists docked into MOD-1.....	66
<b>Figure 3.6</b> Linear correlation between binding energy and logEC <sub>50</sub> of different agonists of MOD-1 .....	67
<b>Figure 3.7</b> Combination of computation and experiment to study the ligand-binding site of the MOD-1 receptor .....	69
<b>Figure 4.1</b> Hydrogen bonding pattern of serotonin in MOD-1 .....	74
<b>Figure 4.2</b> Structures of serotonin analogues used to probe the hydrogen bond between serotonin and Gln 228 .....	76
<b>Figure 4.3</b> Dose-response curves of serotonin analogues in the MOD-1 wild type and L9'T and L9'S mutants .....	77
<b>Figure 4.4</b> Structures of conventional mutations made at position 228 of MOD-1 .....	79

<b>Figure 4.5</b> Dose-response curves of serotonin analogues in Q228N, Q228E, Q228A mutants of MOD-1 .....	79
<b>Figure 4.6</b> AM1 electrostatic potential surfaces (EPS) of the model molecules that represent the Gln analogues .....	82
<b>Figure 4.7</b> The model system used to calculate the binding energies of the hydrogen bonds between the indolic amine of serotonin and Gln analogues .....	83
<b>Figure 4.8</b> The configurations of the HF/6-31G** optimized indole...molecule complex structures.....	85
<b>Figure 4.9</b> Recording results of serotonin on unnatural mutations at position 228 of MOD-1 .....	91
<b>Figure 4.10</b> Structures of conventional mutations made at position 223 of MOD-1 .....	92
<b>Figure 4.11</b> Dose-response curves of serotonin in N223A, N223D, and N223Q mutants of MOD-1 .....	93
<b>Figure 4.12</b> Structures of serotonin analogues used to probe the hydrogen bond between the backbone carbonyl group of Tyr 180 and serotonin .....	94
<b>Figure 4.13</b> The amide-to-ester mutation to modify the hydrogen bonding ability of the backbone carbonyl group of Tyr 180 in MOD-1 with serotonin.....	95
<b>Figure 4.14</b> The structures of 4-fluoroglutamine and 4,4-difluoroglutamine .....	97
<b>Figure 5.1</b> The tethered agonist approach to map the acetylcholine (ACh) binding site in nAChR.....	114
<b>Figure 5.2</b> Tethered agonists used in MOD-1 .....	115
<b>Figure 5.3</b> The effect of L9' mutations on channel gating.....	117

<b>Figure 5.4</b> Picrotoxin blockage effect on wild type and L9' mutant MOD-1s .....	118
<b>Figure 5.5</b> Tethered agonist experiments at position 226 of MOD-1 .....	121
<b>Figure 5.6</b> Tethered agonist experiments at position 180 of MOD-1 .....	121
<b>Figure 5.7</b> Efficiencies of tethered agonists in MOD-1 .....	122

## List of Tables

<b>Table 1.1</b> The common diseases associated with the Cys-loop superfamily of LGICs.....	15
<b>Table 2.1</b> Mutations of Tyr 180 of MOD-1 .....	38
<b>Table 2.2</b> Mutations of key aromatic residues .....	40
<b>Table 3.1</b> Docking results of serotonin in MOD-1 from the twelve initial binding orientations.....	61
<b>Table 3.2</b> MOD-1 residues around 5 Å of serotonin.....	62
<b>Table 3.3</b> Binding Energy and EC <sub>50</sub> of different agonists of MOD-1.....	66
<b>Table 4.1</b> EC <sub>50</sub> values of serotonin analogues in MOD-1 wild type and L9'T and L9'S mutants.....	78
<b>Table 4.2</b> EC <sub>50</sub> values of serotonin analogues in Q228N, Q228E and Q228A mutants of MOD-1 .....	80
<b>Table 4.3</b> Total energies of indole and acetone analogues.....	84
<b>Table 4.4</b> Total energies of the indole···molecule complexes .....	84
<b>Table 4.5</b> The hydrogen bond binding energies of the model system, which mimics the hydrogen bonds between the indolic amine of serotonin and Gln analogues.....	85
<b>Table 4.6</b> EC <sub>50</sub> values of serotonin analogues for unnatural mutations at position 228 of MOD-1.....	90

<b>Table 4.7</b> EC <sub>50</sub> values of N-Me-serotonin, bufotenin, and $\alpha$ -Me-serotonin in MOD-1 wild type.....	94
<b>Table 5.1</b> EC <sub>50</sub> of L9' mutations in MOD-1 using serotonin.....	117

## List of Schemes

<b>Scheme 2.1</b> Synthetic scheme for aminoacylated dCA.....	47
<b>Scheme 4.1</b> Synthesis of dCA-Asn analogues .....	87
<b>Scheme 4.2</b> Synthesis of <i>N</i> -PMP-protected $\gamma$ -keto- $\alpha$ -amino acid derivatives .....	88
<b>Scheme 4.3</b> Failed synthetic route for 2-amino-5,5,5-trifluoro-4-oxopentanoic acid derivatives using a carboxylic acid as the starting material.....	89
<b>Scheme 4.4</b> Proposed synthetic route for 2-amino-5,5,5-trifluoro-4-oxopentanoic acid derivatives using a carboxylic ester as the starting material.....	89
<b>Scheme 4.5</b> Synthesis of NVOC-Gln cyanomethyl ester .....	106
<b>Scheme 4.6</b> General procedure for coupling of amino acids to dCA.....	107
<b>Scheme 4.7</b> Synthesis of 2-(benzofuran-3-yl)ethylamine .....	108

## **Chapter 1**

### **Introduction**

## 1.1 Chemical Neurobiology

Neurobiology is a challenging field in biological science due to its complexity. The ultimate goal of neurobiology is to understand how the human mind works to perceive, move, learn, and memorize.<sup>1</sup> The human brain makes use of nerve cells called neurons and the connections between them to respond to the information obtained from a complicated network of sensory receptors. Even if we just do some simple numerical estimations of the human brain, we will find that understanding the brain seems daunting. A human brain has roughly  $10^{11}$  neurons, which can be divided into at least 1000 different types. Communication among the vast majority of neurons occurs through minute clefts as small as 20–40 nm called synapses (Figure 1.1). A neuron can form thousands of synapses with other neurons, which will yield over 100 trillion synapses in the brain.<sup>2</sup>

Signal transmission is a combination of electrical and chemical processes. An electrical impulse can travel along the long axon of a neuron. When this impulse reaches the axon terminal, vesicles in the pre-synaptic neuron release small chemicals called neurotransmitters, such as acetylcholine and serotonin. Neurotransmitters will diffuse very quickly across the tiny synapse and bind to the corresponding post-synaptic receptors, such as G-protein-coupled receptors (GPCRs) and ion channels. This binding behavior leads to a change of the local electrical activity, which can be transmitted to induce downstream neurotransmitter release for further communication between neurons. The post-synaptic neuroreceptors, which are membrane proteins, play important roles in regulating the signal transmission process, and will be discussed in detail in the following.

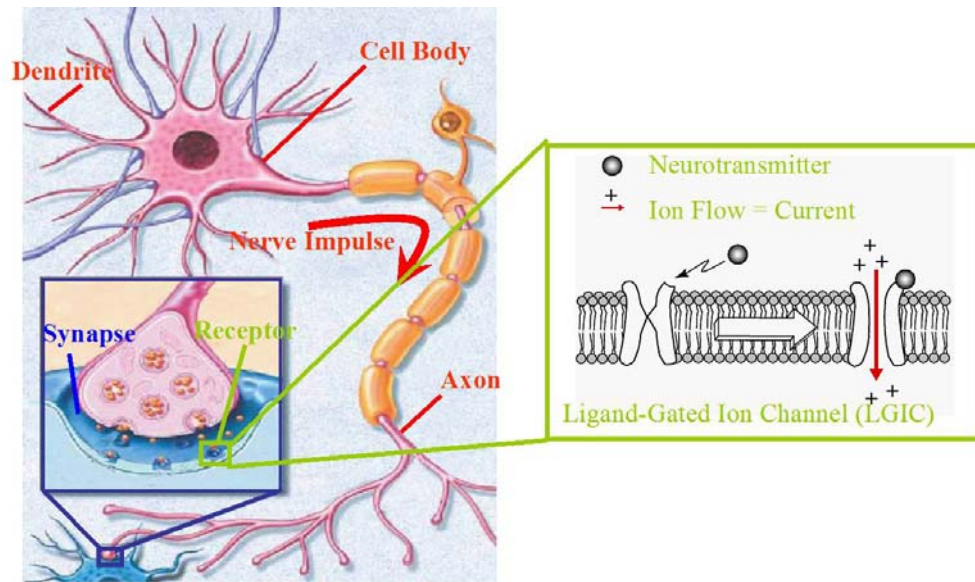


**Figure 1.1** Neurons and signal transmission through synapses. Neurotransmitters from a pre-synaptic nerve terminal diffuse across the synapse and bind to corresponding post-synaptic receptors such as GPCRs and ion channels.

To understand how neuroreceptors function seems difficult due to their structural complexity. Fortunately, with the development of structural biology, molecular biology, and electrophysiology, it is now possible to perform a thorough structure-function study on neuroreceptors at the molecular level. Evidently, to understand the mechanism by which the receptors work, we need to gain information on the following three aspects.

First, high-resolution structural data need to be obtained. A few decades ago, it was thought that it was impossible to determine crystal structures of integral membrane proteins due to the difficulty of obtaining their crystals. With the recent advance of crystallography, now many membrane proteins have been successfully crystallized at high resolution.<sup>3</sup> The breakthrough was marked by two high-resolution ion channel crystal structures in 1998.<sup>4,5</sup> The structural data will undoubtedly benefit the functional

study of the proteins although high-throughput crystallography methods still should be further developed.

Second, the structures of neuroreceptors need to be modified to provide further insights into their functions. Recombinant DNA technology has revolutionized biochemistry since its appearance in the 1970s. Together with the invention of the polymerase chain reaction in the 1980s, in principle, according to our needs, we can modify the cDNA that encodes the target protein, and obtain the desired mutant protein after translation. Therefore, now we can change the structure of neuroreceptors easily at the molecular level. A single amino acid mutation can be introduced by site-directed mutagenesis; a chimera protein can also be built by cutting and ligating several regions of interest. The neuroreceptor proteins can be expressed in different systems, such as *Xenopus* oocytes and human embryonic kidney (HEK) cells.

Finally, we need a sensitive functional assay to monitor the effect that the structural changes cause. In the case of neuroreceptors, the technique of electrophysiology is utilized. The voltage clamp technique, fully developed by Hodgkin and Huxley in the 1950s,<sup>6</sup> enables the whole cell recording of currents during channel activation. Furthermore, the patch clamp technique was invented by Neher and Sakmann in the 1970s<sup>7</sup> and further refined in early 1980s,<sup>8</sup> which can be used to record single channel activity. These electrophysiology tools provide a powerful method to measure channel activity in real time under relatively physiological conditions.

Molecular neurobiology is developing very quickly, and the mechanism of how neuroreceptors work is being disclosed from structure-function studies as well as the emergence of high-resolution structures.

Recently, the field of chemical biology grasped the attention of many chemists and biologists. From the view of the editors of *Nature Chemical Biology*, “Chemical Biology has emerged as a field grounded in technological advances brought about by the close collaboration of chemists and biologists. Using diverse experimental and theoretical techniques, chemical biologists have tackled challenging problems in biology, ranging from cellular signaling to drug development and neurobiology.”<sup>9</sup>

Here we focus on chemical biology of neuroreceptors. We continue the efforts of neurobiology from a molecular level to a chemical level. Therefore, the term chemical neurobiology is used here to describe a chemical-scale study on the molecules of the nervous system, namely, neuroreceptors.<sup>10</sup>

To change the atomic structure of neuroreceptors, conventional site-directed mutagenesis is restricted to the twenty natural amino acids. Systematic study of the role of one specific amino acid is limited by this method. Fortunately, unnatural amino acids can be incorporated into neuroreceptors by using the *in vivo* nonsense suppression methodology.<sup>11</sup> This method provides much greater structural diversity and delivers very subtle modifications to proteins. Unnatural amino acid mutagenesis combined with electrophysiology recording allows us to perform a chemical-scale study on neuroreceptors.

## **1.2 Incorporation of Unnatural Amino Acids into Proteins**

Most of the current studies on unnatural amino acid methodology focus on the site-specific incorporation of one unnatural amino acid into a protein *in vitro* or *in vivo*.<sup>12</sup>

These studies can be categorized into two fields: first, chemically acylated suppressor tRNAs are used; second, the twenty-first aminoacyl-tRNA synthetase is engineered to incorporate unnatural amino acids.

In the first field, the unnatural amino acid is introduced into the expression system after chemical acylation to an *in vitro* transcribed suppressor tRNA. This suppression method has been well-developed since its introduction in the 1980s.<sup>13-15</sup> It is illustrated in Figure 1.2. The chemical acylation process of an unnatural amino acid to an *in vitro* transcribed suppressor tRNA is shown in Figure 1.3. An unnatural amino acid, which is chemically acylated to a suppressor tRNA, is transferred to the site of interest, which is encoded by a proper codon. For an *in vitro* application, translation mixtures from *E. coli* and rabbit reticulocyte can be used. For an *in vivo* application, both mRNA and tRNA can be injected into the *Xenopus* oocyte expression system for translation. Recently, unnatural amino acids have been site-specifically expressed into receptors expressed in mammalian cells.<sup>16</sup> The main limitation of this method is that the aminoacylated tRNA is consumed as a stoichiometric reagent. Therefore, the translated protein amount is limited by the amount of the aminoacylated tRNA that can be introduced into the translation system.<sup>17</sup> One critical requirement of this method is that the suppressor tRNA must not be aminoacylated by any of the endogenous aminoacyl-tRNA synthetases (aaRSs), i.e., the suppressor tRNA should be orthogonal to endogenous aaRSs. A variety of suppressor tRNAs and their corresponding codons have been developed.

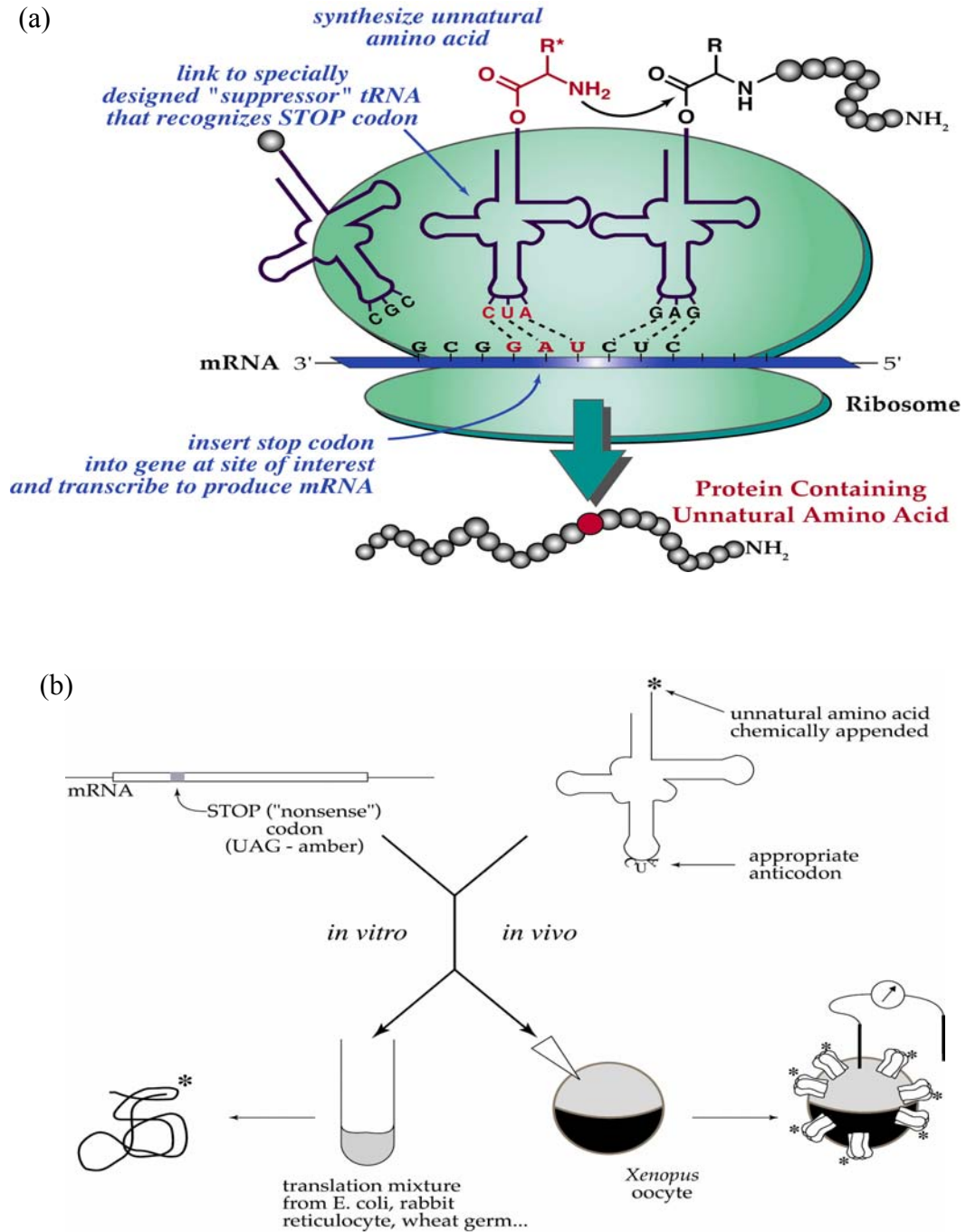


**Figure 1.2** The nonsense suppression methods *in vitro* and *in vivo*. (a) The principle of nonsense suppression method. (b) The application in *in vitro* and *in vivo* systems.

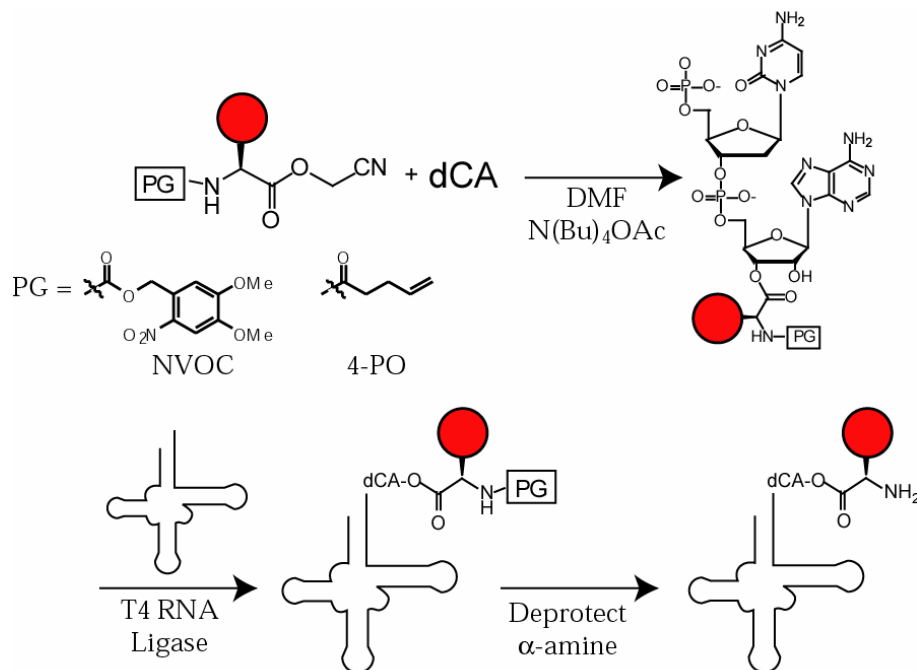


**Figure 1.3** Chemical acylation of an unnatural amino acid to an *in vitro* transcribed suppressor tRNA. The red dot represents an unnatural amino acid.

The use of different expression systems led to the development of a variety of suppressor tRNAs. In 1989, the Schultz group originally used a yeast tRNA<sup>Phe</sup> (CUA) suppressor in the *E. coli* translation system based on the idea that yeast tRNAs are not recognized by *E. coli* aminoacyl tRNA synthetases.<sup>15</sup> Later, they generated an *E. coli* tRNA<sup>Asn</sup>-derived suppressor in the *E. coli* translation system.<sup>18</sup> This new suppressor showed a significant improvement in suppression efficiency. In early studies, Chamberlin and co-workers developed an *E. coli* tRNA<sup>Gly</sup>-derived suppressor. They used this suppressor in a rabbit reticulocyte expression system.<sup>14</sup> Dougherty and co-workers tried to generate an optimal suppressor tRNA for the oocyte expression system.<sup>19</sup> At first, tRNA-MN3, a suppressor modified from the yeast tRNA<sup>Phe</sup> (CUA), was used.<sup>11</sup> However,

in some cases natural amino acids were unexpectedly inserted, probably due to the reacylation of chemically acylated tRNA-MN3 by endogenous aaRSs. To overcome this, a new nonsense suppressor tRNA based on tRNA<sup>Gln</sup>(CUA) from the eukaryote *Tetrahymena thermophila* was designed.<sup>20</sup> A major modification was to mutate U73 to G to reduce recognition by the oocyte's endogenous glutamine acyltransferase. This new suppressor tRNA significantly improved the suppression efficiency.

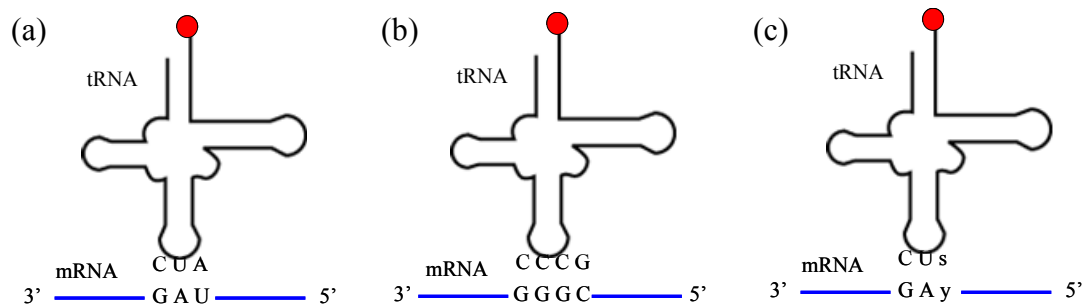


**Figure 1.4** Codons used in response to the aminoacylated suppressor tRNAs to incorporate unnatural amino acids into proteins. (a) Amber codon. An amber codon is recognized by aa-tRNA containing a CUA anticodon. (b) Four-base codon. CGGG is recognized by aa-tRNA containing a CCCG anticodon. (c) Unnatural base pairs yAG-CUs as the codon-anticodon pair. The red dots represent unnatural amino acids.

In response to the aminoacylated suppressor tRNA, several kinds of codons are used, such as stop codons, four-base codons, and unnatural bases (Figure 1.4).<sup>21</sup>

Amber (UAG) suppressors have been the most widely used both *in vitro* and *in vivo*.<sup>11, 15</sup> Chamberlin and co-workers reported that opal (UGA) and ochre (UAA) suppressors gave reasonably good suppression levels in rabbit reticulocyte lysate.<sup>22</sup>

However, Schultz and co-workers reported that an opal suppressor showed a high level of readthrough in *E. coli*.<sup>18</sup> Recently, RajBhandary and co-workers reported that an ochre suppressor tRNA was imported into mammalian cells.<sup>23</sup> Amber (UAG) suppressors have been successfully applied in different expression systems. Dougherty and co-workers have been using oocytes as the translation system to perform structure-function studies *in vivo*.<sup>19</sup> *In vitro* protein synthesis is performed in rabbit reticulocyte lysate, wheat germ extract, or bacterial S-30 extract.<sup>24, 25</sup> Due to the competition of release factors in these translation systems, the nonsense suppressor tRNAs have relatively low efficiency. The use of an *E. coli* S-30 extract deficient in release factor 1 improves the suppression efficiency.<sup>26</sup> With the development of the RNAi technique, it is possible to remove release factor 1 in the translation system to improve the suppression efficiency.<sup>27</sup>

Recently, four-base codons and corresponding frameshift suppressor tRNAs have been developed *in vitro*.<sup>28, 29</sup> This frameshift suppression method can avoid the competition between the suppressor tRNA and endogenous release factors. It has also demonstrated higher suppression efficiency than nonsense suppression. Furthermore, the diversity of the four-base codons can be used to incorporate multiple unnatural amino acids into a protein. Using a set of two four-base codons, AGGU and CGGG, the Sisido group successfully incorporated two different unnatural amino acids into streptavidin in *E. coli*.<sup>30</sup> Later they utilized another set of two four-base codons, CGGG and GGGU, to give a higher suppression efficiency.<sup>31</sup> Their work has been reviewed.<sup>28</sup> The four-base codons they used are summarized in Figure 1.5. Among the reported four-base codons, CGGG, GGGU, and CUCU have higher frameshift suppression efficiency. Further investigation of five-base codons *in vitro*<sup>32</sup> and four-base codons *in vivo*<sup>33, 34</sup> also appeared. The limits

of codon and anticodon size were explored and it was found that three to five bases codons could be well-tolerated by the translation machinery.<sup>35</sup>

	U	C	A	G
U	UUU Phe UUC UUA Leu UUG	UCU Ser UCC UCA UCG	UAU Tyr UAC UAA Stop UAG	UGU Cys UGC UGA Stop UGG Trp
C	CUU CUC CUA Leu CUG	CCU CCC Pro CCA CCG	CAU His CAC CAA Gln CAG	CGU Arg CGC CGA CGG
A	AUU Ile AUC AUA AUG Met	ACU Thr ACC ACA ACG	AAU Asn AAC AAA Lys AAG	AGU Ser AGC AGA Arg AGG
G	GUU Val GUC GUA GUG	GCU Ala GCC GCA GCG	GAU Asp GAC GAA Glu GAG	GGU Gly GGC GGA GGG

**Figure 1.5** Four-base codons assigned to unnatural amino acids. Adapted from Ref<sup>28</sup>.

Another strategy is to choose unnatural base pairs as codon/anticodon pairs. In collaboration with the Benner group, the Chamberlin group successfully applied an isoC and isoG unnatural base pair in the codon-anticodon loops for unnatural amino acid incorporation.<sup>36</sup> However, both the tRNA and mRNA containing unnatural base pairs needed to be synthesized by chemical methods. Recently, another unnatural base pair, y (pyridine-2-one) and s (2-amino-6-(2-thienyl)purine), was used with high efficiency.<sup>37</sup> The mRNA containing y can be transcribed from corresponding DNA template, although the tRNA containing s needs to be synthesized. This strategy could be very useful in multiple unnatural amino acid incorporation if both mRNA and tRNA containing unnatural base pairs can be easily obtained through transcription.

In the second field, efforts have been made to engineer the 21st aminoacyl-tRNA synthetase-suppressor tRNA pairs. Although the 21st aaRS-tRNA pairs are intriguing, it was demonstrated to be extremely difficult to introduce an unnatural amino acid using this method.<sup>38</sup> The 21st aaRS-tRNA pairs must meet two critical requirements. First, the suppressor tRNA must not be aminoacylated by any of the endogenous aminoacyl-tRNA synthetases. Second, the aminoacyl-tRNA synthetase must aminoacylate the suppressor tRNA with the desired unnatural amino acid but no other tRNAs in the cell. The most striking progress in this field was the successful incorporation of *O*-methyl-L-tyrosine into proteins in *E. coli* with high fidelity (greater than 99%).<sup>39</sup> In this experiment, a general and systematic selection approach was developed to generate mutant synthetases that could selectively aminoacylate their cognate orthogonal tRNA with unnatural amino acids. Later, some other efficient selection methods were further developed.<sup>40, 41</sup> To date, over thirty novel amino acids have been successfully incorporated into proteins in *E. coli*.<sup>42</sup> However, challenges still exist for the incorporation of unnatural amino acids that differ significantly from their natural counterparts.

Thus far, the nonsense suppression method has been the most widely used. Since report of this method, over 100 amino acids have been site-specifically incorporated into dozens of proteins including soluble and membrane proteins of virtually any size except D-amino acids or  $\beta$ -amino acids.<sup>12</sup> The structures of incorporated unnatural amino acids are shown in Figure 1.6. They were applied to study ligand-binding sites, protein conformational changes, and protein-protein interactions.

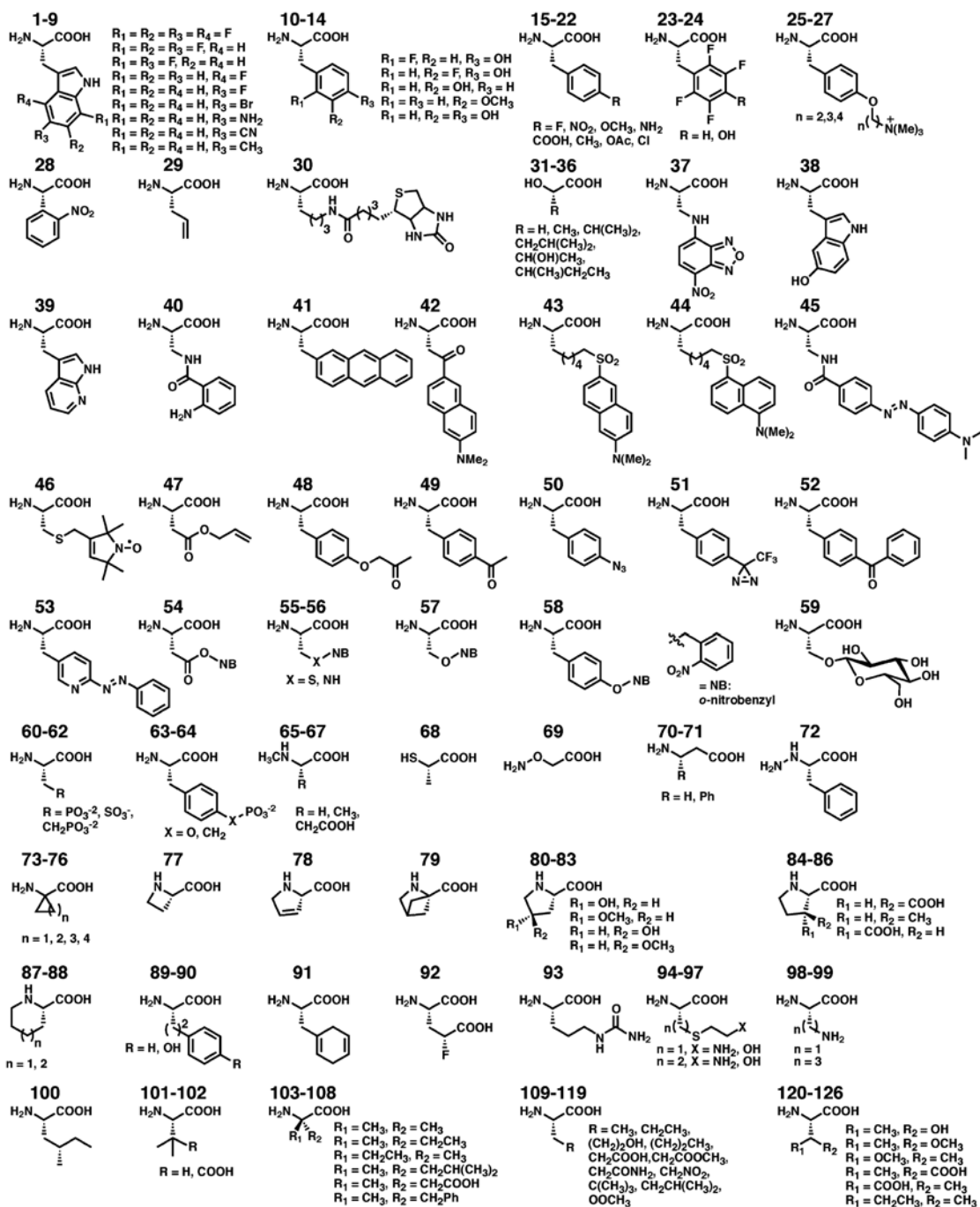


**Figure 1.6** Structures of unnatural amino acids incorporated into proteins using nonsense suppression method. Adapted from Ref<sup>12</sup>.

In our case, we are interested in applying this nonsense suppression method to study neuroreceptors, more specifically, ligand-gated ion channels. *Xenopus* oocytes are excellent expression systems for ion channels.<sup>43</sup> A chemical-scale structure-function study can be fulfilled by this powerful unnatural amino acid mutagenesis method.<sup>44</sup>

### **1.3 The Cys-Loop Superfamily of Ligand-Gated Ion Channels and Insights from the Crystal Structure of Acetylcholine Binding Protein (AChBP)**

Ion channels are membrane proteins.<sup>45</sup> They exist in prokaryotic and eukaryotic organisms, and perform diverse functions. Channels have families: they can be ligand-gated or voltage-gated. Upon stimulation, ion channels open and transport ions across the surface membrane, thus delivering the corresponding signals.

Malfunction of ion channels can lead to serious problems in the cell, and can cause ion channel diseases called channelopathies.<sup>46</sup> Channelopathies can arise from different pathways. The most common sources are due to mutations in the ion channel proteins themselves. Mutations may make the ion pore more difficult to open, or mutations may lead to misfolding of the proteins, therefore reducing the surface expression of the ion channels. We are most interested in the Cys-loop superfamily of ligand-gated ion channels (LGICs). The common diseases related to the Cys-loop superfamily of LGICs are summarized in Table 1.1.<sup>47</sup> The study of these ion channels will benefit the treatment of many diseases, such as Alzheimer's disease, Parkinson's disease, and epilepsy.

**Table 1.1** The common diseases associated with the Cys-loop superfamily of LGICs.<sup>a</sup>

Receptor	Diseases associated with receptor defects	Aims of drugs affecting receptor	Toxin	Abuse
Nicotinic ACh	ADNFLE, slow-channel myasthenic syndrome	Treatment of schizophrenia, Alzheimer's disease, pain, Parkinson's disease, ADHD, Crohn's disease, ADNFLE, cognitive enhancement, smoking cessation, insecticidal effects	Conotoxins, snake toxins, lophotoxin epibatidine	Nicotine addiction
5-HT <sub>3</sub>	NR	Treatment of emesis, irritable bowel syndrome	NR	NR
GABA <sub>A</sub>	Epilepsy	Treatment of anxiety, epilepsy, insomnia, anesthesia	Convulsant toxins	Addiction
Glycine	Startle disease	Enhance GABA <sub>A</sub> transmission	Strychnine	NR

<sup>a</sup> Abbreviations: NR, not reported.

As a major class of LGICs, the Cys-loop superfamily is characterized by the cysteine loop located in the large extracellular N-terminus.<sup>47-49</sup> The Cys-loop is separated by 13 amino acids. The Cys-loop superfamily includes the excitatory cation channels and the inhibitory chloride channels. Cation channels include nicotinic acetylcholine (nAChR),<sup>50, 51</sup> serotonin type 3 (5-HT<sub>3</sub>R; to date three subunits have been identified, namely 5-HT<sub>3</sub>A, 5-HT<sub>3</sub>B, and 5-HT<sub>3</sub>C),<sup>52</sup> zinc-activated (ZAC),<sup>53</sup> and excitatory GABA-gated (EXP-1)<sup>54</sup> receptors. Inhibitory channels include GABA<sub>A</sub><sup>55, 56</sup> and GABA<sub>C</sub>,<sup>57</sup> glycine,<sup>58, 59</sup> MOD-1,<sup>60</sup> and glutamate-gated chloride (GluCl)<sup>61</sup> receptors. To date, EXP-1, MOD-1 and GluCl receptors have been found only in invertebrates.

Upon stimulation, neurotransmitters diffuse across the synapse within a few microseconds and bind to the corresponding ion channels. This binding behavior will induce a conformation change allosterically, and open the ion pore. After a few milliseconds, the channels will return to the closed state again. To understand how ion

channels function, we need to study the neurotransmitter binding behavior and the gating mechanism.

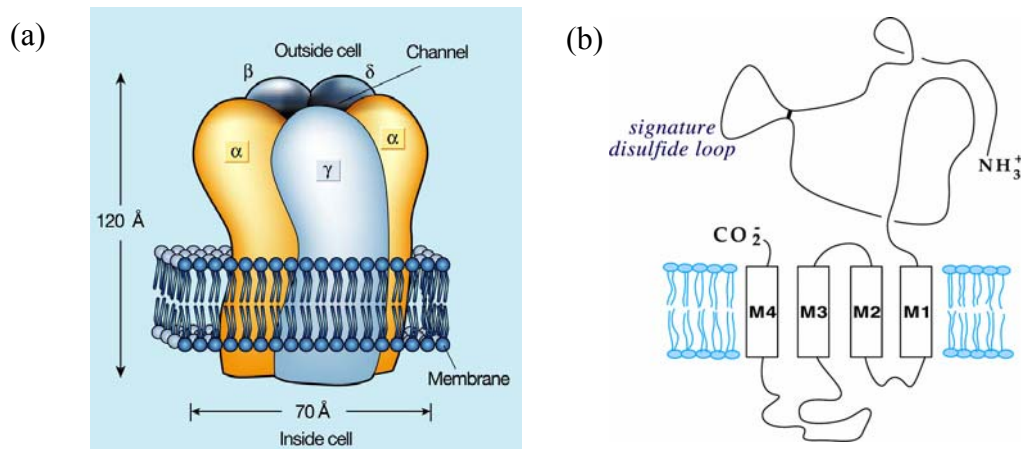


**Figure 1.7** Structural features of nAChR. (a) Subunit arrangement. (b) Subunit topology, with four transmembrane helices (M1- M4) and a large extracellular N-terminal domain.

The Cys-loop superfamily of ligand-gated ion channels shares some common structural characteristics. Most of our knowledge on the structures of the Cys-loop superfamily comes from nAChR.<sup>62</sup> The structure of nAChR was observed at the 9 Å and later at 4.6 Å resolution by the Unwin group using cryoelectron microscopy.<sup>63, 64</sup> Recently, the structure was further refined to 4 Å resolution.<sup>65, 66</sup> The nAChR is pentameric, composed of two  $\alpha$  subunits, one  $\beta$  subunit, one  $\gamma$  subunit, and one  $\delta$  subunit (Figure 1.7). Each subunit has four transmembrane helices, M1–M4, with M2 lining the interior of the pore. A large extracellular N-terminus contains the ligand-binding site.

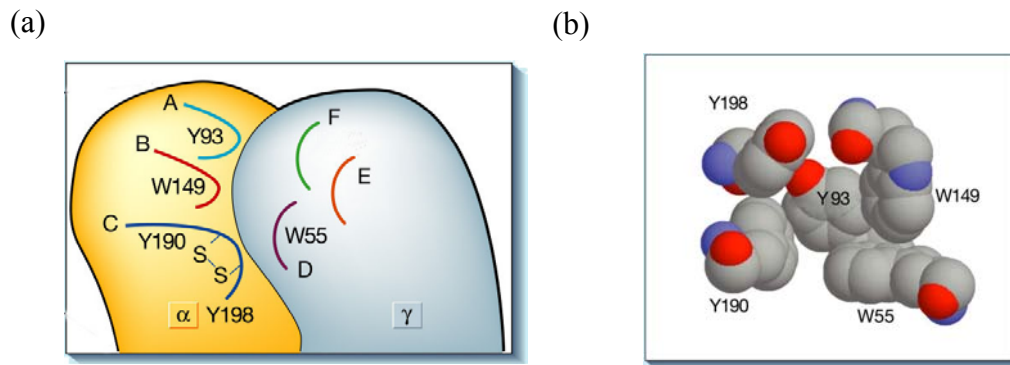


**Figure 1.8** Ligand-binding sites of nAChR. (a) One ligand-binding site between two adjacent subunits:  $\alpha$  and  $\gamma$ . Loop A to loop F are important in binding the ligand. (b) The key aromatic residues around the ligand-binding site.

The resolution of the 4 Å nAChR structure is not high enough to give information on the ligand-binding sites at the atomic level. Photoaffinity labeling, radioligand binding, and mutational studies were used to study the ligand-binding sites of nAChR. The two binding sites lie between subunit interfaces: one between  $\alpha$  and  $\gamma$ ; the other between  $\alpha$  and  $\delta$ . Several loops (loop A to loop F), which are different regions of sequence, define the ligand-binding sites. A large number of aromatic residues are present in the loops (Figure 1.8).<sup>62</sup>

In 2001, the soluble acetylcholine binding protein (AChBP) from the snail *Lymnaea stagnalis* (Ls-AChBP), which is highly homologous to the extracellular domain of the Cys-loop superfamily, was successfully crystallized at 2.7 Å resolution by the Sixma group.<sup>67, 68</sup> AChBP is a homopentamer; each subunit shares about 20% sequence identity with the Cys-loop superfamily. The core structure of each subunit is ten  $\beta$ -strands, which are connected by loops or turns. The key loops (loop A to loop F), as well

as the key aromatic residues, which are important in binding the ligand, are well-conserved (Figure 1.9).

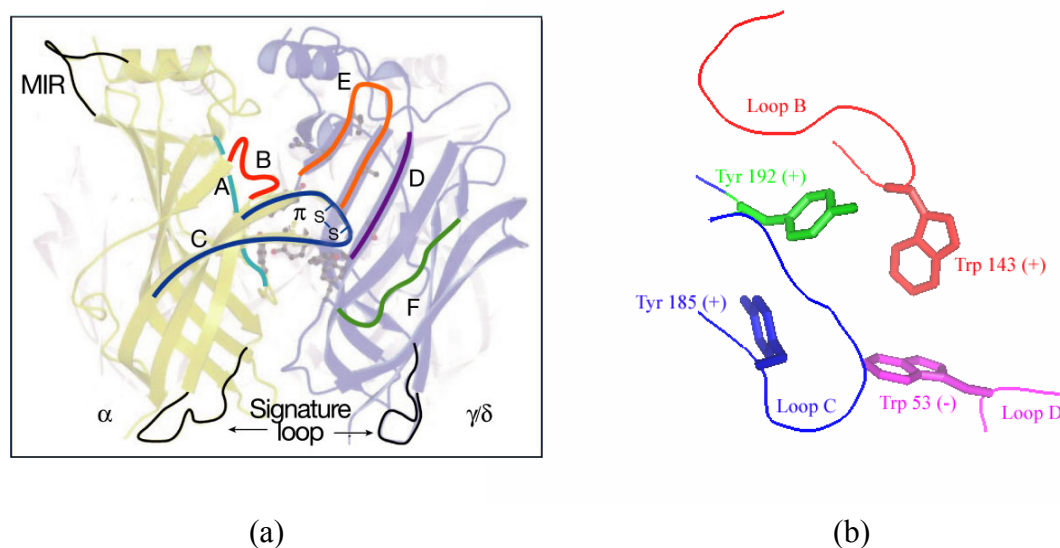


**Figure 1.9** Crystal structure of AChBP. (a) Homopentamer of AChBP. The key loops are conserved between two subunits interface. (b) The key aromatic residues in AChBP near the binding sites.

Later, the crystal structures of AChBP with the agonist nicotine or carbamylcholine bound were resolved at high resolution.<sup>69</sup> It was found that nicotine formed a hydrogen bond with the carbonyl group of Trp143 in AChBP. This hydrogen bond was proven by an unnatural amino acid study using an  $\alpha$ -hydroxy acid in nAChR.<sup>70</sup> Recently, the crystal structures of AChBP from different species (*Bulinus truncates* and *Aplysia californica*) with or without ligands bound were solved.<sup>71, 72</sup> Comparison of these structures with those from Ls-AChBP will help us improve the structure-function study.

The appearance of AChBP greatly stimulated the research field of the Cys-loop ligand-gated ion channels in several aspects.

First, this AChBP structure confirmed all the previous experimental data on the ligand-binding domains of nAChR. This high-resolution structure showed the effectiveness of the loop model for binding, and gave details on the binding pockets. It gave the structural basis for further study of the binding of agonists, antagonists, and other toxin molecules, and should benefit drug design.

Second, with the development of computational chemistry, the AChBP can serve as a reliable template to build homology models for the Cys-loop superfamily. The homology models will give valuable insights into the whole Cys-loop superfamily.

Third, although AChBP does not contain the transmembrane domains and cannot gate, the structural information can be used to study the coupling between binding and gating. It is clear from the structure that loop 5 is near the ligand-binding site and that loop 2 and loop 7 regions are close to the transmembrane domains. The Auerbach group proposed a conformational wave model for gating.<sup>73</sup> They performed single channel studies on the ligand-binding sites, loop 5, loop 2 and loop 7, the M2-M3 linker, and the ion pore regions of nAChR. It was proposed that after binding, loop 5 moved first, and loop 2/loop 7 domains moved afterwards. This stepwise movement was termed conformational wave, which was then extended to the M2-M3 linker and the ion pore region.<sup>74</sup> Harrison and co-workers focused on the coupling between loop 2/loop 7 regions and the M2-M3 linker in the  $\alpha_1$  subunit of GABA<sub>A</sub> receptors.<sup>75</sup> They performed charge-reversal double mutations and proposed that electrostatic interactions between Asp 149

in loop 7 and Lys 279 in the M2-M3 linker provided a potential mechanism for the coupling process. However, Unwin's nAChR structure suggested that hydrophobic interactions between Val 44 in loop 2 and residues in the M2-M3 linker contributed to the coupling process.<sup>66</sup> Now it seems that the coupling between loop 2/loop 7 regions and the M2-M3 linker is complicated, and cannot be elucidated only by the simple electrostatic interactions or hydrophobic interactions. The Sine group studied the initial coupling of binding to gating in nAChR. Using simulation and intrinsic tryptophan fluorescence, it was shown that after binding, loop C moved inward to occlude the entrance of the binding pockets.<sup>76</sup> Beyond the initial binding pockets, using single channel recording, the Sine group showed that upon binding of the agonist, Tyr 190 in loop C moved inside the binding pocket. This movement could destroy a salt bridge between Lys 145 in  $\beta$ -strand 7 and Asp 200 in  $\beta$ -strand 10 and loosen their contact. It was proposed that this process is involved in initiating the coupling of binding to gating.<sup>77</sup> The coupling process of the Cys-loop receptors is still an active research field. The actual coupling mechanism remains to be elucidated.

The structure of the transmembrane domains of nAChR was recently solved at 4.0 Å resolution.<sup>66</sup> It showed that hydrophobic interactions between Leu 251 in the M2 region contributed to the actual gate of the ion pore, which was consistent with previous mutational gating studies.<sup>78</sup> Using knowledge from the crystal structure of AChBP, the Unwin group built the structure of the whole nAChR at 4.0 Å resolution (Figure 1.10).<sup>65</sup> This structure will benefit the study of the whole Cys-loop receptor superfamily, especially on the gating process.

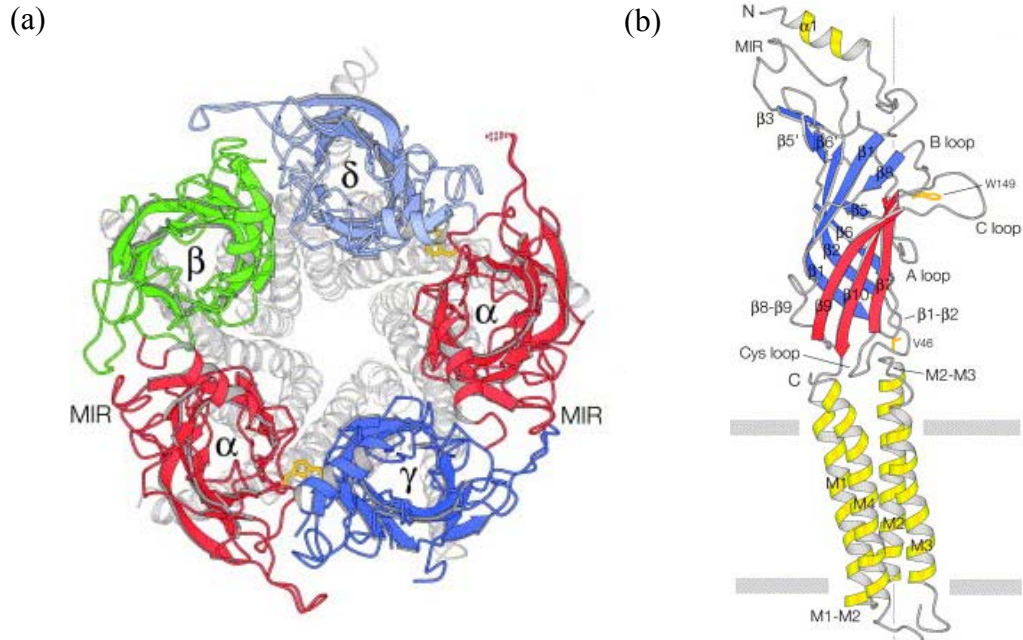


**Figure 1.10** Structure of the whole receptor of nAChR. (a) View from the synaptic cleft. (b) A single  $\alpha$  subunit of a side view. Adapted from Ref<sup>65</sup>.

## 1.4 Summary

We aim to perform a thorough structure-function study on the ligand-binding site of the Cys-loop superfamily of the LGICs. From the viewpoint of a chemist, we would like to obtain a detailed map of the ligand in the binding pocket. It is evident that non-covalent interactions contribute to directing the agonist to the binding pocket. We want to know the specific orientation of the agonist in the binding pocket and what kind of non-covalent interactions play the major role.

In this thesis, our target protein is the MOD-1 receptor.<sup>60</sup> The MOD-1 receptor was discovered in 2000. It is a serotonin-gated chloride channel that modulates locomotory behavior in the nematode *Caenorhabditis elegans*. The gene *mod-1* is responsible for modulation of locomotion; therefore, the protein is termed MOD-1. It belongs to the Cys-loop superfamily of ligand-gated ion channels (LGICs). This receptor is unique in that its agonist, serotonin (5-hydroxytryptamine or 5-HT), is the agonist of excitatory 5-HT<sub>3</sub> receptors while its anion selectivity is characteristic of inhibitory receptors such as the GABA<sub>A</sub> receptor and glycine receptor.

We will use chemistry to study the ligand-binding site of MOD-1. A high-resolution crystal structure of AChBP is available. Computational chemistry can be used to build a homology model of MOD-1 using the AChBP template. We proceed to dock the agonist into the binding pocket. This modeling study is presented in Chapter 3. The binding pattern from the model can give us insights and guidance for experimental study.

Unnatural amino acid mutagenesis is a powerful tool to modify the structure of the protein at the chemical level. Systematic perturbations can be introduced at a specific amino acid. Therefore, specific non-covalent interactions, such as hydrogen bonding, hydrophobic interactions, and cation- $\pi$  interactions can be probed. In Chapter 2, we prove that cation- $\pi$  interactions between the agonist serotonin and Trp 226 in loop C of MOD-1 play a key role in binding the ligand. Surprisingly, this cation- $\pi$  site in MOD-1 is different from that in 5-HT<sub>3</sub>R although these two receptors both bind serotonin and are highly homologous. In Chapter 4, we further show that hydrogen bonds between serotonin and Gln 228 and Asn 223 in MOD-1 are also important in the binding process.

In Chapter 5, we apply another strategy called the tethered agonist approach to further probe the agonist binding site. The tethered agonists are incorporated into the protein so that the channel will be in the spontaneously open state even without the addition of the natural agonist. This is another elegant example of the effectiveness of the nonsense suppression method.

In summary, we perform a chemical-scale study on the ligand-binding site of a serotonin-gated ion channel, MOD-1. Therefore, it is possible to perform chemical neurobiology on this extremely complicated system. Progress in this challenging field is being made with the development of structural biology, molecular biology, electrophysiology, organic synthesis, and computational modeling. This is an example in the developing field of chemical biology, which will benefit drug design and human health.

## 1.5 References

1. Kandel, E. R.; Schwartz, J. H.; Jessell, T. M., *Principles of Neural Science*. 4th ed.; The McGraw-Hill Companies, Inc.: 2000.
2. Nestler, E. J.; Hyman, S. E.; Malenka, R. C., *Molecular Neuropharmacology: A Foundation for Clinical Neuroscience*. The McGraw-Hill Companies, Inc.: 2001.
3. Rees, D. C.; Chang, G.; Spencer, R. H., Crystallographic analyses of ion channels: Lessons and challenges. *J. Biol. Chem.* **2000**, *275*, 713–716.
4. Chang, G.; Spencer, R. H.; Lee, A. T.; Barclay, M. T.; Rees, D. C., Structure of the MscL homolog from *Mycobacterium tuberculosis*: A gated mechanosensitive ion channel. *Science* **1998**, *282*, 2220–2226.

5. Doyle, D. A.; Cabral, J. M.; Pfuetzner, R. A.; Kuo, A. L.; Gulbis, J. M.; Cohen, S. L.; Chait, B. T.; MacKinnon, R., The structure of the potassium channel: Molecular basis of K<sup>+</sup> conduction and selectivity. *Science* **1998**, 280, 69–77.
6. Hodgkin, A. L.; Huxley, A. F., A quantitative description of membrane current and its application to conduction and excitation in nerve. *J. Physiol.-London* **1952**, 117, 500–544.
7. Neher, E.; Sakmann, B., Single-channel currents recorded from membrane of denervated frog muscle-fibers. *Nature* **1976**, 260, 799–802.
8. Hamill, O. P.; Marty, A.; Neher, E.; Sakmann, B.; Sigworth, F. J., Improved patch-clamp techniques for high-resolution current recording from cells and cell-free membrane patches. *Pflugers Arch.* **1981**, 391, 85–100.
9. Editorial, A community of chemists and biologists. *Nat Chem Biol* **2005**, 1, 3.
10. Dougherty, D. A., Is the brain ready for physical organic chemistry? *J. Phys. Org. Chem.* **1998**, 11, 334–340.
11. Nowak, M. W.; Kearney, P. C.; Sampson, J. R.; Saks, M. E.; Labarca, C. G.; Silverman, S. K.; Zhong, W.; Thorson, J.; Abelson, J. N.; Davidson, N.; Schultz, P. G.; Dougherty, D. A.; Lester, H. A., Nicotinic receptor-binding site probed with unnatural amino-acid-incorporation in intact-cells. *Science* **1995**, 268, 439–442.
12. England, P. M., Unnatural amino acid mutagenesis: A precise tool for probing protein structure and function. *Biochemistry* **2004**, 43, 11623–11629.
13. Heckler, T. G.; Chang, L. H.; Zama, Y.; Naka, T.; Chorghade, M. S.; Hecht, S. M., T4 RNA ligase mediated preparation of novel chemically misacylated transfer-RNA Phe. *Biochemistry* **1984**, 23, 1468–1473.
14. Bain, J. D.; Glabe, C. G.; Dix, T. A.; Chamberlin, A. R.; Diala, E. S., Biosynthetic site-specific incorporation of a non-natural amino-acid into a polypeptide. *J. Am. Chem. Soc.* **1989**, 111, 8013–8014.
15. Noren, C. J.; Anthonycahill, S. J.; Griffith, M. C.; Schultz, P. G., A general method for site-specific incorporation of unnatural amino-acids into proteins. *Science* **1989**, 244, 182–188.
16. Monahan, S. L.; Lester, H. A.; Dougherty, D. A., Site-specific incorporation of unnatural amino acids into receptors expressed in mammalian cells. *Chem. Biol.* **2003**, 10, 573–580.
17. Dougherty, D. A., Unnatural amino acids as probes of protein structure and function. *Curr. Opin. Chem. Biol.* **2000**, 4, 645–652.
18. Cload, S. T.; Liu, D. R.; Froland, W. A.; Schultz, P. G., Development of improved tRNAs for *in vitro* biosynthesis of proteins containing unnatural amino acids. *Chem. Biol.* **1996**, 3, 1033–1038.

19. Nowak, M. W.; Gallivan, J. P.; Silverman, S. K.; Labarca, C. G.; Dougherty, D. A.; Lester, H. A., *In vivo* incorporation of unnatural amino acids into ion channels in *Xenopus* oocyte expression system. *Method Enzymol.* **1998**, 293, 504–529.
20. Saks, M. E.; Sampson, J. R.; Nowak, M. W.; Kearney, P. C.; Du, F. Y.; Abelson, J. N.; Lester, H. A.; Dougherty, D. A., An engineered *Tetrahymena* tRNA(Gln) for *in vivo* incorporation of unnatural amino acids into proteins by nonsense suppression. *J. Biol. Chem.* **1996**, 271, 23169–23175.
21. Hohsaka, T.; Sisido, M., Incorporation of non-natural amino acids into proteins. *Curr. Opin. Chem. Biol.* **2002**, 6, 809–15.
22. Bain, J. D.; Diala, E. S.; Glabe, C. G.; Wacker, D. A.; Lyttle, M. H.; Dix, T. A.; Chamberlin, A. R., Site-specific incorporation of nonnatural residues during *in vitro* protein-biosynthesis with semisynthetic aminoacyl-transfer RNAs. *Biochemistry* **1991**, 30, 5411–5421.
23. Kohrer, C.; Xie, L.; Kellerer, S.; Varshney, U.; Rajbhandary, U. L., Import of amber and ochre suppressor tRNAs into mammalian cells: A general approach to site-specific insertion of amino acid analogues into proteins. *Proc. Natl. Acad. Sci. U. S. A.* **2001**, 98, 14310–14315.
24. Karginov, V. A.; Mamaev, S. V.; An, H. Y.; VanCleve, M. D.; Hecht, S. M.; Komatsoulis, G. A.; Abelson, J. N., Probing the role of an active site aspartic acid in dihydrofolate reductase. *J. Am. Chem. Soc.* **1997**, 119, 8166–8176.
25. Ludlam, C. F. C.; Sonar, S.; Lee, C. P.; Coleman, M.; Herzfeld, J.; Rajbhandary, U. L.; Rothschild, K. J., Site-directed isotope labeling and Atr-Ftir difference spectroscopy of bacteriorhodopsin: The peptide carbonyl group of Tyr-185 is structurally active during the Br-N-Transition. *Biochemistry* **1995**, 34, 2–6.
26. Short, G. F.; Golovine, S. Y.; Hecht, S. M., Effects of release factor 1 on *in vitro* protein translation and the elaboration of proteins containing unnatural amino acids. *Biochemistry* **1999**, 38, 8808–8819.
27. Carnes, J.; Jacobson, M.; Leinwand, L.; Yarus, M., Stop codon suppression via inhibition of eRF1 expression. *RNA-Publ. RNA Soc.* **2003**, 9, 648–653.
28. Sisido, M.; Hohsaka, T., Introduction of specialty functions by the position-specific incorporation of nonnatural amino acids into proteins through four-base codon/anticodon pairs. *Appl. Microbiol. Biotechnol.* **2001**, 57, 274–281.
29. Hohsaka, T.; Ashizuka, Y.; Murakami, H.; Sisido, M., Incorporation of nonnatural amino acids into streptavidin through *in vitro* frame-shift suppression. *J. Am. Chem. Soc.* **1996**, 118, 9778–9779.
30. Hohsaka, T.; Ashizuka, Y.; Sasaki, H.; Murakami, H.; Sisido, M., Incorporation of two different nonnatural amino acids independently into a single protein through extension of the genetic code. *J. Am. Chem. Soc.* **1999**, 121, 12194–12195.

31. Hohsaka, T.; Ashizuka, Y.; Taira, H.; Murakami, H.; Sisido, M., Incorporation of nonnatural amino acids into proteins by using various four-base codons in an *Escherichia coli in vitro* translation system. *Biochemistry* **2001**, *40*, 11060–11064.
32. Hohsaka, T.; Ashizuka, Y.; Murakami, H.; Sisido, M., Five-base codons for incorporation of nonnatural amino acids into proteins. *Nucleic Acids Res.* **2001**, *29*, 3646–3651.
33. Magliery, T. J.; Anderson, J. C.; Schultz, P. G., Expanding the genetic code: Selection of efficient suppressors of four-base codons and identification of "shifty" four-base codons with a library approach in *Escherichia coli*. *J. Mol. Biol.* **2001**, *307*, 755–769.
34. Moore, B.; Persson, B. C.; Nelson, C. C.; Gesteland, R. F.; Atkins, J. F., Quadruplet codons: Implications for code expansion and the specification of translation step size. *J. Mol. Biol.* **2000**, *298*, 195–209.
35. Anderson, J. C.; Magliery, T. J.; Schultz, P. G., Exploring the limits of codon and anticodon size. *Chem. Biol.* **2002**, *9*, 237–244.
36. Bain, J. D.; Switzer, C.; Chamberlin, A. R.; Benner, S. A., Ribosome-mediated incorporation of a nonstandard amino-acid into a peptide through expansion of the genetic-code. *Nature* **1992**, *356*, 537–539.
37. Hirao, I.; Ohtsuki, T.; Fujiwara, T.; Mitsui, T.; Yokogawa, T.; Okuni, T.; Nakayama, H.; Takio, K.; Yabuki, T.; Kigawa, T.; Kodama, K.; Yokogawa, T.; Nishikawa, K.; Yokoyama, S., An unnatural base pair for incorporating amino acid analogs into proteins. *Nat. Biotechnol.* **2002**, *20*, 177–182.
38. Saks, M. E., Making sense out of nonsense. *Proc. Natl. Acad. Sci. U. S. A.* **2001**, *98*, 2125–2127.
39. Wang, L.; Brock, A.; Herberich, B.; Schultz, P. G., Expanding the genetic code of *Escherichia coli*. *Science* **2001**, *292*, 498–500.
40. Santoro, S. W.; Wang, L.; Herberich, B.; King, D. S.; Schultz, P. G., An efficient system for the evolution of aminoacyl-tRNA synthetase specificity. *Nat. Biotechnol.* **2002**, *20*, 1044–8.
41. Pastrnak, M.; Schultz, P. G., Phage selection for site-specific incorporation of unnatural amino acids into proteins *in vivo*. *Bioorg. Med. Chem.* **2001**, *9*, 2373–9.
42. Wang, L.; Schultz, P. G., Expanding the genetic code. *Angew. Chem.-Int. Edit.* **2005**, *44*, 34–66.
43. Brown, D. D., A tribute to the *Xenopus laevis* oocyte and egg. *J. Biol. Chem.* **2004**, *279*, 45291–45299.
44. Beene, D. L.; Dougherty, D. A.; Lester, H. A., Unnatural amino acid mutagenesis in mapping ion channel function. *Curr. Opin. Neurobiol.* **2003**, *13*, 264–270.

45. Hille, B., *Ion Channels of Excitable Membranes*. 3rd ed.; Sinauer Associates, Inc.: 2001.
46. Ashcroft, F. M., *Ion Channels and Disease: Channelopathies*. Academic press: 2000.
47. Lester, H. A.; Dibas, M. I.; Dahan, D. S.; Leite, J. F.; Dougherty, D. A., Cys-loop receptors: New twists and turns. *Trends Neurosci.* **2004**, *27*, 329–336.
48. Karlin, A.; Akabas, M. H., Toward a structural basis for the function of nicotinic acetylcholine receptors and their cousins. *Neuron* **1995**, *15*, 1231–1244.
49. Ortells, M. O.; Lunt, G. G., Evolutionary history of the ligand-gated ion-channel superfamily of receptors. *Trends Neurosci.* **1995**, *18*, 121–127.
50. Karlin, A., Emerging structure of the nicotinic acetylcholine receptors. *Nat. Rev. Neurosci.* **2002**, *3*, 102–114.
51. Corringer, P. J.; Le Novère, N.; Changeux, J. P., Nicotinic receptors at the amino acid level. *Annu. Rev. Pharmacol. Toxicol.* **2000**, *40*, 431–458.
52. Reeves, D. C.; Lummis, S. C. R., The molecular basis of the structure and function of the 5-HT<sub>3</sub> receptor: a model ligand-gated ion channel (Review). *Mol. Membr. Biol.* **2002**, *19*, 11–26.
53. Davies, P. A.; Wang, W.; Hales, T. G.; Kirkness, E. F., A novel class of ligand-gated ion channel is activated by Zn<sup>2+</sup>. *J. Biol. Chem.* **2003**, *278*, 712–717.
54. Beg, A. A.; Jorgensen, E. M., EXP-1 is an excitatory GABA-gated cation channel. *Nat. Neurosci.* **2003**, *6*, 1145–1152.
55. Korpi, E. R.; Grunder, G.; Luddens, H., Drug interactions at GABA(A) receptors. *Prog. Neurobiol.* **2002**, *67*, 113–159.
56. Chebib, M.; Johnston, G. A. R., GABA-activated ligand gated ion channels: Medicinal chemistry and molecular biology. *J. Med. Chem.* **2000**, *43*, 1427–1447.
57. Enz, R., GABA(C) receptors: A molecular view. *Biol. Chem.* **2001**, *382*, 1111–1122.
58. Laube, B.; Maksay, G.; Schemm, R.; Betz, H., Modulation of glycine receptor function: a novel approach for therapeutic intervention at inhibitory synapses? *Trends Pharmacol. Sci.* **2002**, *23*, 519–527.
59. Breiting, H. G.; Becker, C. M., The inhibitory glycine receptor: Simple views of a complicated channel. *Chembiochem* **2002**, *3*, 1043–1052.
60. Ranganathan, R.; Cannon, S. C.; Horvitz, H. R., MOD-1 is a serotonin-gated chloride channel that modulates locomotory behaviour in *C. elegans*. *Nature* **2000**, *408*, 470–475.

61. Cully, D. F.; Vassilatis, D. K.; Liu, K. K.; Paress, P. S.; Vanderploeg, L. H. T.; Schaeffer, J. M.; Arena, J. P., Cloning of an avermectin-sensitive glutamate-gated chloride channel from *Caenorhabditis elegans*. *Nature* **1994**, 371, 707–711.
62. Dougherty, D. A.; Lester, H. A., Neurobiology: Snails, synapses and smokers. *Nature* **2001**, 411, 252–254.
63. Miyazawa, A.; Fujiyoshi, Y.; Stowell, M.; Unwin, N., Nicotinic acetylcholine receptor at 4.6 angstrom resolution: Transverse tunnels in the channel wall. *J. Mol. Biol.* **1999**, 288, 765–786.
64. Unwin, N., Nicotinic acetylcholine-receptor at 9-angstrom resolution. *J. Mol. Biol.* **1993**, 229, 1101–1124.
65. Unwin, N., Refined structure of the nicotinic acetylcholine receptor at 4 angstrom resolution. *J. Mol. Biol.* **2005**, 346, 967–989.
66. Miyazawa, A.; Fujiyoshi, Y.; Unwin, N., Structure and gating mechanism of the acetylcholine receptor pore. *Nature* **2003**, 423, 949–955.
67. Brejc, K.; van Dijk, W. J.; Klaassen, R. V.; Schuurmans, M.; van der Oost, J.; Smit, A. B.; Sixma, T. K., Crystal structure of an ACh-binding protein reveals the ligand-binding domain of nicotinic receptors. *Nature* **2001**, 411, 269–276.
68. Smit, A. B.; Syed, N. I.; Schaap, D.; van Minnen, J.; Klumperman, J.; Kits, K. S.; Lodder, H.; van der Schors, R. C.; van Elk, R.; Sorgedraeger, B.; Brejc, K.; Sixma, T. K.; Geraerts, W. P. M., A glia-derived acetylcholine-binding protein that modulates synaptic transmission. *Nature* **2001**, 411, 261–268.
69. Celie, P. H. N.; van Rossum-Fikkert, S. E.; van Dijk, W. J.; Brejc, K.; Smit, A. B.; Sixma, T. K., Nicotine and carbamylcholine binding to nicotinic acetylcholine receptors as studied in AChBP crystal structures. *Neuron* **2004**, 41, 907–914.
70. Cashin, A. L.; Petersson, E. J.; Lester, H. A.; Dougherty, D. A., Using physical chemistry to differentiate nicotinic from cholinergic agonists at the nicotinic acetylcholine receptor. *J. Am. Chem. Soc.* **2005**, 127, 350–356.
71. Celie, P. H. N.; Klaassen, R. V.; van Rossum-Fikkert, S. E.; van Elk, R.; van Nierop, P.; Smit, A. B.; Sixma, T. K., Crystal structure of acetylcholine-binding protein from *Bulinus truncatus* reveals the conserved structural scaffold and sites of variation in nicotinic acetylcholine receptors. *J. Biol. Chem.* **2005**, 280, 26457–26466.
72. Celie, P. H. N.; Kasheverov, I. E.; Mordvintsev, D. Y.; Hogg, R. C.; van Nierop, P.; van Elk, R.; van Rossum-Fikkert, S. E.; Zhmak, M. N.; Bertrand, D.; Tsetlin, V.; Sixma, T. K.; Smit, A. B., Crystal structure of nicotinic acetylcholine receptor homolog AChBP in complex with an [alpha]-conotoxin PnIA variant. *Nat. Struct. Mol. Biol.* **2005**, 12, 582.
73. Grosman, C.; Zhou, M.; Auerbach, A., Mapping the conformational wave of acetylcholine receptor channel gating. *Nature* **2000**, 403, 773–776.

74. Chakrapani, S.; Bailey, T. D.; Auerbach, A., Gating dynamics of the acetylcholine receptor extracellular domain. *J. Gen. Physiol.* **2004**, 123, 341–356.
75. Kash, T. L.; Jenkins, A.; Kelley, J. C.; Trudell, J. R.; Harrison, N. L., Coupling of agonist binding to channel gating in the GABA(A) receptor. *Nature* **2003**, 421, 272–275.
76. Gao, F.; Bren, N.; Burghardt, T. P.; Hansen, S.; Henchman, R. H.; Taylor, P.; McCammon, J. A.; Sine, S. M., Agonist-mediated conformational changes in acetylcholine-binding protein revealed by simulation and intrinsic tryptophan fluorescence. *J. Biol. Chem.* **2005**, 280, 8443–8451.
77. Mukhtasimova, N.; Free, C.; Sine, S. M., Initial coupling of binding to gating mediated by conserved residues in the muscle nicotinic receptor. *J. Gen. Physiol.* **2005**, 126, 23–39.
78. Labarca, C.; Nowak, M. W.; Zhang, H. Y.; Tang, L. X.; Deshpande, P.; Lester, H. A., Channel gating governed symmetrically by conserved leucine residues in the M2 domain of nicotinic receptors. *Nature* **1995**, 376, 514–516.

## **Chapter 2**

# **Different Cation- $\pi$ Sites at Two Homologous Serotonin Receptors, MOD-1 and 5-HT<sub>3</sub>R**

## 2.1 Introduction

The cation- $\pi$  interaction is an important non-covalent binding force in structural biology.<sup>1-3</sup> Our initial goal is to explore new ion channel systems to confirm that this non-covalent interaction is general.

Previous studies on the nicotinic acetylcholine receptor (nAChR) show that a cation- $\pi$  interaction exists between the agonist acetylcholine (for the molecular structure, see Figure 2.1) and Trp 149 in the  $\alpha$  subunit of nAChR.<sup>4</sup> This cation- $\pi$  interaction is further supported by the crystal structure of acetylcholine binding protein (AChBP) (Figure 1.9).<sup>5</sup> The nAChR is the most well-studied and serves as the prototype of the whole Cys-loop superfamily of LGICs.

MOD-1 and 5-HT<sub>3</sub>R are highly homologous in the ligand-binding domains. They both bind serotonin (for the molecular structure, see Figure 2.1) for activation. Trp 183 in 5-HT<sub>3</sub>R, a homolog of Trp 149 in nAChR, forms a strong cation- $\pi$  interaction with serotonin.<sup>6</sup> In this chapter, we continue our effort to identify the cation- $\pi$  site of serotonin in the MOD-1 receptor.

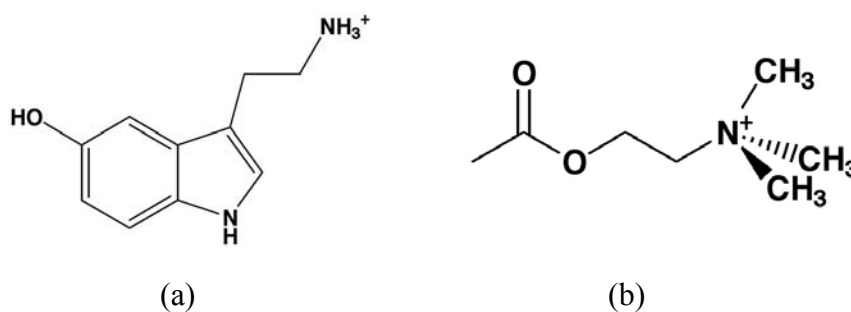


**Figure 2.1** Molecular structures of serotonin and acetylcholine. (a) Serotonin. (b) Acetylcholine.

### 2.1.1 Cation- $\pi$ Interactions

The cation- $\pi$  interaction is an important general force in structural biology.<sup>7</sup> Numerous studies have shown that the cation- $\pi$  interaction is important in biological recognition.<sup>2, 8</sup> In evaluating drug-receptor interactions, the cation- $\pi$  interaction should be considered along with other non-covalent interactions.<sup>1</sup>

Cations bind to the  $\pi$ -face of an aromatic ring through a strong non-covalent force termed the cation- $\pi$  interaction (Figure 2.2 (a)). The simple model of benzene as the aromatic ring qualitatively shows that this interaction arises from the quadrupole moment of benzene, which will interact with properly positioned charges through electrostatic forces (Figure 2.2 (b)).

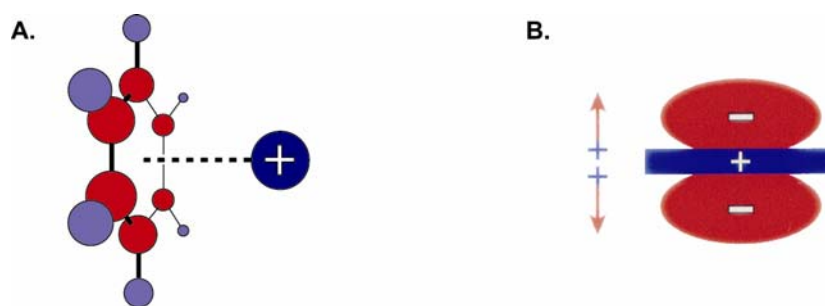


**Figure 2.2** The cation- $\pi$  interaction. (a) A generic cation interacting with benzene. (b) Quadrupole moment of benzene.

In the biological context, the aromatic side chains of Phe, Tyr, and Trp participate in cation- $\pi$  interactions. Their cation- $\pi$  binding energies were evaluated by a simple model system of a sodium cation with a series of aromatic systems using the Hartree-Fock method at the 6-31G\*\* level.<sup>9</sup> The calculated numbers were used to correlate with the experimental results.<sup>4</sup>

Recently, some purely computational efforts have been made to explore more diverse systems to study cation- $\pi$  interactions using high-level MP2 or DFT methods. Different cations, such as Li<sup>+</sup>, K<sup>+</sup>, alkaline earth cations, and ammonium cations, and different aromatic compounds, such as naphthalene, heterocycles, and complete aromatic residues of Phe, Tyr, and Trp were used.<sup>10-16</sup> Other influences such as counterions and water molecules on cation- $\pi$  systems were also investigated both experimentally and computationally.<sup>12, 17-20</sup> All these studies help us better understand the origin and wide application of cation- $\pi$  interactions.

Electrostatic potential surfaces are a very valuable tool in evaluating cation- $\pi$  interactions.<sup>21</sup> They provide a qualitative guide that faithfully tracks more quantitative efforts. Electrostatic potential surfaces were generated by mapping 6-31G\*\* electrostatic potentials onto surfaces of molecular electron density. It is very interesting that AM1 electrostatic potential surfaces represent very good approximations to the *ab initio* surfaces. Therefore, AM1 can provide a useful guideline for electrostatic potential surfaces.

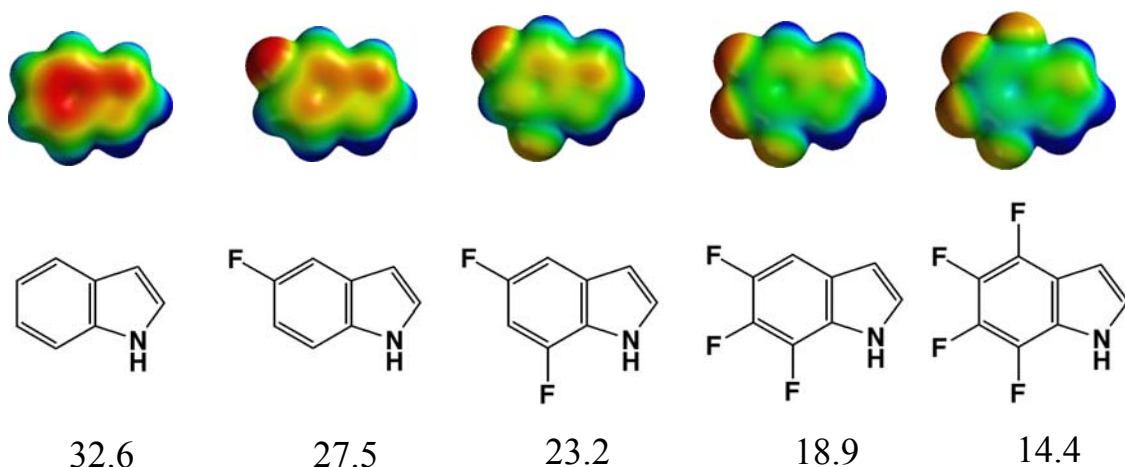


**Figure 2.3** *Ab initio* electrostatic potential surfaces (EPS) of fluorinated Trp side chains. Blue region is positively charged while red region is negatively charged. The structure and number correspond to the EPS right above them. The numbers are the calculated sodium cation binding energy (kcal/mol) using HF/6-31G\*\*.

Fluorination of the indole ring of Trp withdraws the electron density from the aromatic system. As is illustrated from electrostatic potential surfaces, progressive fluorination of the Trp side chains makes charges in the ring centers less negative, diminishing cation- $\pi$  interactions additively (Figure 2.3). The binding energies are calculated from the sodium and indole model system using HF/6-31G\*\*. The progressive fluorination series can give convincing evidence for cation- $\pi$  interactions in a ligand-receptor recognition process.

### 2.1.2 The MOD-1 Receptor

The MOD-1 receptor was discovered in 2000.<sup>22</sup> It is a serotonin-gated chloride channel that modulates locomotory behavior in *C. elegans*. It belongs to the Cys-loop superfamily of ligand-gated ion channels (LGICs).

The MOD-1 receptor is unique. It is activated by serotonin (5-hydroxytryptamine or 5-HT), similar to 5-HT<sub>3</sub>R.<sup>23</sup> In contrast to 5-HT<sub>3</sub>R, it is not blocked by calcium ions or 5-HT<sub>3</sub>-specific antagonists; instead, it is inhibited by the metabotropic 5-HT receptor antagonists, such as mianserin and methiothepin. MOD-1 conducts chloride anions, which is characteristic of inhibitory receptors such as the GABA<sub>A</sub> and glycine receptors. Besides chloride, MOD-1 channels are also permeable to other anions, such as thiocyanate and bromide.

Based on the structure of the nAChR, it is predicted that the MOD-1 receptor is a pentamer. To date, only one subunit has been reported. Each subunit has four transmembrane segments, M1–M4, with the M2 domain presumably lining the interior of the pore. A large extracellular N-terminus contains the ligand binding site (Figure 1.7).

	Loop D			Loop B			Loop C	
AchRG	52	TNV- <b>W</b> IE <b>M</b>	AchRA	148	<b>T</b> W <b>T</b> YDGSV	189	<b>F</b> YSCCPTTP <b>Y</b> LD	
AchBP	50	VVF- <b>W</b> QQT	AchBP	142	<b>S</b> W <b>T</b> THHSRE	184	<b>T</b> YSCCP-EAYED	
5HT3A	87	TYI- <b>W</b> YRQ	5HT3A	182	<b>S</b> WLHTIQD	225	- <b>F</b> SIDISNS <b>Y</b> AE	
MOD-1	79	IDIL <b>E</b> FT-Q	MOD-1	179	<b>S</b> YSHNSEE	220	<b>L</b> YPNG--- <b>Y</b> WDQ	

**Figure 2.4** Sequence alignments for the key regions of the agonist binding sites. AchRG represents the  $\gamma$  subunit of nAChR; AchRA,  $\alpha$  subunit.

In the region of the agonist binding site, MOD-1 and 5-HT<sub>3</sub>R are highly homologous. MOD-1 is 24% identical and 45% similar to 5-HT<sub>3</sub>R. Importantly, key aromatic residues of the agonist binding site are conserved in the two receptors (Figure 2.4).

Most of what we know about the agonist binding site of the Cys-loop family of receptors came from studies of the nAChR.<sup>24</sup> Extensive biochemical studies implicated a large number of aromatic residues as contributing to the binding site. These are associated with six so-called “loops” (loop A to loop F), which are different regions of sequence space that define the agonist binding site. Here we discuss only loops B, C, and D, as these are most conserved among the receptors considered (Figure 2.4). Studies of the nAChR using unnatural amino acid mutagenesis identified a key tryptophan, Trp 149 in loop B, as making a potent cation- $\pi$  interaction with acetylcholine in the binding site. The key to this study was the incorporation of a series of fluorinated Trp derivatives (F<sub>*n*</sub>-Trp, *n* = 1–4), showing that agonist potency tracked linearly with the cation- $\pi$  binding abilities of the fluorinated rings (Table 2.2, Figure 2.7). These findings were subsequently supported by the crystal structure of AChBP (Figure 1.9), a soluble protein that is highly homologous to the agonist binding site of the nAChR.

Recently, the same approach was used to establish a similar binding motif for serotonin in the 5-HT<sub>3</sub> receptor. In particular, Trp 183, the analogue of nAChR Trp 149, makes a strong cation- $\pi$  interaction to the ammonium of serotonin, as evidenced by the fluorinated Trp study (Table 2.2, Figure 2.7).

As shown in Figure 2.4, MOD-1 also contains aromatic residues at the key locations, but with a subtle difference. The residue that aligns with Trp 183 of 5-HT<sub>3</sub>R is Tyr 180 of MOD-1. The key tryptophan that makes a cation- $\pi$  interaction with serotonin (and acetylcholine) is now a Tyr. Of course, Tyr (and Phe) can also participate in cation- $\pi$  interactions,<sup>3</sup> and so this conservative change (Trp to Tyr) is not startling.

## 2.2 Electronic and Steric Effects on Ligand-Binding at Position 180 of MOD-1

MOD-1 thus presents an opportunity to quantify a cation- $\pi$  interaction between serotonin and a Tyr, allowing a direct comparison with the serotonin...Trp interaction in 5-HT<sub>3</sub>R.

As a qualitative test of whether a cation- $\pi$  interaction is important at position 180, we mutated Tyr to Phe and Trp. The EC<sub>50</sub> of the Phe mutant (1.1  $\mu$ M) is very close to that of wild type (1.2  $\mu$ M) while EC<sub>50</sub> of the Trp mutant (35.1  $\mu$ M) is much greater (Table 2.1). The calculated cation- $\pi$  binding energies for Tyr, Phe, and Trp are 26.9, 27.1, 32.6 kcal/mol, respectively (Figure 2.3 and Figure 2.5). The Tyr to Trp mutant increases the side chain size, partially occludes the agonist binding site, and leads to an increased EC<sub>50</sub>. Phenylalanine has a very similar effect as tyrosine at position 180 on both the EC<sub>50</sub> values and the cation- $\pi$  binding ability, which indicates that the absence of a hydroxyl group does not produce a significant perturbation. Since the fluorination of tyrosine may perturb its pK<sub>a</sub>, we used phenylalanine at position 180 as the reference state to evaluate cation- $\pi$  interactions in the following experiments.

**Table 2.1** Mutations of Tyr 180 of MOD-1

Residue	EC <sub>50</sub> (μM)	n <sub>Hill</sub>
Tyr (Wild type)	1.2 ± 0.2	1.09 ± 0.18
Phe	1.1 ± 0.1	1.08 ± 0.12
4-F-Phe	213 ± 57	0.96 ± 0.12
4-Cl-Phe	202 ± 52	0.81 ± 0.09
4-Br-Phe	196 ± 46	0.88 ± 0.10
3,4,5-F <sub>3</sub> -Phe	210 ± 69	0.71 ± 0.13
4-Me-Phe	90.0 ± 8.6	0.90 ± 0.05
4-MeO-Phe	316 ± 181	0.85 ± 0.13
Trp	35.1 ± 7.0	0.90 ± 0.11
5-F-Trp	127 ± 46	0.58 ± 0.07

We used the *in vivo* nonsense suppression methodology for unnatural amino acid incorporation to substitute Tyr 180 of MOD-1 with several Phe analogues, including fluorinated residues of the sort that were so informative in studying the tryptophan interaction (Table 2.1).

The EC<sub>50</sub> values for 4-F-Phe, 4-Cl-Phe, and 4-Br-Phe at position 180 of MOD-1 are 213 μM, 202 μM, and 196 μM, respectively, which are essentially the same. Since cation-π binding energies for 4-F-Phe (21.9 kcal/mol), 4-Cl-Phe (21.5 kcal/mol), and 4-Br-Phe are close while steric effects are different, it seems that an electronic effect rather than a steric effect is important here.

The electrostatic potential surfaces (EPS) for the side chains of some phenylalanine derivatives used in the current studies are shown in Figure 2.5. F-Phe, Cl-Phe, and Br-Phe, which have similar EPS, form much weaker cation-π interactions than

Phe, Tyr, 4-Me-Phe, and 4-MeO-Phe, which also have similar EPS among them. To further probe steric effects at Tyr 180, 4-Me-Phe and 4-MeO-Phe were incorporated into this position.

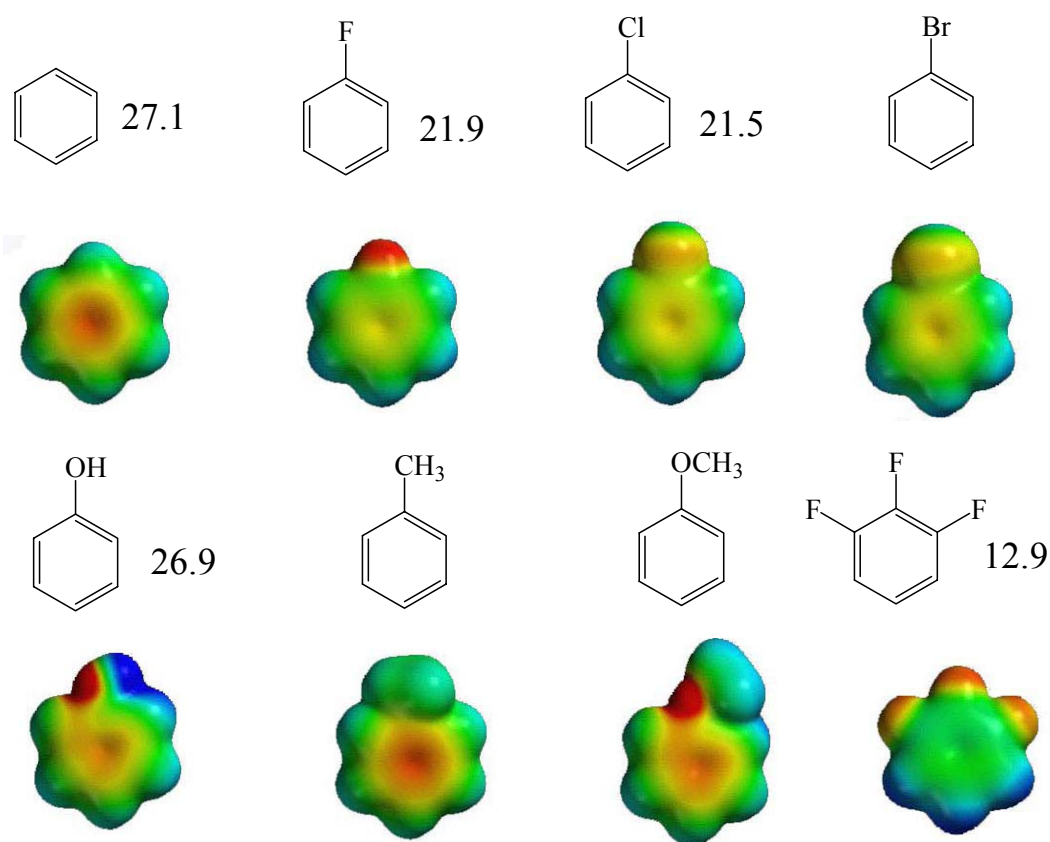


**Figure 2.5** AM1 electrostatic potential surfaces of the side chains of phenylalanine derivatives. Blue region is positively charged while red region is negatively charged. The numbers beside molecular structures are the calculated sodium cation binding energy (kcal/mol) using HF/6-31G\*\*.

The  $EC_{50}$  values for 4-Me-Phe and 4-MeO-Phe are 90.0  $\mu$ M and 316  $\mu$ M, respectively. This result possibly means that a steric effect actually plays an important role at this site, too. However, Tyr and Phe have similar  $EC_{50}$  values; 4-F-Phe, 4-Cl-Phe,

and 4-Br-Phe also give similar behavior, which contradicts the importance of steric effect here.

We found that these mutation studies yield puzzling and sometimes contradictory results. Possibly many factors play important roles at this site. The data showed no clear trend, and certainly not the remarkable trend seen when studying the Trp residues in 5-HT<sub>3</sub>R or nAChR.

### 2.3 Cation- $\pi$ Interactions between Serotonin and Trp 226 of MOD-1

Given these puzzling results, we considered a second subtle difference between MOD-1 and other Cys-loop receptors. Another canonical aromatic residue of the agonist binding site is Tyr 198 of the nAChR, aligning with Tyr 234 of 5-HT<sub>3</sub>R and Tyr 192 of AChBP. This Tyr is conserved in essentially all members of the family, but it is Trp 226 in MOD-1. Given our earlier successes with studies of fluorinated Trp derivatives, we decided to apply the same protocol to Trp 226 of MOD-1.

**Table 2.2** Mutations of key aromatic residues (EC<sub>50</sub>,  $\mu$ M)

Residue	149 nAChR <sup>a</sup>	183 5-HT <sub>3</sub> <sup>b</sup>	226 MOD-1	Cation- $\pi$ Binding <sup>c</sup>
Trp	1.2 $\pm$ 0.1	1.2 $\pm$ 0.1	1.2 $\pm$ 0.3	32.6
5-F-Trp	4.7 $\pm$ 0.1	6.0 $\pm$ 0.5	12 $\pm$ 1	27.5
5,7-F <sub>2</sub> -Trp	13 $\pm$ 0.1	37 $\pm$ 3	66 $\pm$ 11	23.3
5,6,7-F <sub>3</sub> -Trp	34 $\pm$ 0.1	240 $\pm$ 8	240 $\pm$ 50	18.9
4,5,6,7-F <sub>4</sub> -Trp	65 $\pm$ 0.3	–	1600 $\pm$ 210	14.4

a. Ref<sup>4</sup>. The receptor has a Leu9'Ser mutation in M2. b. Ref<sup>6</sup>. c. kcal/mol

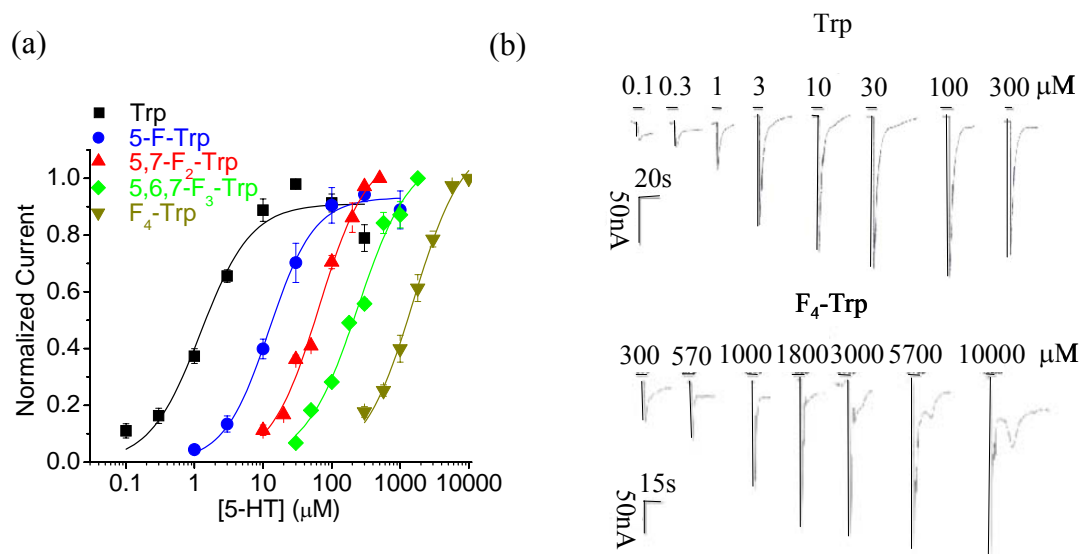


**Figure 2.6** Electrophysiology recording of fluorinated tryptophans at position 226 of MOD-1. (a) Dose-response curves. (b) Representative voltage-clamp current traces for oocytes expressing suppressed MOD-1.

The dose-response curves and representative electrophysiology traces are shown in Figure 2.6. The  $EC_{50}$  results are summarized in Table 2.2. We know that  $EC_{50}$  is a value reflecting both binding and gating of ion channels. However, since all the subtle mutations here are only made in the binding site and far away from the actual gating position, we assume that the mutations only affect binding, and that these  $EC_{50}$  values can represent the binding constants. Therefore, we can draw the plot of  $\log [EC_{50}/EC_{50}(wt)]$  vs. cation- $\pi$  interaction ability (Figure 2.7). Stunningly, the exact same trend seen for Trp 183 of 5-HT<sub>3</sub>R is seen for Trp 226 of MOD-1. Both serotonin lines have steeper slopes than the analogous acetylcholine line, and the two serotonin lines have identical slopes. It

is thus estimated that cation- $\pi$  interactions contribute to ligand binding in nAChR and serotonin receptors by ca. 2 kcal/mol and ca. 4 kcal/mol, respectively.<sup>6</sup> Such agreement can only be interpreted to mean that the primary ammonium of serotonin makes a strong cation- $\pi$  interaction with a Trp in both systems, but the two homologous receptors use a different tryptophan to make the cation- $\pi$  interaction to serotonin.<sup>25</sup>

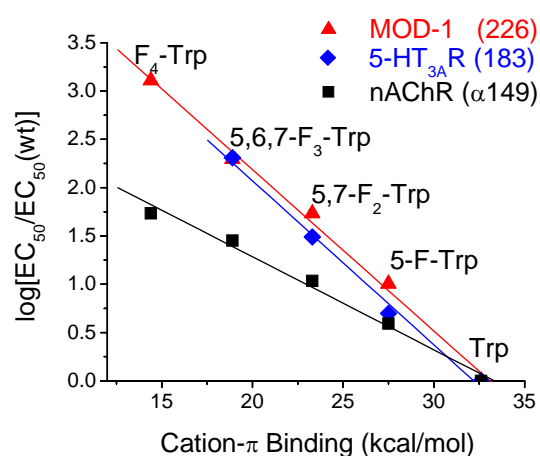


**Figure 2.7** Fluorination effects versus cation- $\pi$  binding energies. Red line represents cation- $\pi$  site at Trp 226 in MOD-1; blue line, Trp 183 in 5-HT<sub>3R</sub>; black line, Trp 149 in nAChR.

It thus appears that Nature has moved the critical cation- $\pi$  binding interaction from the loop B site to the second loop C site on going from 5-HT<sub>3R</sub> to MOD-1. We emphasize that these are highly homologous receptors. On the basis of the AChBP structure, we estimate that the two critical residues are about 9 Å apart. Thus, while much of the serotonin molecule might occupy the same position in the two receptors, a significant rearrangement of the alkylammonium unit must occur on going from one receptor to the other. Note also that binding is not all that is happening. In both systems,

serotonin induces a large conformational change in the receptor, gating the ion channel. This makes it all the more remarkable that two binding orientations are possible.

## 2.4 Switch of Tyr 180 and Trp 226 in MOD-1

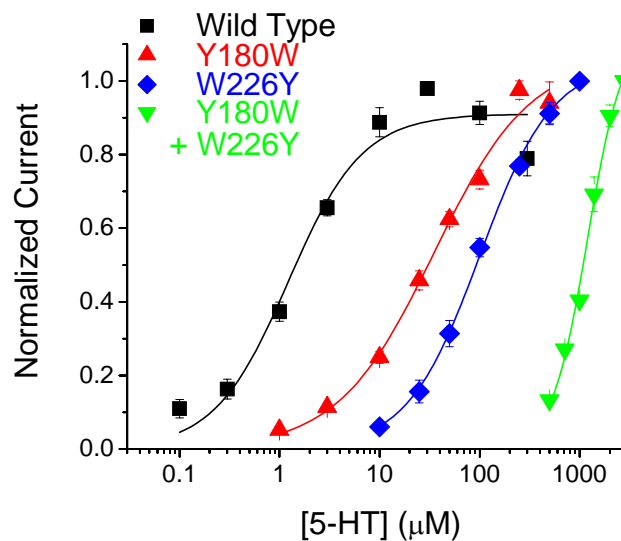


**Figure 2.8** Dose-response curves for the switch between Tyr 180 and Trp 226 of MOD-1.

Superficially, it appears that Nature has simply swapped the Trp/Tyr pair of the agonist binding site. That is, we have Trp...Tyr in the nAChR (149...198) and the 5-HT<sub>3</sub> receptor (183...234), but Tyr...Trp in MOD-1 (180...226). To test this notion, we prepared the MOD-1 double mutant Y180W/W226Y by conventional mutagenesis. The results are shown in Figure 2.8. EC<sub>50</sub> of the double mutant receptor (1200 μM) is 1000-fold higher than that of wild type (1.2 μM). Both single mutants Y180W (EC<sub>50</sub>, 35.1 μM) and

W226Y ( $EC_{50}$ , 101  $\mu$ M) are also substantially compromised. Similarly, the W183Y 5-HT<sub>3</sub>R single mutant shows a 90-fold increase in  $EC_{50}$ .<sup>26</sup>

Thus, the MOD-1 and 5-HT<sub>3</sub> receptors are precisely designed to bind serotonin, as would be expected. But the designs are different, and serotonin accommodates both. Another perspective on these data is that they provide testimony to the strength of the  $RNH_3^+ \cdots Trp$  cation- $\pi$  interaction. Even when a perfectly acceptable Tyr is positioned in the “classical” cation- $\pi$  site (the one used in nAChR and 5-HT<sub>3</sub>R), a Trp is preferable, and the ligand adjusts to reach it.

## 2.5 Discussion

The “lock and key” model for drug-receptor interactions has evolved over time. Certainly, proteins and small molecules are more flexible than their metaphorical counterparts, and some adaptation of one to the other is common. Nevertheless, the notion that proteins craft well-defined binding sites that are custom-tailored to their ligands remains central to analyses of biological recognition and drug discovery.

The notion of a ligand held in a precise location by specific contacts to the protein has served enzymology, and drug discovery around enzymes, well. However, perhaps for receptors, molecules for which ligand binding induces a structural change that launches a signaling process, such a structured model is not necessary. Perhaps all that is required is for the ligand to occupy the binding region, acting more like a wedge, to initiate the conformational change. Standard forces of molecular recognition are required to direct

the ligand to the binding site, but the precise details of the binding interaction are less critical. In the present case, a cation- $\pi$  interaction plays an important role in delivering serotonin to the binding site, but there is some flexibility as to the precise location of that interaction.

Two highly homologous serotonin receptors, namely, MOD-1 and 5-HT<sub>3</sub>R, make use of different cation- $\pi$  sites to bind the same agonist serotonin. While the full implications of these results for studies of drug-receptor interactions remain to be established, they immediately provide a caution for efforts to model binding sites based on sequence homology. It is entirely reasonable to assume that, since serotonin makes a cation- $\pi$  interaction with Trp 183 in 5-HT<sub>3</sub>R, it would also make a cation- $\pi$  interaction with Tyr 180 in MOD-1; any researcher would be comfortable with this modest substitution. However, our results show that instead of settling for the tyrosine, the agonist reorients in the binding site to contact a nearby tryptophan and thus maximize the cation- $\pi$  interaction.

## **2.6 Methods**

### **2.6.1 Electrophysiology**

Electrophysiological recordings were made 24–72 hours after injection. Whole-cell currents from stage VI oocytes of *Xenopus laevis* were measured in standard two-electrode voltage clamp mode.<sup>27</sup> Microelectrodes were filled with 3M KCl and the resistances were between 0.5 and 2 M $\Omega$ . Oocytes were continuously perfused with calcium-free ND96 bath solution. Serotonin was purchased from Sigma/Aldrich and all

drugs were prepared in calcium-free ND96 solution. Macroscopic serotonin-induced currents were recorded in response to bath application of the desired agonist concentration at a holding potential of -60 mV or -80 mV. Dose-response data were obtained from 3 to 5 oocytes and data were reported as mean  $\pm$  standard error. Curves were fit to the Hill equation,  $I/I_{\max} = 1/[1 + (EC_{50}/[A])^{n_H}]$ , where  $I$  is the current for agonist concentration  $[A]$ ,  $I_{\max}$  is the maximum current,  $EC_{50}$  is the concentration to elicit a half-maximum response, and  $n_H$  is the Hill coefficient.

## **2.6.2 Incorporation of Unnatural Amino Acids by *in vivo* Nonsense Suppression**

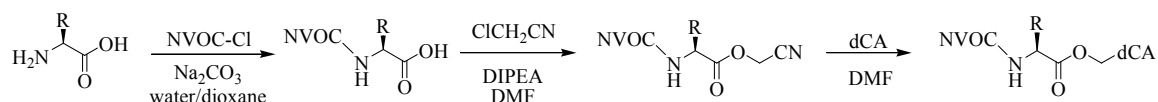
### **Methods**

For suppression experiments, 25 ng of tRNA and 10 ng of mRNA were co-injected in a total volume of 50 nL per oocyte. Immediately before the microinjection, the NVOC-aminoacyl-tRNA was deprotected by photolysis. The ligation of aminoacyl-dCA to tRNA and gene construction of suppressor tRNA have been described previously.<sup>28, 29</sup> The MOD-1 gene was subcloned into the plasmid pBlueScript. The MOD-1 TAG mutants were made by the Quickchange<sup>TM</sup> site-directed mutagenesis method and were monitored by DNA sequencing. Plasmid DNAs were linearized with *KpnI*, and mRNA was transcribed using the Ambion T3 mMESSAGE mMACHINE kit.

For wild type and conventional mutation experiments, only 5 ng mRNA was injected into oocytes in a 50 nL volume per cell. The remaining procedure was the same as above.

### 2.6.3 Synthesis of Aminoacyl dCA (dCA-AA)

dCA-NVOC-4-fluorophenylalanine and dCA-NVOC-3,4,5-trifluorophenylalanine were synthesized according to previous procedures, as demonstrated in Scheme 2.1.<sup>30</sup>



**Scheme 2.1** Synthetic scheme for aminoacylated dCA.

**NVOC-4-fluorophenylalanine (1a).** 100 mg (0.55 mmol) of 4-fluorophenylalanine and 87 mg (0.82 mmol, 1.5 eq) of sodium carbonate were dissolved in 12 ml of water and 10 ml of dioxane. A solution of 152 mg (0.55 mmol) of NVOC-Cl in 10 ml of dioxane was added dropwise. One hour later, the bright yellow reaction mixture was extracted with 3 × 25 ml of methylene chloride. The organic extracts were combined, dried over Na<sub>2</sub>SO<sub>4</sub>, filtered, and rotary-evaporated. The crude product was purified by flash chromatography using 1:1 ethyl acetate/petroleum ether to pure ethyl acetate to give a bright yellow solid (120 mg, 52%). <sup>1</sup>H NMR (300 MHz, d<sup>6</sup>-acetone) δ 7.69 (s, 1H), 7.35 (t, 2H), 7.13 (s, 1H), 7.05 (t, 2H), 6.90 (d, 1H), 5.42 (m, 2H), 4.49 (m, 1H), 3.93 (s, 3H), 3.89 (s, 3H), 3.24 (m, 1H), 3.03 (m, 1H), 1.96 & 2.05 (m, 0.5H).

**NVOC-3,4,5-trifluorophenylalanine (1b).** This compound was prepared by the procedure described above except using 3,4,5-fluorophenylalanine as the starting material. Yield: 60%. <sup>1</sup>H NMR (300 MHz, d<sup>6</sup>-acetone) δ 7.69 (s, 1H), 7.20 (m, 2H), 6.98 (d, 1H),

5.42 (m, 2H), 4.49 (m, 1H), 3.93 (s, 3H), 3.89 (s, 3H), 3.24 (m, 1H), 3.03 (m, 1H), 1.96 & 2.05 (m, 1H).

**NVOC-4-fluorophenylalanine cyanomethyl ester (2a).** 60 mg (0.14 mmol) of NVOC-4-fluorophenylalanine (*1a*) was dissolved in 5 ml of anhydrous DMF. DIPEA (30  $\mu$ l, 0.17 mmol, 1.2 eq) and chloroacetonitrile (210  $\mu$ l, 3.27 mmol, 23 eq) were added slowly. The reaction was stirred under argon at room temperature overnight. After 14 hours, the reaction was quenched by adding 10 ml of 0.1 M  $\text{KH}_2\text{PO}_4$  and 20 ml of water and then extracted with 3  $\times$  40 ml of ethyl acetate. The combined organic layers were washed with 50 ml of water, dried over  $\text{Na}_2\text{SO}_4$ , and rotary-evaporated. Flash chromatography purification (1:3 to 1:2 to 2:1 ethyl acetate/petroleum ether) gave 40 mg (62%) of product.  $^1\text{H}$  NMR (300 MHz,  $\text{CD}_2\text{Cl}_2$ )  $\delta$  7.70 (s, 1H), 7.21 (m, 2H), 7.06 (m, 2H), 6.99 (s, 1H), 5.48 (m, 4H), 4.73 & 4.80 (m, 3H), 3.92 (d, 6H), 3.18 (m, 2H), 2.93 (s, 0.5H), 2.84 (s, 0.5H).

**NVOC-3,4,5-trifluorophenylalanine cyanomethyl ester (2b).** Prepared as above except using *1b* as the starting material. Yield: 90%.  $^1\text{H}$  NMR (300 MHz,  $\text{CD}_2\text{Cl}_2$ )  $\delta$  7.70 (s, 1H), 7.05 (s, 1H), 6.90 (t, 2H), 5.80 (d, 1H), 5.45 (m, 2H), 4.65 & 4.80 (m, 3H), 3.92 (d, 6H), 3.18 (m, 2H), 2.93 (s, 2H), 2.84 (s, 2H).

**dCA-NVOC-4-fluorophenylalanine (3a).** NVOC-4-fluorophenylalanine-cyanomethyl ester (*2a*, 10 mg, 0.021 mmol) was mixed with the tetra-*n*-butyl-ammonium salt of the dCA dinucleotide (10 mg, 0.007 mmol) in 400  $\mu$ l of anhydrous DMF. The

reaction was stirred under argon at room temperature. After 1 hour TBA acetate (12 mg, 0.04 mmol) was added to continue the reaction for another 2 hours. The crude product was separated using reverse-phase semi-preparative HPLC with a gradient from 25 mM ammonium acetate (pH 4.5) to CH<sub>3</sub>CN. The desired fractions containing the aminoacyl dinucleotide were combined, frozen, and lyophilized. Ammonium ions were removed by redissolving the product in 10 mM aqueous acetic acid/acetonitrile, followed by lyophilization. The product (3.9 mg, 20%) was quantified by UV/Vis spectra and characterized by mass spectrometry. ESI-MS: found [M-H]<sup>-</sup>: 1039.4, calculated for C<sub>38</sub>H<sub>43</sub>N<sub>10</sub>O<sub>20</sub>P<sub>2</sub>F 1040.4.

**dCA-NVOC-3,4,5-trifluorophenylalanine (3b).** Prepared as above except using *2b* as the starting material. Yield: 23%. ESI-MS: found [M-H]<sup>-</sup>: 1075.4, calculated for C<sub>38</sub>H<sub>41</sub>N<sub>10</sub>O<sub>20</sub>P<sub>2</sub>F<sub>3</sub> 1076.4.

## 2.7 References

1. Zacharias, N.; Dougherty, D. A., Cation- $\pi$  interactions in ligand recognition and catalysis. *Trends Pharmacol. Sci.* **2002**, 23, 281–287.
2. Ma, J. C.; Dougherty, D. A., The cation- $\pi$  interaction. *Chem. Rev.* **1997**, 97, 1303–1324.
3. Dougherty, D. A., Cation- $\pi$  interactions in chemistry and biology: A new view of benzene, Phe, Tyr, and Trp. *Science* **1996**, 271, 163-168.
4. Zhong, W. G.; Gallivan, J. P.; Zhang, Y. O.; Li, L. T.; Lester, H. A.; Dougherty, D. A., From *ab initio* quantum mechanics to molecular neurobiology: A cation- $\pi$  binding site in the nicotinic receptor. *Proc. Natl. Acad. Sci. U. S. A.* **1998**, 95, 12088–12093.
5. Brejc, K.; van Dijk, W. J.; Klaassen, R. V.; Schuurmans, M.; van der Oost, J.; Smit, A. B.; Sixma, T. K., Crystal structure of an ACh-binding protein reveals the ligand-binding domain of nicotinic receptors. *Nature* **2001**, 411, 269–276.

6. Beene, D. L.; Brandt, G. S.; Zhong, W. G.; Zacharias, N. M.; Lester, H. A.; Dougherty, D. A., Cation- $\pi$  interactions in ligand recognition by serotonergic (5-HT<sub>3A</sub>) and nicotinic acetylcholine receptors: The anomalous binding properties of nicotine. *Biochemistry* **2002**, 41, 10262–10269.
7. Gallivan, J. P.; Dougherty, D. A., Cation- $\pi$  interactions in structural biology. *Proc. Natl. Acad. Sci. U. S. A.* **1999**, 96, 9459–9464.
8. Scrutton, N. S.; Raine, A. R. C., Cation- $\pi$  bonding and amino-aromatic interactions in the biomolecular recognition of substituted ammonium ligands. *Biochem. J.* **1996**, 319, 1–8.
9. Mecozzi, S.; West, A. P.; Dougherty, D. A., Cation- $\pi$  interactions in simple aromatics: Electrostatics provide a predictive tool. *J. Am. Chem. Soc.* **1996**, 118, 2307–2308.
10. Ruan, C. H.; Rodgers, M. T., Cation- $\pi$  interactions: Structures and energetics of complexation of Na<sup>+</sup> and K<sup>+</sup> with the aromatic amino acids, phenylalanine, tyrosine, and tryptophan. *J. Am. Chem. Soc.* **2004**, 126, 14600–14610.
11. Zhu, W. L.; Tan, X. J.; Shen, J. H.; Luo, X. M.; Cheng, F.; Mok, P. C.; Ji, R. Y.; Chen, K. X.; Jiang, H. L., Differentiation of cation- $\pi$  bonding from cation- $\pi$  intermolecular interactions: A quantum chemistry study using density-functional theory and Morokuma decomposition methods. *J. Phys. Chem. A* **2003**, 107, 2296–2303.
12. Cheng, Y. H.; Liu, L.; Fu, Y.; Chen, R.; Li, X. S.; Guo, Q. X., Counterion effects on the cation- $\pi$  interaction between alkaline earth cations and benzene. *J. Phys. Chem. A* **2002**, 106, 11215–11220.
13. Tsuzuki, S.; Yoshida, M.; Uchamaru, T.; Mikami, M., The origin of the cation/ $\pi$  interaction: The significant importance of the induction in Li<sup>+</sup> and Na<sup>+</sup> complexes. *J. Phys. Chem. A* **2001**, 105, 769–773.
14. Felder, C.; Jiang, H. L.; Zhu, W. L.; Chen, K. X.; Silman, I.; Botti, S. A.; Sussman, J. L., Quantum/classical mechanical comparison of cation- $\pi$  interactions between tetramethylammonium and benzene. *J. Phys. Chem. A* **2001**, 105, 1326–1333.
15. Gapeev, A.; Yang, C. N.; Klippenstein, S. J.; Dunbar, R. C., Binding energies of gas-phase metal ions with pyrrole: Experimental and quantum chemical results. *J. Phys. Chem. A* **2000**, 104, 3246–3256.
16. Dunbar, R. C., Complexation of Na<sup>+</sup> and K<sup>+</sup> to aromatic amino acids: A density functional computational study of cation- $\pi$  interactions. *J. Phys. Chem. A* **2000**, 104, 8067–8074.
17. Xu, Y. C.; Shen, J. H.; Zhu, W. L.; Luo, X. M.; Chen, K. X.; Jiang, H. L., Influence of the water molecule on cation- $\pi$  interaction: *Ab initio* second order Moller-Plesset perturbation theory (MP2) calculations. *J. Phys. Chem. B* **2005**, 109, 5945–5949.

18. Hunter, C. A.; Low, C. M. R.; Rotger, C.; Vinter, J. G.; Zonta, C., The role of the counteranion in the cation- $\pi$  interaction. *Chem. Commun.* **2003**, 834–835.
19. Gapeev, A.; Dunbar, R. C., Binding of alkaline earth halide ions  $MX^+$  to benzene and mesitylene. *J. Phys. Chem. A* **2000**, 104, 4084–4088.
20. Gallivan, J. P.; Dougherty, D. A., A computational study of cation- $\pi$  interactions vs. salt bridges in aqueous media: Implications for protein engineering. *J. Am. Chem. Soc.* **2000**, 122, 870–874.
21. Mecozzi, S.; West, A. P.; Dougherty, D. A., Cation- $\pi$  interactions in aromatics of biological and medicinal interest: Electrostatic potential surfaces as a useful qualitative guide. *Proc. Natl. Acad. Sci. U. S. A.* **1996**, 93, 10566–10571.
22. Ranganathan, R.; Cannon, S. C.; Horvitz, H. R., MOD-1 is a serotonin-gated chloride channel that modulates locomotory behaviour in *C. elegans*. *Nature* **2000**, 408, 470–475.
23. Maricq, A. V.; Peterson, A. S.; Brake, A. J.; Myers, R. M.; Julius, D., Primary structure and functional expression of the 5-HT<sub>3</sub> receptor, a serotonin-gated ion channel. *Science* **1991**, 254, 432–437.
24. Lester, H. A.; Dibas, M. I.; Dahan, D. S.; Leite, J. F.; Dougherty, D. A., Cys-loop receptors: New twists and turns. *Trends Neurosci.* **2004**, 27, 329–336.
25. Mu, T. W.; Lester, H. A.; Dougherty, D. A., Different binding orientations for the same agonist at homologous receptors: A lock and key or a simple wedge? *J. Am. Chem. Soc.* **2003**, 125, 6850–6851.
26. Spier, A. D.; Lummis, S. C. R., The role of tryptophan residues in the 5-hydroxytryptamines receptor ligand binding domain. *J. Biol. Chem.* **2000**, 275, 5620–5625.
27. Quick, M. W.; Lester, H. A., Methods for expression of excitability proteins in *Xenopus* oocytes. *Methods in Neurosciences* **1994**, 19, 261–279.
28. Nowak, M. W.; Gallivan, J. P.; Silverman, S. K.; Labarca, C. G.; Dougherty, D. A.; Lester, H. A., *In vivo* incorporation of unnatural amino acids into ion channels in *Xenopus* oocyte expression system. *Method Enzymol.* **1998**, 293, 504–529.
29. Saks, M. E.; Sampson, J. R.; Nowak, M. W.; Kearney, P. C.; Du, F. Y.; Abelson, J. N.; Lester, H. A.; Dougherty, D. A., An engineered *Tetrahymena* tRNA(Gln) for *in vivo* incorporation of unnatural amino acids into proteins by nonsense suppression. *J. Biol. Chem.* **1996**, 271, 23169–23175.
30. Kearney, P. C.; Nowak, M. W.; Zhong, W.; Silverman, S. K.; Lester, H. A.; Dougherty, D. A., Agonist binding site of the nicotinic acetylcholine receptor: Tests with novel side chains and with several agonists. *Mol. Pharmacol.* **1996**, 50, 1401–1412.

## **Chapter 3**

### **Prediction of the Ligand-Binding Site of MOD-1: Implications for the Hydrogen Bonding Pattern of Serotonin**

### 3.1 Introduction

In Chapter 2, using the unnatural amino acid mutagenesis methodology, we showed that the primary ammonium group of serotonin forms a cation- $\pi$  interaction with Trp 226 of MOD-1 (Figure 2.6).<sup>1</sup> Here, we continue our efforts to obtain more details on the ligand-binding site.

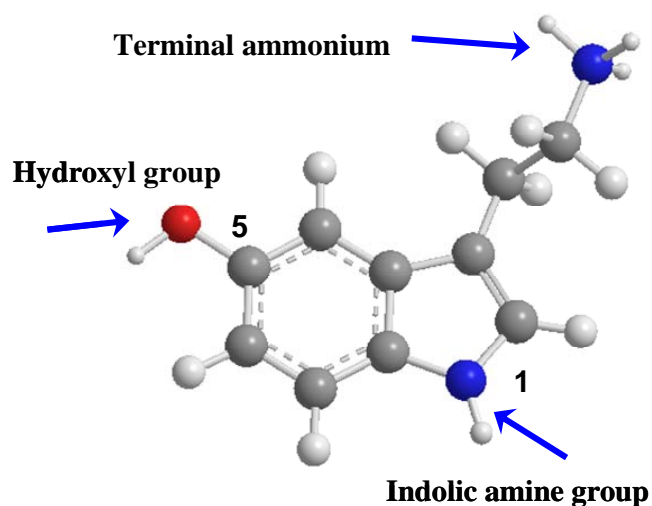


**Figure 3.1** Potential hydrogen bonding positions of serotonin in the MOD-1 receptor. As indicated by the arrows, the terminal ammonium, indolic amine group, hydroxyl group can potentially form hydrogen bonds with the receptors.

Upon binding, the agonist serotonin can potentially form hydrogen bonds with the MOD-1 receptor at three positions. As shown in Figure 3.1, the terminal primary ammonium cation and the indolic amine group can act as hydrogen bond donors; the hydroxyl group can act as both a hydrogen donor and an acceptor. If we can identify the hydrogen bonding pattern of serotonin inside the binding pocket, the entire orientation of

the ligand will be fixed at the chemical level, and non-covalent interactions responsible for binding will be elucidated. Ultimately, we will obtain high-resolution information on the binding pocket with the ligand bound.

However, this task is challenging. We do not have crystal structures of MOD-1. Most of our knowledge on the ligand-binding site of the Cys-loop superfamily comes from nAChR.<sup>2</sup> The ligand binding site lies in the large N-terminal extracellular domain between two subunits of the receptor. Photoaffinity labeling, radioligand binding, and mutational studies have been used to establish that several loops (loop A to loop F), which are different regions of sequence, define the ligand-binding sites (Figure 1.8). Currently, for MOD-1, we only know that a cation- $\pi$  interaction exists between the primary ammonium of serotonin and Trp 226 of MOD-1. Sequence alignments of MOD-1 with nAChR indicate that residues from loop A to loop F in MOD-1 are important in binding the ligand. Both the main chains and side chains of many residues are the hydrogen bond candidates; in addition, there are three possible hydrogen bonding positions in serotonin. The hydrogen bond pattern of serotonin inside the binding pocket can have a large amount of variations. Therefore, it is difficult to establish this hydrogen bonding pattern without further guidance.

Fortunately, our anxiety over this challenging task is relieved by the determination of the crystal structure of the acetylcholine binding protein (AChBP) and the development of computational modeling methods.

Recently, Sixma and co-workers reported the crystal structure of acetylcholine binding protein (AChBP), which is homologous to the extracellular domain of the Cys-loop superfamily.<sup>3</sup> AChBP shares about 20% sequence identity with the Cys-loop

superfamily and has the key loops (loop A to loop F), which are important in binding the ligand. AChBP is an excellent template to perform the homology modeling study on the Cys-loop superfamily.

Therefore, we can obtain a homology model of a receptor using AChBP as the template. In order to obtain the orientation of the ligand, we need to further dock the ligand into the binding site of the receptor. Some homology modeling tools such as MODELLER, and docking programs such as DOCK have been developed, and their applications in structure-based ligand and drug design have been reviewed.<sup>4</sup>

Many modeling studies on the Cys-loop superfamily have appeared since the arrival of the AChBP crystal structure. The structures of nAChR with agonists such as acetylcholine, nicotine, or epibatidine, in the binding site were modeled.<sup>5, 6</sup> Using molecular dynamics simulations, the Sine group showed that the curariform antagonists adopted different orientations in both AChBP and nAChR, which was further confirmed by corresponding experiments.<sup>7-9</sup> More recently, the Sine group revealed that upon agonist binding in AChBP, loop C moved inward to occlude the entrance of the binding site.<sup>10</sup> The ligand orientations in the binding pockets have also been predicted in the GABA<sub>A</sub> and 5-HT<sub>3</sub> receptors.<sup>11-13</sup>

In this chapter, HierDock was used to dock serotonin and several other agonists into the extracellular domain of MOD-1, which was built from the AChBP template. The cation- $\pi$  interaction between the primary ammonium cation of serotonin and Trp 226 was demonstrated. Most impressively, a hydrogen bonding pattern of serotonin in the binding pocket was suggested. Side chains of Asn 223 and Gln 228, and the main chain carbonyl group of Tyr 180 form hydrogen bonds with the hydroxyl group, indolic amine group,

and the terminal ammonium of serotonin, respectively. This detailed binding pattern will give us directions for further experiments.

## **3.2 Methods**

### **3.2.1 Sequence Alignment**

The extracellular domains of MOD-1 and 5-HT<sub>3</sub>R were aligned with AChBP (pdb id: 1I9B) using the program CLUSTALW.<sup>14</sup> Some manual adjustments were made according to the knowledge of the binding sites.

### **3.2.2 3-D Model Building**

The program MODELLER (Version 6) was used to perform homology modeling of MOD-1 using AChBP as the template.<sup>15</sup> Each subunit was built separately. The coordinates of the five subunits were then assembled to generate the whole homopentamer of MOD-1.

Hydrogens were added using Biograf. Protein was described by CHARMM22 charges,<sup>16</sup> and counterions (Na<sup>+</sup> and Cl<sup>-</sup>) were added to balance charged residues. The solvation effect was simulated by the surface-generalized Born (SGB) implicit solvation model.<sup>17</sup> The whole protein was then minimized using MPSim<sup>18</sup> with the Dreiding force field.<sup>19</sup> Since the sequence identity between MOD-1 and AChBP is about 16% and the sequence similarity is about 60%, the quality of the minimized MOD-1 protein was evaluated by the Protein Health Utility implemented in QUANTA.

### 3.2.3 Agonist Docking by HierDock

HierDock is a recently developed docking algorithm.<sup>20-22</sup> It has been successfully applied to predict the binding sites of GPCRs and aminoacyl-tRNA synthetases.<sup>21, 23</sup> The HierDock protocol is based on DOCK 4.0.<sup>24</sup>

The charges of all the agonists were taken from quantum chemical calculations at the B3LYP/6-31G\*\* level after full optimization using Jaguar 4.0. Although the protein is a homopentamer, only one agonist was chosen to be docked into one of the ligand-binding sites.

First, we needed to define the binding pocket for the agonist. We know that the ligand-binding site lies between two subunit interfaces. Previous study on MOD-1 shows that a cation- $\pi$  interaction exists between the terminal primary ammonium of serotonin and Trp 226. Therefore, serotonin was manually docked to the subunit interfaces with the primary amine N atom in serotonin sandwiched between Tyr 180 and Trp 226 of one subunit. In order to probe the agonist conformation space more thoroughly inside the binding site, we generated twelve starting orientations of the agonist. The hydroxyl group and indole N atom in serotonin were rotated inside the binding pocket to obtain twelve different initial orientations, which sampled the steric-permitted spaces nearby.

For each initial orientation, the corresponding binding site was defined as the cube occupied by the ligand plus a 5 Å margin in each dimension. An energy grid was then generated for the binding region plus a 10 Å margin for each dimension. Therefore, altogether twelve binding regions were defined for further docking.

For each binding region, the Monte Carlo method was used to generate 5000 ligand conformations to match the void regions. The ligand conformation was minimized

and binding energy was calculated. According to the energy scoring function, the top 50 conformations were chosen for further evaluation. MPSim was used to minimize the top 50 conformations in the presence of the receptor. The top five conformations were chosen to run another cycle of minimization including the AVGB solvation model. The one with the lowest energy was chosen as the docking result.

The binding energy (BE) was defined as the following:

$$\text{BE} = \text{Energy (complex)} - \text{Energy (free protein)} - \text{Energy (free ligand)}$$

where the energy included the solvation effect.

Therefore, for twelve initial binding regions, we obtained twelve docking results of serotonin. Comparison of the binding energies as well as the overall orientations of serotonin inside the binding pocket gave us the preferred docking conformation of serotonin for further refinement.

For other agonists, only one initial docking region was used according to that of serotonin, which yielded the final preferred docking conformation. Then the above HierDock procedure was used to obtain the preferred docking conformation for the corresponding agonists. The binding energies from the preferred docking conformations were used to compare with the binding affinities of the agonists.

### **3.2.4 Side Chain Optimization by SCREAM**

Using the preferred binding conformation of serotonin, the side chains for all the residues within 5 Å of the bound serotonin were optimized using the SCREAM side chain optimization program. The rotamer library of amino acids was used to mutate the side chains of those residues. After brief minimizations, the new structure with lowest energy

was taken for further analysis. This step would give more flexibility to the binding pockets thus optimizing the intermolecular interactions, e.g., the hydrogen bonds.

### 3.2.5 Serotonin Re-docking by HierDock

The new structure obtained from SCREAM was applied to the HierDock procedure again for relaxation.

After this re-docking step, we obtained our final docking orientation of serotonin inside this binding site.

## 3.3 Results

```

AChBP FDRADILYNIHQTSRDPDVIPTQRD-R-PVAVSVSLKFINILEVNEITNEVDVVF-WQQTWSDRTLAWNSSHSP-
MOD-1 WSEGKI-MNTIMSNTKMLPDAED-S--VQVNIIEIHVQDMGSLNEISSDFEIDILFTQL-WHDSALSFAPLPAAC-
5-HT3 PALLRLSDHLLANYKKGVRP-VRDWRKPTTVSIVDIVIMYAILNVDEKNQVLTYYI-WYRQYWTDEFQWTFEDFDN
                                         Loop D

AChBP -DQ----VSVPISSLWVPDLAAINAISKPEVLTP---QLARVVSVDGEVLYMPSIRQRFSCDVSGVDTEG-AT-C
MOD-1 -KRNITMETRLLPKIWSPNTCMINSKRRTVHASPSENVMVILYENGTVWINHRLSVKSPCNLDLRQFPFDTQT-C
5-HT3 VTK----LSIPTDSIWVPDILINEFVDVGKSPNI---PYVYVHHRGEVQNYKPLQLVTACSLDIYNFPFD-VQNC
                                         Loop A                               Loop E

AChBP RIKIGSWTHHSREISVDPT---TENSDDSEYFYSQYSRFEILDVTQKKNVTVSCCP-EAEDVEVSLNFRKKG
MOD-1 ILIFESYSHNSEEVELH-W---MEEAVTLMKPIQLPDFDMVHYSTKKEITLLYPNG---YDQLQVTFKRRY
5-HT3 SLTFTSNLHTIQDINITLWRSPEEVRSDKSFIFINQGEWELLEVPQFKE--FSIDISNSAEMKFYVIIRRRP
                                         Loop B                               Loop F                               Loop C

```

**Figure 3.2** Sequence alignment of the amino-terminal domain of MOD-1 (*C. elegans*), 5-HT<sub>3A</sub>R (mouse), and AChBP (snail). The characteristic Cys-loop was colored yellow; the key loops responsible for ligand-binding were also noted; the key aromatic residues were colored red.

### 3.3.1 Model of MOD-1

The sequence alignment of the amino-terminal domain of MOD-1, 5-HT<sub>3A</sub>R, and AChBP is shown in Figure 3.2. The key binding loops (loop A to loop F) are labeled. The model of MOD-1 after minimization is shown in Figure 3.3.

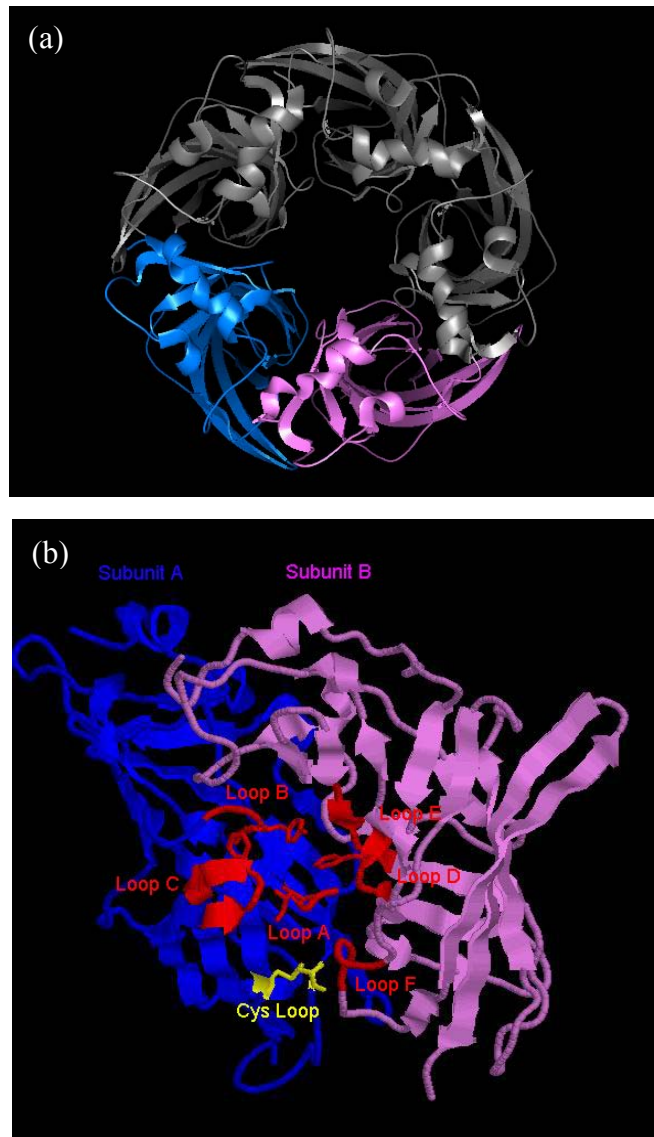


**Figure 3.3** Model of MOD-1 after minimization. Subunit A is colored blue and subunit B violet. (a) Top view of the homopentamer from the synaptic cleft. (b) Side view. Loop A to loop F are colored red. Figures were generated using Pymol (a) and Rasmol (b).

The secondary structures of AChBP are well-conserved in the model of MOD-1: Each subunit starts with a  $\alpha$ -helix and continues with the core  $\beta$  strands. The Cys-loop is positioned between  $\beta_6$  and  $\beta_7$  strands. The binding site of serotonin lies between the subunits interface. As in Figure 3.3, the residues in loops A, B, C from subunit A consist

of the primary binding pocket of serotonin, while the residues in loops D, E, F from subunit B define the complementary part.

### 3.3.2 The Binding Pocket of Serotonin in MOD-1

**Table 3.1** Docking results of serotonin in MOD-1 from the twelve initial binding orientations (DB stands for defined binding orientation).

	Binding energy (kcal/mol)	Hydrogen bond partner of the hydroxyl group in serotonin
DB1	-155.85	Asn223
DB2	-152.66	–
DB3	-161.76	–
DB4	-170.54	Asn223
DB5	-162.14	–
DB6	-162.32	–
DB7	-158.88	–
DB8	-152.00	–
DB9	-162.10	–
DB10	-159.52	–
DB11	-154.79	–
DB12	-164.16	–

The docking results from the twelve initial orientations of serotonin in MOD-1 are summarized in Table 3.1. For all the above twelve docking results, there is no hydrogen bond between the receptor and the indole N atom of serotonin. In two cases, namely, the results from DB1 and DB4, a hydrogen bond forms between the hydroxyl group of

serotonin and Asn 223 of MOD-1. Especially, the docking result from DB4 has the lowest energy among all the twelve and shows that the primary amine N atom of serotonin lies right above the center of the six-membered ring of Trp 226. Therefore, we used the preferred docking result from DB4 for further refinement.

After side chain optimization by SCREAM and re-docking, we obtained the final docking conformation of serotonin in the binding pocket (Figure 3.4). Serotonin is represented using a space-filling model, lying between two subunit interfaces (Figure 3.4 (a)). All the MOD-1 residues within 5 Å of serotonin are summarized in Table 3.2. Impressively, the binding pocket of serotonin including the hydrogen bonding pattern is very informative after this refinement step.

**Table 3.2** MOD-1 residues around 5 Å of serotonin.

Residues	Loops
F83	Loop D (-) <sup>b</sup>
I122	Loop A (+) <sup>a</sup>
I140	Loop E (-)
I176, E178, S179, Y180, S181, H182	Loop B (+)
L219, Y221, N223, W226, D227, Q228	Loop C (+)

<sup>a</sup> “+” means the primary binding pocket on subunit A. <sup>b</sup> (-) means the complementary binding pocket on subunit B.

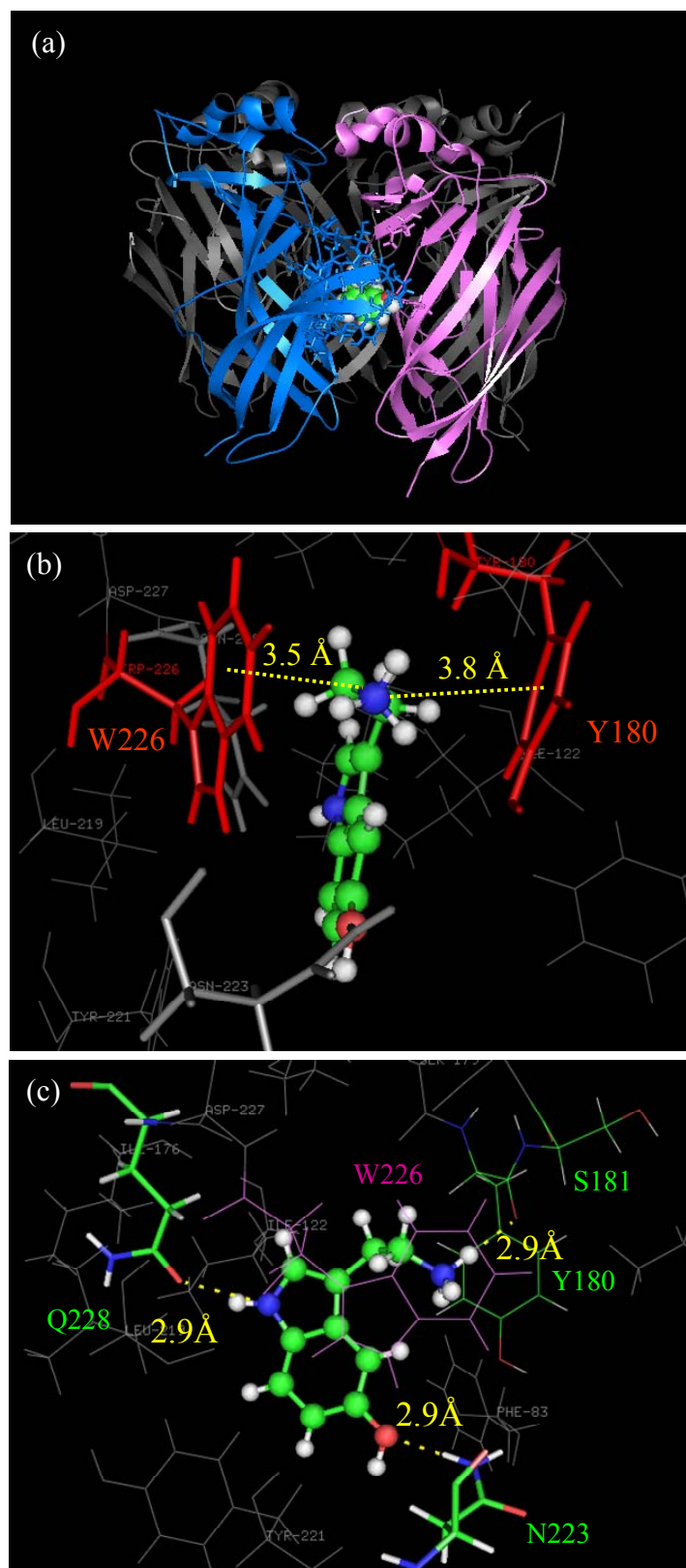


**Figure 3.4** Docking result of serotonin in MOD-1. (a) Overall side view. (b) Cation- $\pi$  interaction pattern. (c) Hydrogen bonding pattern. Figures were generated using Pymol.

From Table 3.2, we can see that at least one residue from loop A to loop E contributes to the binding site. This docking orientation also confirms that loops A, B, and C define the primary binding pocket and that loop D and E form the complementary part. It seems that loop B and loop C are the most important in binding the ligand since more residues from these two loops are around serotonin.

Ile 122 in loop A, the homolog of Tyr 93 in nAChR (Figure 1.8), is above the five-membered ring of serotonin. The shortest distance between Ile 122 and serotonin is only 2.80 Å. Phe 83 in loop D, the homolog of Trp 55 in nAChR (Figure 1.8), is above the six-membered ring of serotonin. The nearest distance between Phe 83 and serotonin is 4.03 Å. The benzene ring of Phe 83 can have a T-shape aromatic interaction with the six-membered ring of serotonin.

The cation- $\pi$  interaction pattern of serotonin is shown in Figure 3.4 (b). The primary amine of serotonin is sandwiched between the aromatic rings of Trp 226 in loop C and Tyr 180 in loop B. The distance between the primary amine N atom of serotonin and the center of the six-membered ring of Trp 226 is 3.5 Å, while the distance between the N atom and the center of the six-membered ring of Tyr 180 is 3.8 Å. However, the primary amine of serotonin lies only well above the center of the six-membered ring of Trp 226. Therefore, the cation- $\pi$  interaction of Trp 226 is much stronger than that of Tyr 180. This cation- $\pi$  interaction acts as an important driving force to direct the primary amine of serotonin into the corresponding position inside the binding pocket.

The hydrogen bonding pattern of serotonin is shown in Figure 3.4 (c). First, the side chain amide carbonyl group of Gln 228 forms a hydrogen bond with the indolic amine group of serotonin. The heavy atom distance is 2.9 Å. Second, the side chain

amide group of Asn 223 hydrogen bonds with the hydroxyl group of serotonin. In our model, one N-H in the amide group of Asn 223 is the hydrogen bond donor and the oxygen atom in the hydroxyl group of serotonin is the acceptor. The heavy atom distance is 2.9 Å. Third, the main chain carbonyl group of Tyr 180 forms a hydrogen bond with the primary ammonium cation of serotonin. The distance between the carbonyl oxygen atom and the amine nitrogen atom is 2.9 Å.

The hydrogen bonding pattern and aromatic interactions between the agonist serotonin and the receptor are well-illustrated by the docking result. This high-resolution image of the binding pocket provides us an excellent direction for our future experiments.

### **3.3.3 Docking of Other Agonists**

Some other agonists were also docked into MOD-1 using the DB4 binding region. The structures of the agonists are shown in Figure 3.5. N-methyl-serotonin and  $\alpha$ -methyl-serotonin are serotonin derivatives, methylated at different sites, which will provide some steric perturbation around the primary amine of serotonin. Tryptamine will explore the importance of the hydroxyl group in serotonin. Although these agonists adopt slightly different orientations inside the binding pocket compared to serotonin, the overall binding pockets remain very similar.

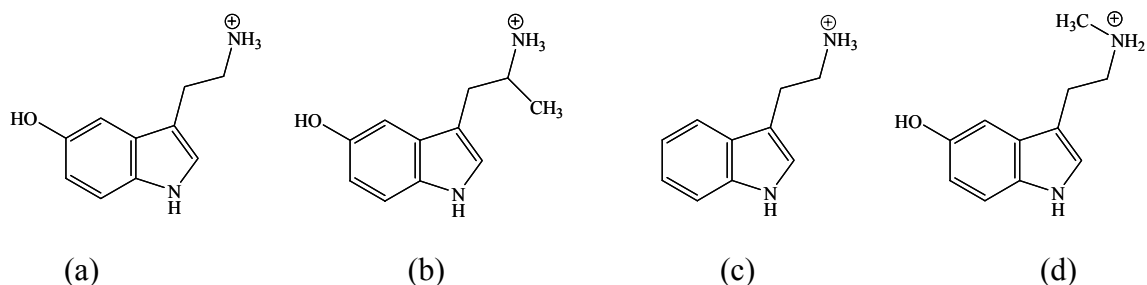


**Figure 3.5** The structures of agonists docked into MOD-1. (a) Serotonin. (b)  $\alpha$ -methyl-serotonin. (c) Tryptamine. (d) N-methyl-serotonin.

The binding energies of the agonists are summarized in Table 3.3. The  $EC_{50}$  values of the agonists from the experiments are also shown. Each agonist will open the channel and elicit some current.  $EC_{50}$  is the concentration at which the agonist will induce half the maximal current.  $EC_{50}$  represents the potency of one agonist.

**Table 3.3** Binding Energy and  $EC_{50}$  of different agonists of MOD-1.

	Binding Energy (kcal/mol)	$EC_{50}$ ( $\mu$ M)
Serotonin	-170.54	$1.2 \pm 0.3$
$\alpha$ -methyl-serotonin	-163.34	$2.8 \pm 0.6$
tryptamine	-158.13	$26 \pm 3$
N-methyl-serotonin	-152.80	$37 \pm 4$

The smaller the binding energy, the more potent the agonist (Table 3.3). From the binding energies of different agonists we can postulate their relative potency. Thus we can have the order of potency: serotonin >  $\alpha$ -methyl-serotonin > tryptamine > N-methyl-serotonin. The more potent the agonist, the smaller the  $EC_{50}$  value. Therefore, a smaller

binding energy corresponds to a smaller  $EC_{50}$  value for an agonist. This is the case when we compare the computed binding energy to the experimentally measured  $EC_{50}$  values of these agonists.

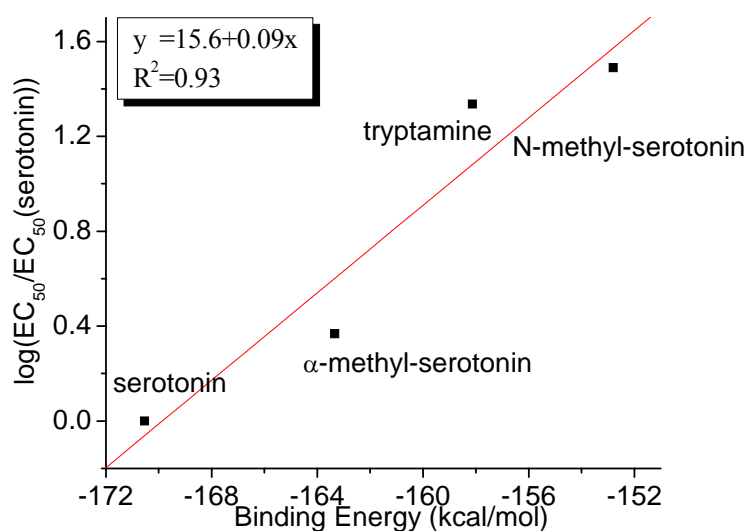


**Figure 3.6** Linear correlation between binding energy and  $\log EC_{50}$  of different agonists of MOD-1.

The  $\log EC_{50}$  value is related to the energy scale. We can plot  $\log(EC_{50}(\text{agonist})/EC_{50}(\text{serotonin}))$  versus the binding energy calculated from the docking. As in Figure 3.6, this yields a nice linear correlation. Therefore, it is possible to use the calculated binding energy to postulate the potency of an unknown agonist, which will benefit structure-based drug design.

It needs to be pointed out that during the binding energy calculation the empirical force field was applied to the whole complicated ligand-protein complex, which possibly

will not fully reflect the behavior of the ligand-binding pocket. If we can describe the ligand-binding pocket with the quantum mechanics (QM) method and other protein portions with the molecular mechanics (MM) method, more accurate binding energies will be obtained, and thus, the relative potency of agonists can be predicted with more confidence. This hybrid method is called QM/MM method and has been applied in other biological systems.<sup>25</sup> The implementation of the QM/MM method into the complicated ligand-receptor recognition system will help us better understand this process.

### **3.4 Conclusions and Discussion**

Serotonin was docked into the ligand-binding pocket of MOD-1 built from the AChBP template. The main purpose of this docking study was to find the hydrogen bonding pattern of serotonin in MOD-1. Most impressively, after the refinement step, a vivid hydrogen bonding pattern was obtained (Figure 3.4).

From the model, the main chain carbonyl group of Tyr 180 can hydrogen bond with the primary amine of serotonin. The incorporation of an  $\alpha$ -hydroxy acid at Ser 181 will introduce the amide-to-ester backbone mutation. The hydrogen bond acceptor ability of the main chain carbonyl group of Tyr 180 will then decrease. This subtle change can be used to prove that hydrogen bond. Hydrogen bonds exist between Asn 223 / Gln 228 and serotonin in the model. We can perturb the receptor as well as the agonist with proper

designs. This forward and reverse pharmacology strategy will be applied to confirm the corresponding hydrogen bonds.

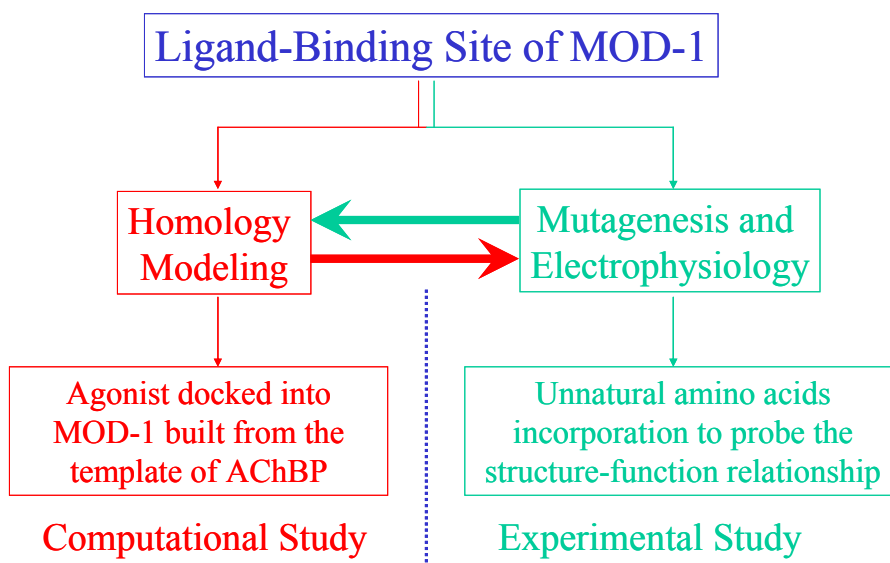


**Figure 3.7** Combination of computation and experiment to study the ligand-binding site of the MOD-1 receptor.

To study the ligand-binding site of MOD-1, we performed some experiments as described in Chapter 2. We mutated the structure using the powerful unnatural amino acid mutagenesis method, monitored the function by electrophysiological recording, and gained some knowledge about the binding site. In order to obtain more detailed information on the binding pocket, in this chapter, based on our current knowledge from experiment, we continued to build a homology model of MOD-1, and docked the agonist into this homology model. We gained a detailed image of the agonist in the binding site. The next step is to prove this model by experiments, which will be discussed in Chapter 4.

Therefore, when used in conjunction with one another, experimental chemistry and computational chemistry complement one another (Figure 3.7).

### 3.5 References

1. Mu, T. W.; Lester, H. A.; Dougherty, D. A., Different binding orientations for the same agonist at homologous receptors: A lock and key or a simple wedge? *J. Am. Chem. Soc.* **2003**, 125, 6850–6851.
2. Lester, H. A.; Dibas, M. I.; Dahan, D. S.; Leite, J. F.; Dougherty, D. A., Cys-loop receptors: New twists and turns. *Trends Neurosci.* **2004**, 27, 329–336.
3. Brejc, K.; van Dijk, W. J.; Klaassen, R. V.; Schuurmans, M.; van der Oost, J.; Smit, A. B.; Sixma, T. K., Crystal structure of an ACh-binding protein reveals the ligand-binding domain of nicotinic receptors. *Nature* **2001**, 411, 269–276.
4. Davis, A. M.; Teague, S. J.; Kleywegt, G. J., Application and limitations of X-ray crystallographic data in structure-based ligand and drug design. *Angew. Chem.-Int. Edit.* **2003**, 42, 2718–2736.
5. Le Novere, N.; Grutter, T.; Changeux, J. P., Models of the extracellular domain of the nicotinic receptors and of agonist- and Ca<sup>2+</sup>-binding sites. *Proc. Natl. Acad. Sci. U. S. A.* **2002**, 99, 3210–3215.
6. Schapira, M.; Abagyan, R.; Totrov, M., Structural model of nicotinic acetylcholine receptor isotypes bound to acetylcholine and nicotine. *BMC Struct. Biol.* **2002**, 2.
7. Sine, S. M.; Wang, H. L.; Gao, F., Toward atomic-scale understanding of ligand recognition in the muscle nicotinic receptor. *Curr. Med. Chem.* **2004**, 11, 559–567.
8. Wang, H. L.; Gao, F.; Bren, N.; Sine, S. M., Curariform antagonists bind in different orientations to the nicotinic receptor ligand binding domain. *J. Biol. Chem.* **2003**, 278, 32284–32291.
9. Gao, F.; Bren, N.; Little, A.; Wang, H. L.; Hansen, S. B.; Talley, T. T.; Taylor, P.; Sine, S. M., Curariform antagonists bind in different orientations to acetylcholine-binding protein. *J. Biol. Chem.* **2003**, 278, 23020–23026.
10. Gao, F.; Bren, N.; Burghardt, T. P.; Hansen, S.; Henchman, R. H.; Taylor, P.; McCammon, J. A.; Sine, S. M., Agonist-mediated conformational changes in acetylcholine-binding protein revealed by simulation and intrinsic tryptophan fluorescence. *J. Biol. Chem.* **2005**, 280, 8443–8451.

11. Thompson, A. J.; Price, K. L.; Reeves, D. C.; Chan, S. L.; Chau, P. L.; Lummis, S. C. R., Locating an antagonist in the 5-HT<sub>3</sub> receptor binding site using modeling and radioligand binding. *J. Biol. Chem.* **2005**, *280*, 20476–20482.
12. Reeves, D. C.; Sayed, M. F. R.; Chau, P. L.; Price, K. L.; Lummis, S. C. R., Prediction of 5-HT<sub>3</sub> receptor agonist-binding residues using homology modeling. *Biophys. J.* **2003**, *84*, 2338–2344.
13. Cromer, B. A.; Morton, C. J.; Parker, M. W., Anxiety over GABA(A) receptor structure relieved by AChBP. *Trends Biochem.Sci.* **2002**, *27*, 280–287.
14. Thompson, J. D.; Higgins, D. G.; Gibson, T. J., ClustalW: Improving the sensitivity of progressive multiple sequence alignment through sequence weighting, position-specific gap penalties and weight matrix choice. *Nucleic Acids Res.* **1994**, *22*, 4673–4680.
15. Sali, A.; Blundell, T. L., Comparative protein modeling by satisfaction of spatial restraints. *J. Mol. Biol.* **1993**, *234*, 779–815.
16. MacKerell, A. D.; Bashford, D.; Bellott, M.; Dunbrack, R. L.; Evanseck, J. D.; Field, M. J.; Fischer, S.; Gao, J.; Guo, H.; Ha, S.; Joseph-McCarthy, D.; Kuchnir, L.; Kuczera, K.; Lau, F. T. K.; Mattos, C.; Michnick, S.; Ngo, T.; Nguyen, D. T.; Prodhom, B.; Reiher, W. E.; Roux, B.; Schlenkrich, M.; Smith, J. C.; Stote, R.; Straub, J.; Watanabe, M.; Wiorkiewicz-Kuczera, J.; Yin, D.; Karplus, M., All-atom empirical potential for molecular modeling and dynamics studies of proteins. *J. Phys. Chem. B* **1998**, *102*, 3586–3616.
17. Ghosh, A.; Rapp, C. S.; Friesner, R. A., Generalized born model based on a surface integral formulation. *J. Phys. Chem. B* **1998**, *102*, 10983–10990.
18. Lim, K. T.; Brunett, S.; Iotov, M.; McClurg, R. B.; Vaidehi, N.; Dasgupta, S.; Taylor, S.; Goddard, W. A., Molecular dynamics for very large systems on massively parallel computers: The MPSim program. *J. Comput. Chem.* **1997**, *18*, 501–521.
19. Mayo, S. L.; Olafson, B. D.; Goddard, W. A., Dreiding: A generic force-field for molecular simulations. *J. Phys. Chem.* **1990**, *94*, 8897–8909.
20. Trabanino, R. J.; Hall, S. E.; Vaidehi, N.; Floriano, W. B.; Kam, V. W. T.; Goddard, W. A., First principles predictions of the structure and function of G-protein-coupled receptors: Validation for bovine rhodopsin. *Biophys. J.* **2004**, *86*, 1904–1921.
21. Vaidehi, N.; Floriano, W. B.; Trabanino, R.; Hall, S. E.; Freddolino, P.; Choi, E. J.; Zamanakos, G.; Goddard, W. A., Prediction of structure and function of G protein-coupled receptors. *Proc. Natl. Acad. Sci. U. S. A.* **2002**, *99*, 12622–12627.
22. Floriano, W. B.; Vaidehi, N.; Goddard, W. A.; Singer, M. S.; Shepherd, G. M., Molecular mechanisms underlying differential odor responses of a mouse olfactory receptor. *Proc. Natl. Acad. Sci. U. S. A.* **2000**, *97*, 10712–10716.

23. Wang, P.; Vaidehi, N.; Tirrell, D. A.; Goddard, W. A., Virtual screening for binding of phenylalanine analogues to phenylalanyl-tRNA synthetase. *J. Am. Chem. Soc.* **2002**, 124, 14442–14449.
24. Ewing, T. J. A.; Kuntz, I. D., Critical evaluation of search algorithms for automated molecular docking and database screening. *J. Comput. Chem.* **1997**, 18, 1175–1189.
25. Shurki, A.; Warshel, A., Structure/function correlations of proteins using MM, QM/MM, and related approaches: Methods, concepts, pitfalls, and current progress. In *Protein Simulations*, 2003; Vol. 66, pp 249–313.

## **Chapter 4**

### **Hydrogen Bonding Pattern of Serotonin in MOD-1**

## 4.1 Introduction

The modeling study in Chapter 3 showed that serotonin could form three hydrogen bonds in the binding pocket of MOD-1 (Figure 3.4). First, the side chain amide carbonyl group of Gln 228 forms a hydrogen bond with the indolic amine group of serotonin (Figure 4.1 (a)). Second, the side chain amide group of Asn 223 hydrogen bonds with the hydroxyl group of serotonin (Figure 4.1 (b)). Third, the main chain carbonyl group of Tyr 180 forms a hydrogen bond with the primary ammonium cation of serotonin (Figure 4.1 (c)). Therefore, we had a high-resolution model of the binding pocket with serotonin bound.

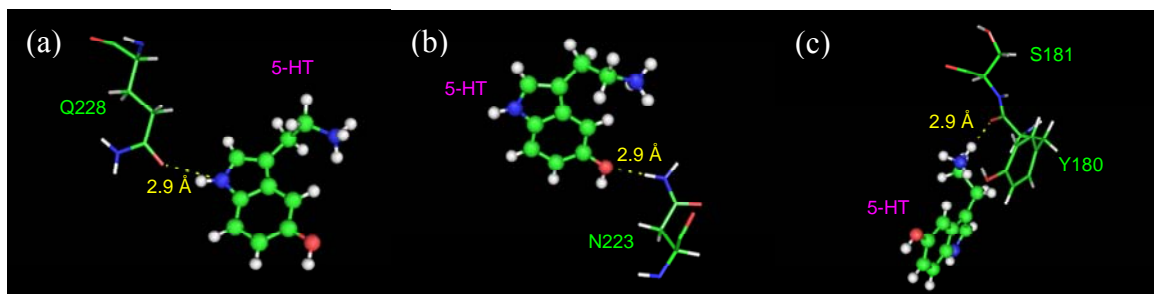


**Figure 4.1** Hydrogen bonding pattern of serotonin in MOD-1. (a) H-bond between Q228 and 5-HT. (b) H-bond between N223 and 5-HT. (c) H-bond between the main chain carbonyl group of Y180 and 5-HT.

In this chapter, we aim to prove this hydrogen bonding pattern experimentally. In order to confirm the hydrogen bond between a ligand and a specific residue in a receptor, we need to show: first, the specific residue forms a hydrogen bond; second, the ligand is the actual hydrogen bond partner of this specific residue. To prove the first point that a

specific residue forms a hydrogen bond, we can change the structure of this residue to perturb its hydrogen bonding ability and monitor the resulting functional change. Conventional mutations can be used as a starting point for this purpose. Furthermore, with the powerful unnatural amino acid mutagenesis methodology,<sup>1</sup> we can finely tune the hydrogen bonding ability of this residue and thus confirm this point with more confidence. To prove the second point that the ligand is the actual hydrogen bond partner of this specific residue, we need to modify the hydrogen bonding ability of the ligand. Such a study can then be performed on structures where both the ligand and the residue change, which will give compelling evidence on the hydrogen bond between the ligand and the specific residue. If forward pharmacology is used to describe the structural modification of the ligand, and reverse pharmacology to the residue, this strategy can then be termed as the forward and reverse pharmacology method.

The forward and reverse pharmacology method was applied to test the hydrogen bonding pattern of serotonin in MOD-1. The hydrogen bond between the indolic amine group of serotonin and Gln 228 was confirmed. Furthermore, the EC<sub>50</sub> values measured in the experiments were in good agreement with the hydrogen bond binding energies calculated from the *ab initio* quantum chemical method. Our current results showed that it is possible that the two hydrogen bonds between serotonin and Asn 223 and the main chain carbonyl group of Tyr 180 exist. Therefore, we obtained a high-resolution image of the orientation of serotonin in the binding pocket, which could benefit the study of the Cys-loop superfamily of ligand-gated ion channels and drug design efforts.

## 4.2 Hydrogen Bond between Gln 228 and the Indolic Amine Group of Serotonin

### 4.2.1 Use of Serotonin Analogues and Conventional Mutations to Probe the Hydrogen Bond between Gln 228 and Serotonin

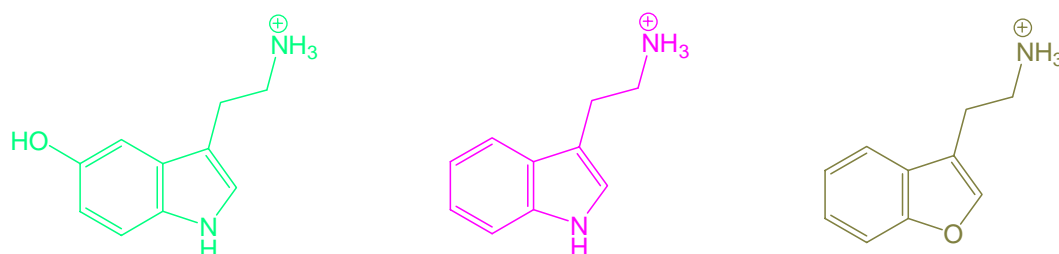


**Figure 4.2** Structures of serotonin analogues used to probe the hydrogen bond between serotonin and Gln 228. The molecule in green is serotonin; the molecule in magenta is tryptamine; the molecule in dark yellow is 2-(benzofuran-3-yl)ethylamine (BFEA).

Several serotonin analogues were used to probe the hydrogen bond between serotonin and Gln 228. As shown in Figure 4.2, serotonin is colored green, tryptamine colored magenta, and 2-(benzofuran-3-yl)ethylamine (BFEA) colored dark yellow. Compared to serotonin, tryptamine only lacks a hydroxyl group, deleting the potential hydrogen bond formation ability at this position. Compared to tryptamine, BFEA substitutes the indole nitrogen with an oxygen atom, removing the hydrogen bond donor ability at this position. Tryptamine and BFEA modify the hydrogen bonding ability of serotonin at different positions. The use of these three drugs simultaneously will give valuable information on the hydrogen bond partners of serotonin in the binding pocket.

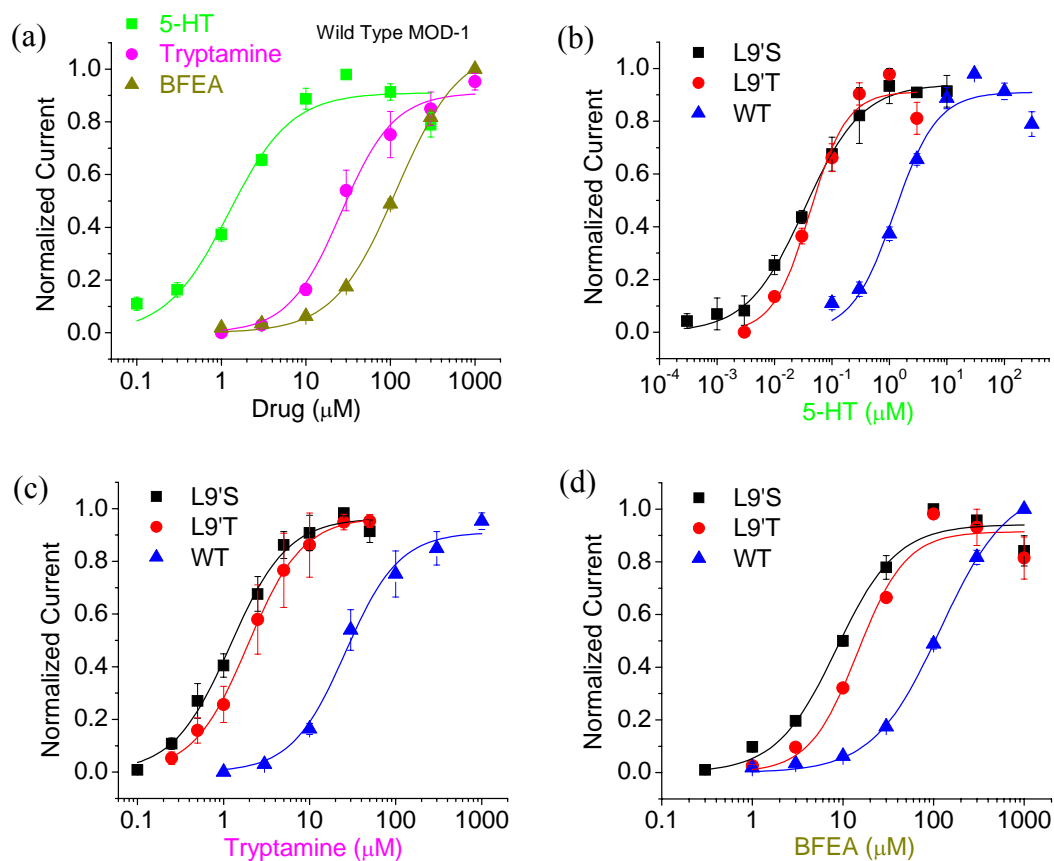


**Figure 4.3** Dose-response curves of serotonin analogues in the MOD-1 wild type and L9'T and L9'S mutants. (a) Serotonin analogues recorded in wild type. (b) Serotonin curves recorded in wild type and L9'T and L9'S mutants. (c) Tryptamine curves recorded in wild type and L9'T and L9'S mutants. (d) BFEA curves recorded in wild type and L9'T and L9'S mutants.

We measured dose-response curves of these drugs in the MOD-1 wild type. The results are summarized in Figure 4.3 (a) and Table 4.1. Tryptamine had a higher  $\text{EC}_{50}$  value (26  $\mu\text{M}$ ) than serotonin (1.22  $\mu\text{M}$ ), and BFEA had an even higher  $\text{EC}_{50}$  value (118  $\mu\text{M}$ ) although much lower efficacy than serotonin and tryptamine. This  $\text{EC}_{50}$  trend agreed with the docking result that both the hydroxyl group and the indolic amine of serotonin

formed hydrogen bonds with the receptor because deletion of the hydrogen bonding ability at either of these two positions impaired the drug potency.

**Table 4.1** EC<sub>50</sub> values of serotonin analogues in MOD-1 wild type and L9'T and L9'S mutants.

		5-HT	Tryptamine	BFEA
WT	EC <sub>50</sub> (μM)	1.22±0.30	26±3	118±7
	n <sub>Hill</sub>	1.17±0.06	1.39±0.22	1.17±0.06
L9'T	EC <sub>50</sub> (μM)	0.042±0.005	1.92±0.09	14.5±2.0
	n <sub>Hill</sub>	1.36±0.12	1.36±0.07	1.62±0.22
L9'S	EC <sub>50</sub> (μM)	0.033±0.003	1.20±0.11	8.51±1.64
	n <sub>Hill</sub>	0.87±0.10	1.31±0.12	1.31±0.28

Next, we did a simple test to see whether these three drugs had similar gating mechanisms. From the study of nAChR, it is known that Leu 9' in the M2 region is the actual gate of the ion pore.<sup>2</sup> In nAChR, L9'T and L9'S mutations can shift the dose-response relationship to lower concentrations.<sup>3, 4</sup> Thus, using these three drugs, we recorded the dose-response curves of the L9'T and L9'S mutants in MOD-1. The results are shown in Figure 4.3 and Table 4.1. Both the L9'T and L9'S mutations shifted the EC<sub>50</sub> curves to the left for all these three drugs with similar trends. Therefore, these three drugs did not differ significantly in their gating pathways, thus, providing good comparisons with each other in studying the binding behavior of MOD-1.

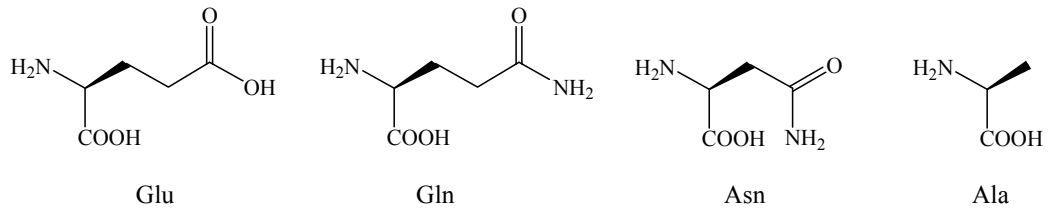


**Figure 4.4** Structures of conventional mutations made at position 228 of MOD-1.

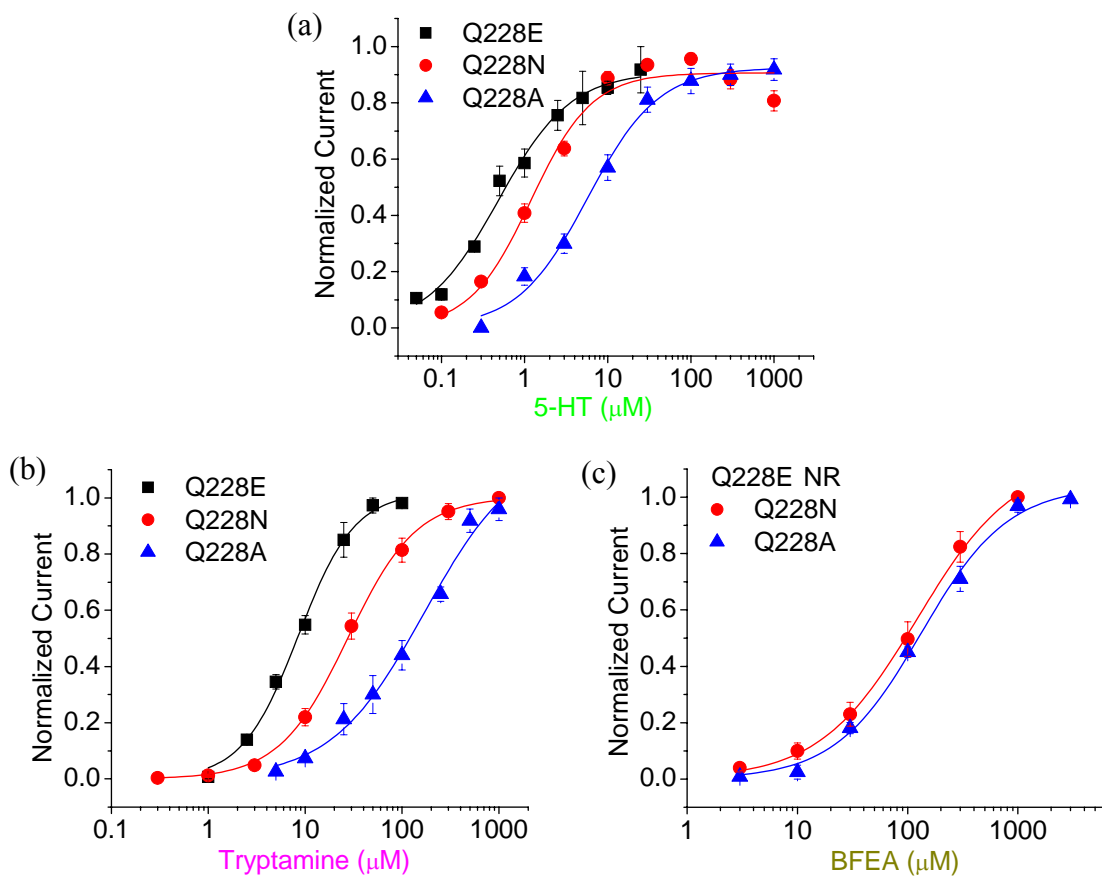


**Figure 4.5** Dose-response curves of serotonin analogues in Q228N, Q228E, Q228A mutants of MOD-1. (a) Serotonin was used for recording. (b) Tryptamine was used for recording. (c) BFEA was used for recording.

With the three serotonin analogues at hand, we mutated Gln 228 to glutamate, asparagine, and alanine to modify its hydrogen bonding ability (Figure 4.4). The dose-response curves of these mutants using the three serotonin analogues were measured. The results are summarized in Figure 4.5 and Table 4.2.

**Table 4.2** EC<sub>50</sub> values of serotonin analogues in Q228N, Q228E and Q228A mutants of MOD-1.

Position 228		5-HT	Tryptamine	BFEA
Q228N	EC <sub>50</sub> (μM)	1.19±0.20	28±1	121±12
	n <sub>Hill</sub>	1.18±0.20	1.23±0.05	1.21±0.06
Q228E	EC <sub>50</sub> (μM)	0.49±0.05	8.50±0.63	NR <sup>a</sup>
	n <sub>Hill</sub>	1.00±0.10	1.50±0.13	
Q228A	EC <sub>50</sub> (μM)	5.75±0.50	170±20	133±10
	n <sub>Hill</sub>	1.02±0.11	0.91±0.10	1.11±0.10

<sup>a</sup> NR represents no response.

When serotonin was used for recording, Asn gave a similar EC<sub>50</sub> value (1.19 μM) to the wild type Gln (1.22 μM), which is indicated by the red dose-response curve (Q228N) in Figure 4.5 (a). Asn has the terminal amide group and is only one carbon shorter than Gln. The Gln to Asn mutation could still keep the hydrogen bond between serotonin and the amide carbonyl group of the residue at position 228, and thus, did not change the EC<sub>50</sub> value. The Glu mutant (EC<sub>50</sub>, 0.49 μM) shifted the dose-response curve to the left, which is indicated by the black curve (Q228E) in Figure 4.5 (a). This was in

accordance with the prediction that the Gln to Glu mutation increased the electron density of the oxygen atom forming the hydrogen bond, thus potentiating the hydrogen bonding ability. The Ala mutant ( $EC_{50}$ , 5.75  $\mu$ M) shifted the dose-response curve to the right, which is indicated by the blue curve (Q228A) in Figure 4.5 (a). This result agreed with the expectation that the Gln to Ala mutation deleted the hydrogen bond, thus impairing the agonist potency. The current study on these mutations showed that Gln 228 participated in hydrogen bond formation, which would be further proved by unnatural amino acid mutations. However, we still needed to confirm that the actual hydrogen bond partner of Gln 228 was the indolic amine of serotonin.

When tryptamine was used for recording, the dose-response curves for the three mutations had the same trend as those using serotonin (Figure 4.5 (b)). The Asn mutant had a similar  $EC_{50}$  to wild type; the Glu mutant, decreased  $EC_{50}$ ; the Ala mutant, increased  $EC_{50}$ . Serotonin and tryptamine had similar responses to the mutations at Gln 228. This result showed that the hydrogen bond partner of Gln 228 was not the hydroxyl group of serotonin. Therefore, the model of the indolic amine of serotonin acting as the hydrogen bond donor was supported.

Finally, we used BFEA to perform the recordings. BFEA had a distinctively different response profile to these mutations at Gln 228 from serotonin and tryptamine (Figure 4.5 (c)). Using BFEA, both the Asn and Ala mutants produced similar  $EC_{50}$  values to wild type. The current of the Glu mutant was too small to calculate the  $EC_{50}$  value. The mutations at Gln 228 did not affect the binding of BFEA, which confirmed that the actual hydrogen bond partner of Gln 228 was the indolic amine of serotonin!

As described above, to probe the hydrogen bond between Gln 228 and serotonin, we modified the hydrogen bonding abilities of both Gln 228 using conventional mutagenesis and serotonin at the specific sites using proper drugs. This purposely designed structure-function study strongly supported the model that a hydrogen bond exists between the side chain amide carbonyl group of Gln 228 and the indolic amine of serotonin (Figure 4.1 (a)).

## 4.2.2 Use of Unnatural Amino Acid Mutations to Further Prove the Hydrogen Bond between Gln 228 and Serotonin

### 4.2.2.1 Model Study of the Hydrogen Bond Binding Energies between Gln 228 and Serotonin

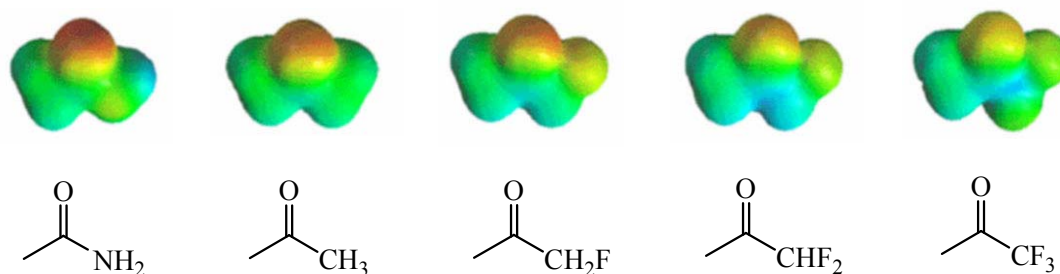


**Figure 4.6** AM1 electrostatic potential surfaces (EPS) of the model molecules that represent the Gln analogues. Red region is negatively charged; blue region is positively charged. The structures shown correspond to the EPS right above them.

Using the powerful unnatural amino acid mutations, we can subtly tune the hydrogen bonding ability of Gln 228. In order to modify the hydrogen bond acceptor ability of the side chain amide carbonyl group in Gln 228, we can substitute the terminal

amine with a methyl group first. This substitution deletes the potential hydrogen bond formation ability of the terminal amine. Then the terminal methyl ketone can be progressively fluorinated, which decreases the hydrogen bond acceptor ability of the carbonyl group little by little. This trend is vividly shown by the electrostatic potential surfaces of some simple model molecules by the AM1 semi-empirical method (Figure 4.6).

As shown in Figure 4.6, acetamide represented glutamine, acetone represented 2-amino-5-oxohexanoic acid, fluoroacetone represented 2-amino-6-fluoro-5-oxohexanoic acid, 1,1-difluoroacetone represented 2-amino-6,6-difluoro-5-oxohexanoic acid, and 1,1,1-trifluoroacetone represented 2-amino-6,6,6-trifluoro-5-oxohexanoic acid. The negatively charged red regions of the oxygen atoms became lighter and lighter from left to right, which reflects the decreasing electron densities of the oxygen atoms, and the hydrogen bond acceptor abilities of the corresponding carbonyl groups are weakened little by little. These EPS surfaces qualitatively showed the relative hydrogen bonding strength of these molecules. However, to obtain quantitative results, we needed to calculate the binding energies of the hydrogen bonds between serotonin and these model molecules.

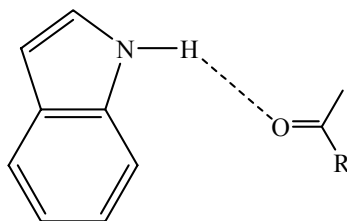


**Figure 4.7** The model system used to calculate the binding energies of the hydrogen bonds between the indolic amine of serotonin and Gln analogues.

A simple model system was used to mimic the hydrogen bonds between the indolic amine of serotonin and Gln analogues (Figure 4.7). Indole represented serotonin and acetone analogues represented Gln analogues. The hydrogen bond binding energy was calculated according to the following equation:

$$\text{Binding Energy} = E(\text{Indole}) + E(\text{Molecule}) - E(\text{Indole}\cdots\text{Molecule Complex})$$

The calculated total energies (TE) of indole and acetone analogues are summarized in Table 4.3. The total energies of the indole $\cdots$ molecule complexes are shown in Table 4.4. The hydrogen bond binding energies of the model system are summarized in Table 4.5. The configurations of the HF/6-31G\*\* optimized indole $\cdots$ molecule complex structures are shown in Figure 4.8.

**Table 4.3** Total energies of indole and acetone analogues.

	TE (Hartree)		
	AM1	HF/6-31G**	MP2/6-31G**
Indole	0.0876483	-361.482918	-362.699316
Acetamide	-0.0808907	207.988975	208.611777
Acetone	-0.0784983	-191.972072	-192.571407
Fluoroacetone	-0.1521816	-290.815136	-291.573003
1,1-difluoroacetone	-0.2298946	-389.672355	-390.591911
1,1,1-trifluoroacetone	-0.310967	-488.539615	-489.621864

**Table 4.4** Total energies of the indole $\cdots$ molecule complexes.

Indole $\cdots$ molecule complexes	TE (Hartree)		
	AM1	HF/6-31G**	MP2/6-31G**
Acetamide	-0.0020535	-569.48447	-571.324855
Acetone	0.0030624	-553.46438	-555.280201
Fluoroacetone	-0.0700851	-652.306647	-654.280768
1,1-difluoroacetone	-0.1466802	-751.162356	-753.296667
1,1,1-trifluoroacetone	-0.2279992	-850.029096	-852.324389

**Table 4.5** The hydrogen bond binding energies of the model system, which mimics the hydrogen bonds between the indolic amine of serotonin and Gln analogues.

Indole...molecule complexes	Binding Energy (kcal/mol)		
	AM1	HF/6-31G**	MP2/6-31G**
Acetamide	5.53	7.89	8.64
Acetone	3.82	5.89	5.95
Fluoroacetone	3.48	5.39	5.30
1,1-difluoroacetone	2.78	4.44	3.41
1,1,1-trifluoroacetone	2.94	4.12	2.01

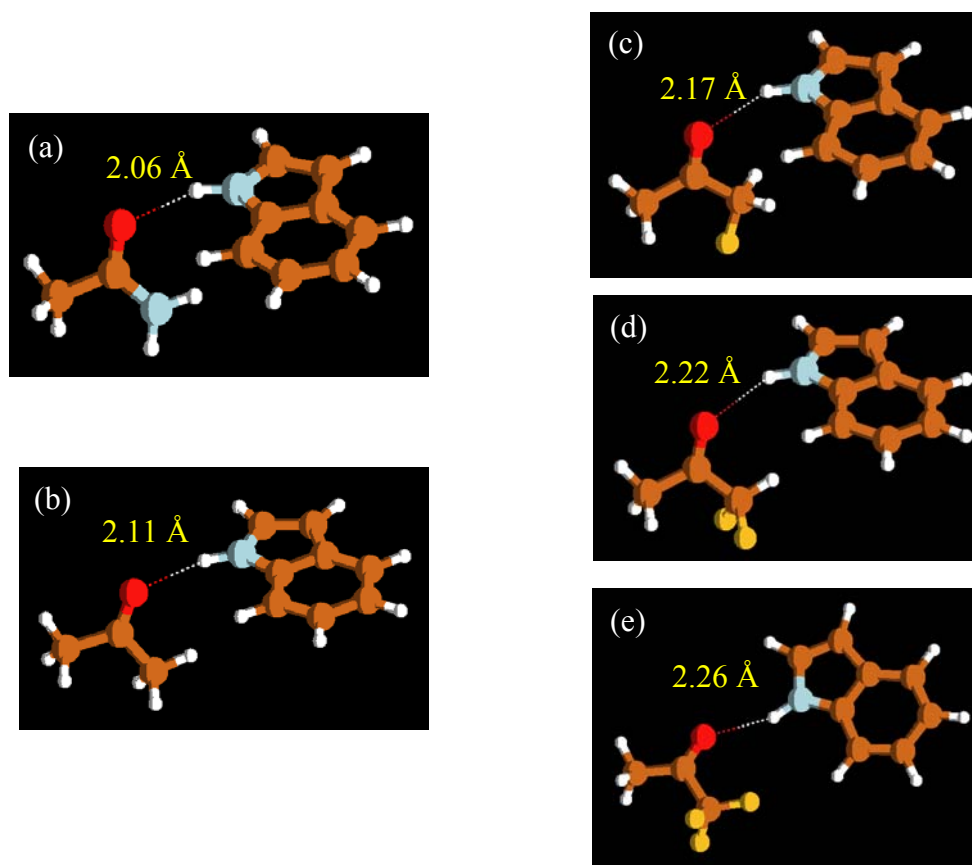


**Figure 4.8** The configurations of the HF/6-31G\*\* optimized indole...molecule complex structures. (a) Indole...acetamide complex. (b) Indole...acetone complex. (c) Indole...fluoroacetone complex. (d) Indole...difluoroacetone complex. (e) Indole...trifluoroacetone complex. Red is oxygen, cyan is nitrogen, yellow is fluorine, dark yellow is carbon, and white is hydrogen. The numbers are the hydrogen bond distances between the oxygen and hydrogen atoms.

The hydrogen bond binding energies of the model system decreased from 7.89 kcal/mol for the acetamide complex to 5.89 kcal/mol for the acetone complex. Progressive fluorinations of acetone decreased the binding energies for the corresponding complexes little by little. Accordingly, as shown in Figure 4.8, the hydrogen bond distance between the oxygen and hydrogen atoms in the acetone complex (2.11 Å) was larger than that in the acetamide complex (2.06 Å). Progressive fluorination of acetone further increased the hydrogen bond distances little by little. This result agreed with the trend seen in the EPS surfaces of the acetone analogues (Figure 4.6).

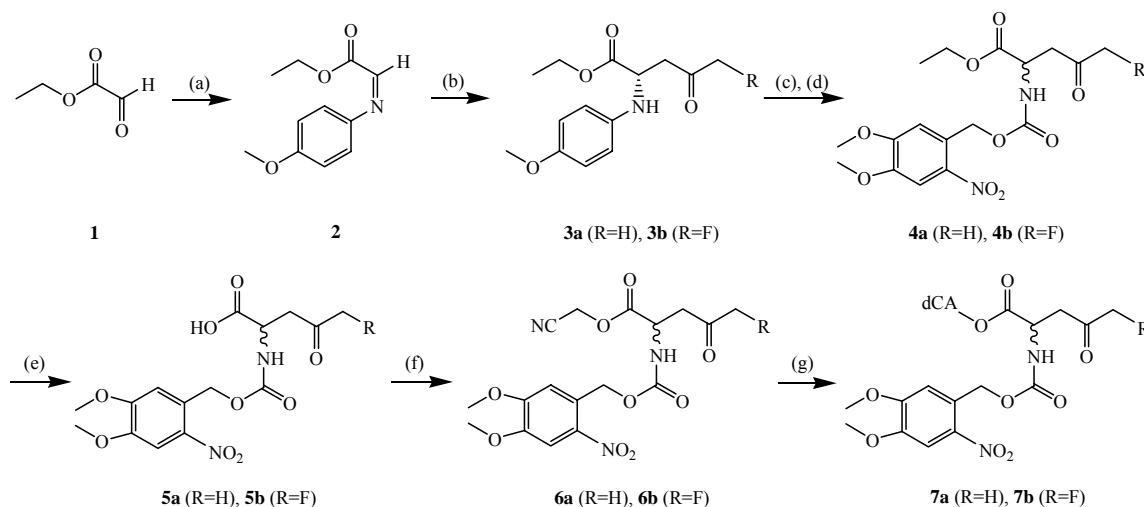
The hydrogen binding energies provided a quantitative estimation of the bond strength, which could be used for comparison with the experimental results.

#### **4.2.2.2 Synthesis of the Asn Analogues to Probe the Hydrogen Bond between Gln 228 and Serotonin**

Since Asn gave similar responses to Gln at position 228 using all three serotonin analogues, for ease of synthesis, we chose to synthesize Asn analogues to probe this hydrogen bond. The synthesis of 2-amino-4-oxopentanoic acid and 2-amino-5-fluoro-4-oxopentanoic acid derivatives is shown in Scheme 4.1.

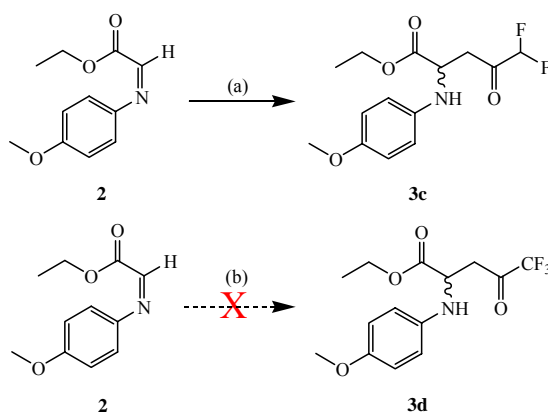
*N*-PMP-protected  $\gamma$ -keto- $\alpha$ -amino acid derivatives can be obtained from an *L*-proline-catalyzed direct asymmetric Mannich reaction with *N*-PMP-protected  $\alpha$ -ethylglyoxylate and proper ketone donors.<sup>5-7</sup> As shown in step (b) of Scheme 4.1, **3a** and **3b** were synthesized with high ee values and good yields according to the reported

procedure.<sup>7</sup> To obtain high ee values and yields of **3a** and **3b**, the starting material **2** needed to be freshly made. The following steps in Scheme 4.1 were not expected to introduce significant racemization according to the literature. However, **3a** and **3b** were kept at room temperature for several days, and racemization occurred. Since for nonsense unnatural amino acid mutagenesis, only L-amino acids would be incorporated into proteins, we did not make further efforts to investigate the chirality of the compounds in the following steps. The PMP group was exchanged with a NVOC protection group via a one-pot oxidative dearylation and re-protection procedure to afford **4a** and **4b**.<sup>8</sup> The ethyl ester group was removed under mild conditions using potassium carbonate aqueous solution to produce **5a** and **5b**.<sup>9, 10</sup> Subsequently, the *N*-NVOC-protected amino acids were activated and coupled to dCA as previously described.<sup>11</sup>



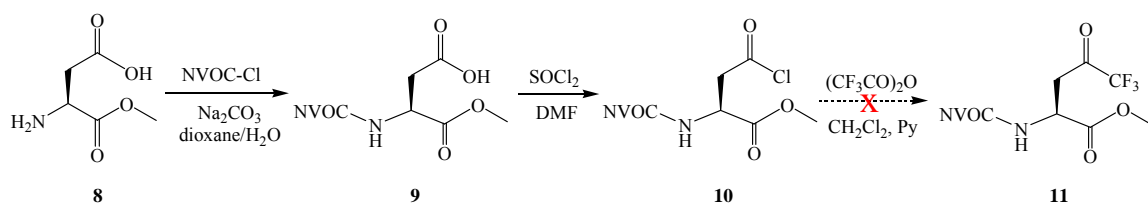
**Scheme 4.1** Synthesis of dCA-Asn analogues. Reagents: (a) p-anisidine, CH<sub>2</sub>Cl<sub>2</sub> (93%). (b) For **3(a)**, acetone, L-Pro, DMSO (71%, 91% ee); for **3(b)**, fluoroacetone, L-Pro, DMSO (75%, 98% ee). (c) CAN, H<sub>2</sub>O/CH<sub>3</sub>CN; (d) NVOC-Cl, dioxane/H<sub>2</sub>O; for **4(a)**, 61%; for **4(b)**, 40%. (e) K<sub>2</sub>CO<sub>3</sub>, aq. MeOH; for **5(a)**, 78%; for **5(b)**, 78%. (f) chloroacetonitrile, triethylamine, DMF; for **6(a)**, 90%; for **6(b)**, 63%. (g) dCA, DMF.

However, by using the standard L-proline-catalyzed Mannich reaction procedure, **3c** and **3d** could not be obtained (Scheme 4.2). The reaction to form **3c** was incomplete after 48 hours, and it was difficult to separate **3c** from starting materials. It was reported that the use of the ionic liquid of 1-butyl-3-methylimidazolium tetrafluoroborate (BMIMBF<sub>4</sub>) as the reaction medium could speed up the L-proline catalyzed Mannich reaction significantly.<sup>12</sup> Therefore, BMIMBF<sub>4</sub> was used to perform the reactions again. The reaction to form **3c** was complete in one hour, and **3c** was successfully separated. The use of **3c** for the following steps to obtain dCA-amino acid is in progress. However, **3d** was not the major product of the corresponding reaction even using BMIMBF<sub>4</sub> as the reaction medium.



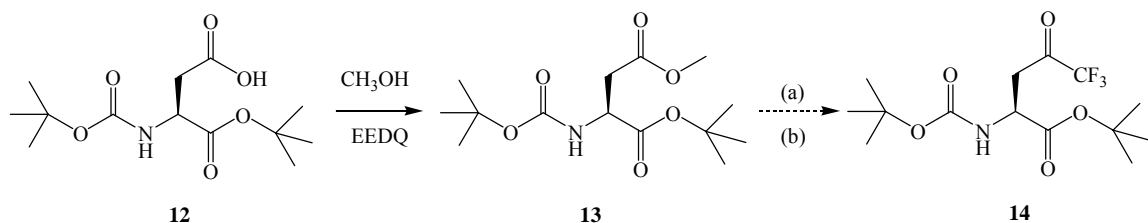
**Scheme 4.2** Synthesis of *N*-PMP-protected  $\gamma$ -keto- $\alpha$ -amino acid derivatives. Reagents: (a) 1,1-difluoroacetone, D,L-Pro, BMIMBF<sub>4</sub> (45%); (b) 1,1,1-trifluoroacetone, D,L-Pro, BMIMBF<sub>4</sub>.

Therefore, we needed to design new synthetic routes for 2-amino-5,5,5-trifluoro-4-oxopentanoic acid derivatives. Several methods have been developed to prepare trifluoromethyl ketones from carboxylic acids and carboxylic esters.<sup>13-17</sup>



**Scheme 4.3** Failed synthetic route for 2-amino-5,5,5-trifluoro-4-oxopentanoic acid derivatives using a carboxylic acid as the starting material.

Starting from a carboxylic acid, we tried the synthetic route shown in Scheme 4.3.<sup>16, 17</sup> However, the key transformation from **10** to **11** did not yield promising results.



**Scheme 4.4** Proposed synthetic route for 2-amino-5,5,5-trifluoro-4-oxopentanoic acid derivatives using a carboxylic ester as the starting material. (a) TMS-CF<sub>3</sub> with either TBAF or CsF as the initiator. (b) H<sup>+</sup>.

Starting from carboxylic esters, we proposed another synthetic route shown in Scheme 4.4. **13** could be easily obtained from **12** with a high yield (91%).<sup>18</sup> Using either anhydrous tetrabutylammonium fluoride (TBAF) or cerium fluoride (CsF) as the initiator, trifluoromethyltrimethylsilane (TMS-CF<sub>3</sub>) can be used to transfer a CF<sub>3</sub> group to the ester, which upon acid hydrolysis, will yield trifluoromethyl ketone.<sup>13, 14</sup> It needs to be mentioned that in step (a), rigorously dry conditions are a prerequisite for a successful reaction. This route seems promising.

#### 4.2.2.3 Electrophysiology Recording of the Asn Analogues at Position 228 of MOD-1

The unnatural Asn analogues obtained above, namely, 2-amino-4-oxopentanoic acid (PAO) and 2-amino-5-fluoro-4-oxopentanoic acid (F-PAO), were incorporated into position 228 of MOD-1. The recording results using the three serotonin analogues are summarized in Table 4.6. The dose-response curves of serotonin on these mutations are shown in Figure 4.9.

**Table 4.6** EC<sub>50</sub> values of serotonin analogues for unnatural mutations at position 228 of MOD-1.

Position 228		5-HT	Tryptamine	BFEA
PAO	EC <sub>50</sub> (μM)	10.0±1.2	485±35	
	n <sub>Hill</sub>	1.89±0.34	2.75±0.47	NR <sup>a</sup>
F-PAO	EC <sub>50</sub> (μM)	36±4		
	n <sub>Hill</sub>	1.68±0.27	NR	NR

<sup>a</sup> NR represents no response.

The substitution of the terminal amine of Asn with a methyl group increased the EC<sub>50</sub> value of serotonin from 1.19 μM to 10.0 μM. Fluorination of PAO shifted the dose-response curve further to the right (Figure 4.9 (a)). This trend was in good agreement with the calculated hydrogen bond binding energies using the model system (Table 4.5). The higher the EC<sub>50</sub> values, the smaller the hydrogen bonding energies. We did a plot of log (EC<sub>50</sub>(mutant)/EC<sub>50</sub>(WT)) versus hydrogen bond binding energy from the HF/6-31G\*\* calculation, and a good linear fit was found (Figure 4.9 (b)). In combination with

previous conventional mutation results (Table 4.2 and Figure 4.5 (a)), the current unnatural mutations provide convincing evidence that the terminal amide carbonyl group of Gln 288 formed a hydrogen bond.

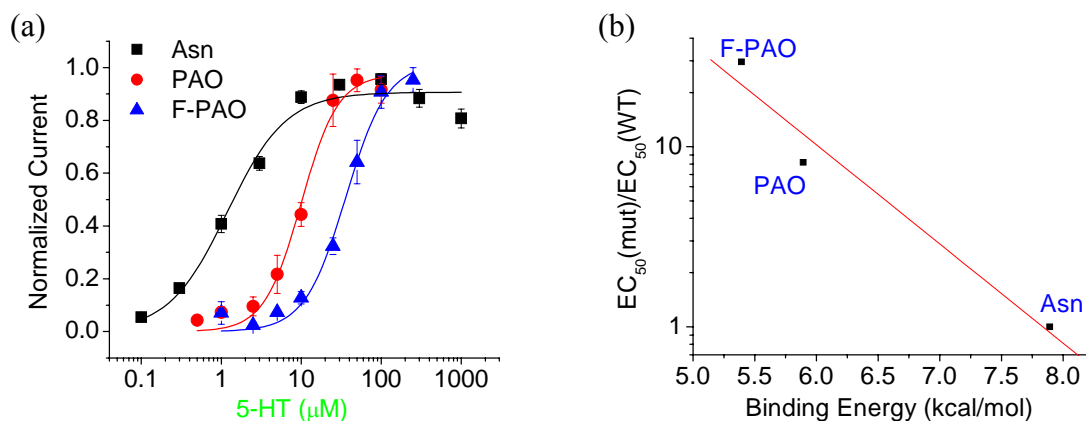


**Figure 4.9** Recording results of serotonin on unnatural mutations at position 228 of MOD-1. (a) Dose-response curves of serotonin. (b) The correlation between the  $\text{EC}_{50}$  values and the hydrogen bond binding energies. The binding energies are from the HF/6-31G\*\* results in Table 4.5.

$\text{EC}_{50}$  recordings of tryptamine on F-PAO, and BFEA on PAO and F-PAO were not successful due to the small currents. By using tryptamine, PAO (485  $\mu\text{M}$ ) had a much larger  $\text{EC}_{50}$  value than Asn (28  $\mu\text{M}$ ). Again, this was supportive evidence for the model that the actual hydrogen bond partner of Gln 228 is the indolic amine rather than the hydroxyl group of serotonin.

The current results from the unnatural amino acids study together with the conventional mutations study unambiguously prove that the terminal amine of Gln forms a hydrogen bond with serotonin, and that it is the indolic amine of serotonin that participates in this hydrogen bond.

In summary, starting from a computational model, a forward and reverse pharmacology strategy was applied to evaluate the MOD-1 binding site. Together with the powerful unnatural amino acid mutagenesis, the current results represent the most up-to-date advancement in studying the ligand-binding sites of ion channels. This hydrogen bond pattern would not be otherwise elucidated.

### 4.3 Hydrogen Bond between Asn 223 and the Hydroxyl Group of Serotonin

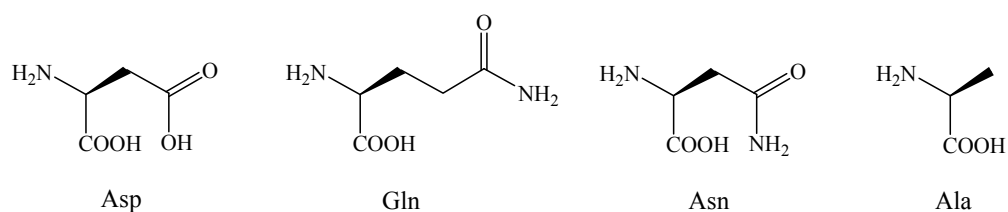


**Figure 4.10** Structures of conventional mutations made at position 223 of MOD-1.

Originally, a strategy similar to what was used in studying Gln 228 was planned as follows. To change the hydrogen bonding ability of Asn 223, we mutated asparagine to aspartate, glutamine, and alanine (Figure 4.10). We measured the dose-response curves of these mutants using serotonin. The results are summarized in Figure 4.11.

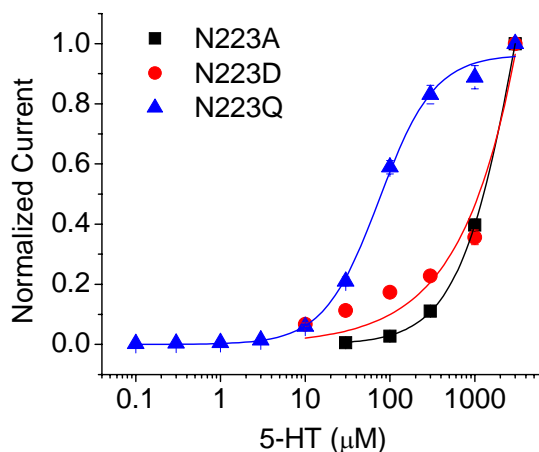


**Figure 4.11** Dose-response curves of serotonin in N223A, N223D, and N223Q mutants of MOD-1.

For serotonin, the N223A and N223D mutations gave huge  $EC_{50}$  values (at least 1 mM), possibly producing a malfunctioning receptor; the N223Q mutant (73  $\mu$ M) increased  $EC_{50}$  about 60-fold. Tryptamine and BFEA were also tried on these three mutants. However, either the measured  $EC_{50}$  values were huge (at least 1 mM) or the currents were too small to calculate  $EC_{50}$  (data not shown). Although no conclusive result was achieved from the experiments, we did find that Asn 223 is very sensitive to mutations. Only the Gln mutation was moderately tolerated, possibly due to the preservation of the terminal amide group, which was proposed to form a hydrogen bond with serotonin in the model.

We also did some recording on MOD-1 wild type using the drug 5-methoxytryptamine, and the  $EC_{50}$  value was huge (at least 1mM, data not shown).

The bottom line was that the present experiments did not disagree with the modeling results (Figure 4.1 (b)).

#### 4.4 Hydrogen Bond between Main Chain Carbonyl Group of Tyr 180 and the Terminal Ammonium of Serotonin

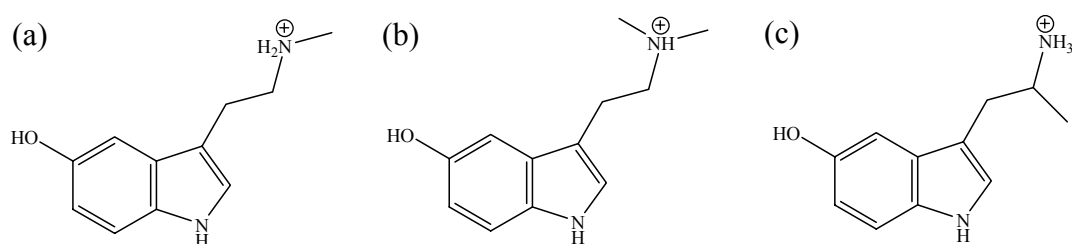


**Figure 4.12** Structures of serotonin analogues used to probe the hydrogen bond between the backbone carbonyl group of Tyr 180 and serotonin. (a) N-Me-serotonin. (b) Bufotenin. (c)  $\alpha$ -Me-serotonin.

**Table 4.7**  $EC_{50}$  values of N-Me-serotonin, bufotenin, and  $\alpha$ -Me-serotonin in MOD-1 wild type.

		N-Me-serotonin	Bufotenin	$\alpha$ -Me-serotonin
	$EC_{50}$ ( $\mu$ M)	$37 \pm 4$	$10 \pm 1$	$2.8 \pm 0.6$
WT	$n_{Hill}$	$1.0 \pm 0.1$	$1.6 \pm 0.3$	$1.3 \pm 0.3$

Several serotonin analogues were used (Figure 4.12). At first, their  $EC_{50}$  values were recorded on wild type MOD-1. The results are shown in Table 4.7.  $\alpha$ -Me-serotonin had a similar  $EC_{50}$  to wild type, while N-Me-serotonin and bufotenin had much larger  $EC_{50}$  values than wild type. N-Me-serotonin has a secondary ammonium, and bufotenin has a tertiary ammonium. Therefore, both of these drugs might form a weaker cation- $\pi$  interaction with Trp 226 and also had a weaker hydrogen bond with the backbone carbonyl group of Tyr 180 according to our model (Figure 4.1 (c)). The potential

hydrogen bonding ability of the terminal ammonium in serotonin could thus be modified by using these serotonin analogues.

To modify the hydrogen bonding ability of the main chain carbonyl group of Tyr 180, we needed to incorporate an  $\alpha$ -hydroxy acid into Ser 181. After incorporation, an amide-to-ester mutation would appear at the backbone peptide bond between Tyr 180 and Ser 181, which could weaken the hydrogen bonding ability of the backbone carbonyl group of Tyr 180 (Figure 4.13). This method was successfully used to prove the hydrogen bond between nicotine and the backbone carbonyl group of Trp 149 in nAChR,<sup>19</sup> which was the sequence homolog of Tyr 180 in MOD-1 (Figure 2.4).

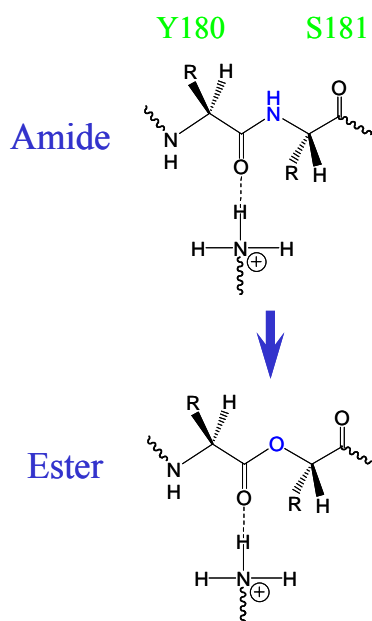


**Figure 4.13** The amide-to-ester mutation to modify the hydrogen bonding ability of the backbone carbonyl group of Tyr 180 in MOD-1 with serotonin.

$\alpha$ -Hydroxytyrosine (Yah) was incorporated into Tyr 180 and incorporation of  $\alpha$ -hydroxyserine (Sah) was attempted at Ser 181. Electrophysiology recording was done

using serotonin. The incorporation of Yah at position 180 did not significantly change the  $EC_{50}$  value (data not shown). Unfortunately, the incorporation of Sah at position 181 did not give recordable currents.

Although the conclusive result could not be obtained from the current experiments, from the  $EC_{50}$  value of N-Me-serotonin in wild type MOD-1 and the result that the backbone carbonyl group of the homologous Trp 149 in nAChR forms a hydrogen bond with nicotine, it is possible that the hydrogen bond also exists between the backbone carbonyl group of Try 180 in MOD-1 and serotonin.

#### **4.5 Conclusions and Future Directions**

Using the forward and reverse pharmacology strategy, we tested the hydrogen bonding pattern of serotonin in MOD-1, which was obtained by the modeling study in Chapter 3. The hydrogen bond between the indolic amine group of serotonin and Gln 228 was confirmed. Our current results showed that it is possible that the two hydrogen bonds between serotonin and Asn 223 and the main chain carbonyl group of Tyr 180 exist. Therefore, we obtained a high-resolution image of the orientation of serotonin in the binding pocket. Moreover, we identified that during the ligand-binding process, both cation- $\pi$  interactions and hydrogen bonds played important roles in directing serotonin to the correct orientation inside the binding pocket. If we considered that cation- $\pi$  interactions played a key role in the other Cys-loop superfamily members such as nAChR, it is quite possible that in MOD-1, cation- $\pi$  interactions direct the primary ammonium of

serotonin to the proper position with some flexibility to activate the channel, and almost simultaneously but a little bit later, the hydrogen bonds between Gln 228/Asn 223 and serotonin fix the orientation of serotonin and thus maximize the activation efficiency.

Future experiments will be focused on finishing the synthesis of 2-amino-5,5-difluoro-4-oxopentanoic acid and 2-amino-5,5,5-trifluoro-4-oxopentanoic acid. After that, they will be incorporated into Gln 228 of MOD-1 for electrophysiology recording, which will complete the intended progressive fluorination series.

Other unnatural amino acids of interest are fluorinated Gln analogues (Figure 4.14). The synthesis of 4-fluoroglutamine and 4,4-difluoroglutamine were reported.<sup>20, 21</sup> 4-fluoroglutamine is also commercially available but expensive. These fluorinated Gln analogues are also useful in probing the hydrogen bonding ability of Gln.

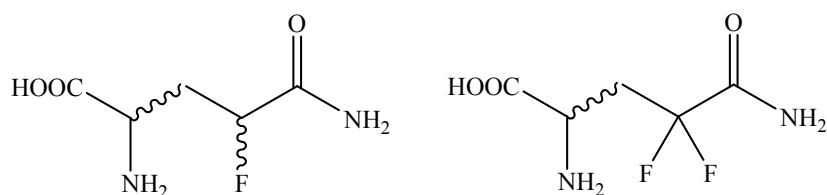


**Figure 4.14** The structures of 4-fluoroglutamine and 4,4-difluoroglutamine.

To sum up, by using both computational modeling and a structure-function experimental study, especially with the aid of the powerful unnatural amino acid mutagenesis method, accurate information on the ligand-binding site and the specific non-covalent interactions responsible for the binding process can be obtained even for a complicated neuroprotein. With this forward and reverse pharmacology method, more

and more progress will be made in the near future while studying the ligand-binding sites of neuroreceptors.

## **4.6 Materials and Methods**

### **4.6.1 Electrophysiology**

Electrophysiological recordings were made 24–72 hours after injection. Whole-cell currents from stage VI oocytes of *Xenopus laevis* were measured in standard two-electrode voltage clamp mode using the OpusXpress<sup>TM</sup> 6000A (Axon Instruments, Union City, California). Microelectrodes were filled with 3M KCl and the resistances were between 0.5 and 2 M $\Omega$ . Oocytes were continuously perfused with calcium-free ND96 or ND96 bath solution at flow rates of 1 ml/min, 4 ml/min during drug application and 3 ml/ml during wash. The holding potential was -60 or -80 mV. Data were sampled at 125 Hz and filtered at 50 Hz. Drug applications were 15 s. Serotonin was purchased from Sigma/Aldrich and all drugs were prepared in ND96 solution. Dose-response data were obtained from 3 to 5 oocytes and data were reported as mean  $\pm$  standard error. Curves were fit to the Hill equation,  $I/I_{\max} = 1/[1 + (EC_{50}/[A])^{n_H}]$ , where  $I$  is the current for agonist concentration  $[A]$ ,  $I_{\max}$  is the maximum current,  $EC_{50}$  is the concentration to elicit a half-maximum response, and  $n_H$  is the Hill coefficient.

## 4.6.2 Incorporation of Unnatural Amino Acids by *in vivo* Nonsense Suppression

### Methods

For suppression experiments, 25 ng of tRNA and 10 ng of mRNA were co-injected in a total volume of 50 nL per oocyte. Immediately before microinjection, the NVOC-aminoacyl-tRNA was deprotected by photolysis. The ligation of aminoacyl-dCA to tRNA and gene construction of suppressor tRNA have been described previously. The MOD-1 gene was subcloned into the plasmid pBlueScript. The MOD-1 TAG mutants were made by the Quickchange<sup>TM</sup> site-directed mutagenesis method and were monitored by DNA sequencing. Plasmid DNAs were linearized with *KpnI*, and mRNA was transcribed using the Ambion T3 mMESSAGE mMACHINE kit.

For wild type and conventional mutation experiments, only 5 ng mRNA was injected into oocytes in a 50 nL volume per cell with the same following procedure as described above.

dCA- $\alpha$ -hydroxyserine was a gift from Niki M. Zacharias at Neurion Pharmaceuticals.

## 4.6.3 Synthesis of Amino Acids, dCA-Amino Acid and Others

### 4.6.3.1 General

Reagents were purchased from Aldrich, Sigma, or other commercial sources. Flash chromatography was on 230–400 mesh silica gel with the solvent indicated. All NMR shifts are reported as  $\delta$  ppm downfield from TMS. <sup>1</sup>H (300 MHz) and <sup>19</sup>F (282 MHz) NMR spectra were recorded using a GE QE-300 or Varian 300 spectrometer. Electrospray ionization (ESI) mass spectrometry was performed at the Caltech

Protein/Peptide Micro Analytical Laboratory. High performance liquid chromatography (HPLC) separations were performed on a Waters dual 510 pump liquid chromatography system equipped with a Waters 996 PDA (photodiode array) UV detector for semi-preparative HPLC. Waters Prep Nova-Pak HR C18 column (7.8x300 mm) was used for semi-preparative HPLC.

#### **4.6.3.2 Synthesis of 2-Amino-4-Oxopentanoic Acid, 2-Amino-5-Fluoro-4-Oxopentanoic Acid, and 2-Amino-5,5-Difluoro-4-Oxopentanoic Acid**

The synthetic routes are shown in Scheme 4.1 and Scheme 4.2.

**N-(Ethoxycarbonylmethylidene)-4-methoxyaniline (2).** 5.089 ml of the ethyl glyoxylate solution (**1**) (50% v/v in toluene, 25 mmol) and 2 g of anhydrous Na<sub>2</sub>SO<sub>4</sub> were added in 30 ml of CH<sub>2</sub>Cl<sub>2</sub> at 0 °C. 3.079 g of p-anisidine (25 mmol) was added to the solution. The mixture was stirred under argon for 5 minutes at 0 °C and another 2 hours at room temperature. The reaction was quenched by the addition of 20 ml of CH<sub>2</sub>Cl<sub>2</sub>, dried over Na<sub>2</sub>SO<sub>4</sub>, and rotary-evaporated. Flash chromatography (1:3 ethyl acetate / petroleum ether) gave 4.817 g (93%) of product as a yellow oil. <sup>1</sup>H NMR (CDCl<sub>3</sub>) δ = 1.36 (t, 3H), 3.78 (s, 3H), 4.36 (q, 2H), 6.88 (d, 2H), 7.32 (d, 2H), 7.89 (s, 1H). ESI-MS calcd for C<sub>11</sub>H<sub>13</sub>NO<sub>3</sub>: 207.09. Found [M+H]<sup>+</sup>: 208.0.

**Ethyl (2S)-2-(p-methoxyphenylamino)-4-oxopentanoate (3a).** 3.105 g of **2** (15 mmol) was dissolved in 120 ml of anhydrous DMSO. 30 ml of acetone was added followed by 345 mg of L-proline (3 mmol, 20 mol%). The mixture was stirred under

argon for 18 hours at room temperature. The reaction was quenched by the addition of 150 ml of half-saturated ammonium chloride solution, and extracted with ethyl acetate (150 ml x 2, 100 ml, 50 ml). The combined organic layer was dried over Na<sub>2</sub>SO<sub>4</sub>, and rotary-evaporated. Flash chromatography (1:1 ethyl acetate / petroleum ether) gave 2.818 g (71%) of product as a yellow oil. Chiral HPLC (Daicel Chiralpak AD column, hexane / i-PrOH = 96:4, flow rate 1 ml/min,  $\lambda$  = 254 nm):  $t_R$  (major) = 46.30 min;  $t_R$  (minor) = 43.75 min; ee = 91%. <sup>1</sup>H NMR (CDCl<sub>3</sub>)  $\delta$  = 1.22 (t, 3H), 2.18 (s, 3H), 2.96 (d, 2H), 3.74 (s, 3H), 4.17 (q, 2H), 4.33 (t, 1H), 6.64 (d, 2H), 6.77 (d, 2H). ESI-MS calcd for C<sub>14</sub>H<sub>19</sub>NO<sub>4</sub>: 265.13. Found [M+H]<sup>+</sup>: 266.0, [M+Na]<sup>+</sup>: 287.8, [M+K]<sup>+</sup>: 303.8.

**Ethyl (2S)-5-fluoro-2-(p-methoxyphenylamino)-4-oxopentanoate (3b).** 1.700 g of **2** (8.2 mmol) was dissolved in 60 ml of anhydrous DMSO. 15 ml of fluoroacetone was added followed by 189 mg of L-proline (1.64 mmol, 20 mol%). The mixture was stirred under argon for 26 hours at room temperature. The reaction was quenched by the addition of 75 ml of half-saturated ammonium chloride solution, extracted with ethyl acetate (75 ml x 2, 50 ml, 25 ml). The combined organic layer was dried over Na<sub>2</sub>SO<sub>4</sub>, and rotary-evaporated. Flash chromatography (1:1 ethyl acetate / petroleum ether) gave 1.729 g (75%) of product as a yellow oil. Chiral HPLC (Daicel Chiralpak AS column, hexane / i-PrOH = 90:10, flow rate 1 ml/min,  $\lambda$  = 254 nm):  $t_R$  (major) = 32.20 min;  $t_R$  (minor) = 44.99 min; ee = 98%. <sup>1</sup>H NMR (CDCl<sub>3</sub>)  $\delta$  = 1.24 (t, 3H), 3.07 (m, 2H), 3.74 (s, 3H), 4.19 (q, 2H), 4.44 (t, 1H), 4.83 (d, 2H, J = 47.4 Hz), 6.67 (d, 2H), 6.77 (d, 2H). <sup>19</sup>F NMR (CDCl<sub>3</sub>)  $\delta$  = 2.51 (t, 1F, J = 47.4 Hz). ESI-MS calcd for C<sub>14</sub>H<sub>18</sub>FNO<sub>4</sub>: 283.12. Found [M+H]<sup>+</sup>: 283.8, [M+Na]<sup>+</sup>: 305.8.

**Ethyl 5,5-difluoro-2-(p-methoxyphenylamino)-4-oxopentanoate (3c).** 4.5 ml of 1,1-difluoroacetone and 173 mg of D,L-proline (1.5 mmol, 60 mol%) were added in 2 ml of the ionic liquid of 1-butyl-3-methylimidazolium tetrafluoroborate (BMIMBF<sub>4</sub>). The mixture was stirred under argon for 20 minutes at room temperature. 518 mg of **2** (2.5 mmol) in 2.5 ml of BMIMBF<sub>4</sub> was added. The reaction was stirred under argon for 2 hours at room temperature. The reaction was extracted with ethyl ether (20 ml x 4). The combined ether layer was rotary-evaporated. Flash chromatography (1:2 ethyl acetate / petroleum ether) gave 337 mg (45%) of product as a brown oil. <sup>1</sup>H NMR (CDCl<sub>3</sub>) δ = 1.24 (t, 3H), 3.17 (d, 2H), 3.74 (s, 3H), 4.19 (q, 2H), 4.45 (t, 1H), 5.73 (t, 1H, J = 53.8 Hz), 6.67 (d, 2H), 6.77 (d, 2H). <sup>19</sup>F NMR (CDCl<sub>3</sub>) δ = -127.61 (d, 2F, J = 53.5 Hz). ESI-MS calcd for C<sub>14</sub>H<sub>17</sub>F<sub>2</sub>NO<sub>4</sub>: 301.11. Found [M+H]<sup>+</sup>: 302.0.

**Ethyl 2-((4,5-dimethoxy-2-nitrobenzyloxy)carbonylamino)-4-oxopentanoate (4a).** 265 mg of **3a** (1 mmol) in 10 ml of CH<sub>3</sub>CN was stirred at 0 °C. 1.645 g of CAN (3 mmol) in 10 ml of H<sub>2</sub>O was added dropwise. The reaction was stirred under argon for 1 hour at 0 °C. The mixture was neutralized using saturated NaHCO<sub>3</sub> aq to pH around 7.0, rotary-evaporated briefly to remove CH<sub>3</sub>CN. To the remaining mixture was added Na<sub>2</sub>S<sub>2</sub>O<sub>3</sub> (316 mg, 2 mmol) and Na<sub>2</sub>CO<sub>3</sub> (160 mg, 1.5 mmol). 276 mg of 2-nitroveratryloxycarbonyl chloride (NVOC-Cl) (1 mmol) in 20 ml of p-dioxane was added. The reaction was stirred under argon for 4 hours at room temperature. The mixture was extracted with CH<sub>2</sub>Cl<sub>2</sub> (20 ml x 2, 10 ml x 3). The combined organic layer was decolorized by activated carbon, filtrated through Celite, dried over Na<sub>2</sub>SO<sub>4</sub>, and rotary-evaporated.

Flash chromatography (1:1 ethyl acetate / petroleum ether) gave 243 mg (61%) of product as a pale-yellow solid. Chiral HPLC (Daicel Chiralpak AS column, hexane / ethanol = 90:10, flow rate 1 ml/min,  $\lambda = 254$  nm):  $t_R$  (major) = 36.67 min;  $t_R$  (minor) = 44.15 min; ee = 5 %, which was mainly due to the use of racemized **3a**.  $^1\text{H NMR}$  ( $\text{CDCl}_3$ )  $\delta = 1.24$  (t, 3H), 2.18 (s, 3H), 3.00 (dd, 1H), 3.25 (dd, 1H), 3.95 (s, 3H), 4.01 (s, 3H), 4.18 (q, 2H), 4.52 (m, 1H), 5.47 and 5.60 (AB, 2H), 5.91 (d, 1H), 7.04 (s, 1H), 7.71 (s, 1H). ESI-MS calcd for  $\text{C}_{17}\text{H}_{22}\text{N}_2\text{O}_9$ : 398.13. Found  $[\text{M}+\text{H}]^+$ : 398.8,  $[\text{M}+\text{Na}]^+$ : 420.8,  $[\text{M}+\text{K}]^+$ : 436.8.

**Ethyl 2-((4,5-dimethoxy-2-nitrobenzyloxy)carbonylamino)-5-fluoro-4-oxopentanoate (4b)**. 567 mg of racemized **3b** (2 mmol) in 20 ml of  $\text{CH}_3\text{CN}$  was stirred at 0 °C. 3.290 g of CAN (6 mmol) in 20 ml of  $\text{H}_2\text{O}$  was added dropwise. The reaction was stirred under argon for 1 hour at 0 °C. The mixture was neutralized using saturated  $\text{NaHCO}_3$  aq to pH around 7.0, rotary-evaporated briefly to remove  $\text{CH}_3\text{CN}$ . To the remaining mixture was added  $\text{Na}_2\text{S}_2\text{O}_3$  (632 mg, 4 mmol) and  $\text{Na}_2\text{CO}_3$  (318 mg, 3 mmol). 551 mg of NVOC-Cl (2 mmol) in 40 ml of p-dioxane was added. The reaction was stirred under argon for 4 hours at room temperature. The mixture was extracted with  $\text{CH}_2\text{Cl}_2$  (40 ml x 2, 20 ml x 3). The combined organic layer was decolorized by activated carbon, filtrated through Celite, dried over  $\text{Na}_2\text{SO}_4$ , and rotary-evaporated. Flash chromatography (1:1 ethyl acetate / petroleum ether) gave 330 mg (40%) of product as a pale-yellow powder.  $^1\text{H NMR}$  ( $\text{CDCl}_3$ )  $\delta = 1.25$  (t, 3H), 3.15 (m, 1H), 3.31 (m, 1H), 3.95 (s, 3H), 4.01 (s, 3H), 4.67 (m, 1H), 4.82 (d, 1H,  $J = 48.0$  Hz), 5.47 and 5.59 (AB, 2H), 5.84 (d, 1H),

7.03 (s, 1H), 7.71 (s, 1H).  $^{19}\text{F}$  NMR ( $\text{CDCl}_3$ )  $\delta$  = 1.49 (t, 1F,  $J$  = 47.7 Hz). ESI-MS calcd for  $\text{C}_{17}\text{H}_{21}\text{FN}_2\text{O}_9$ : 416.12. Found  $[\text{M}+\text{H}]^+$ : 416.8,  $[\text{M}+\text{Na}]^+$ : 439.0,  $[\text{M}+\text{K}]^+$ : 455.0.

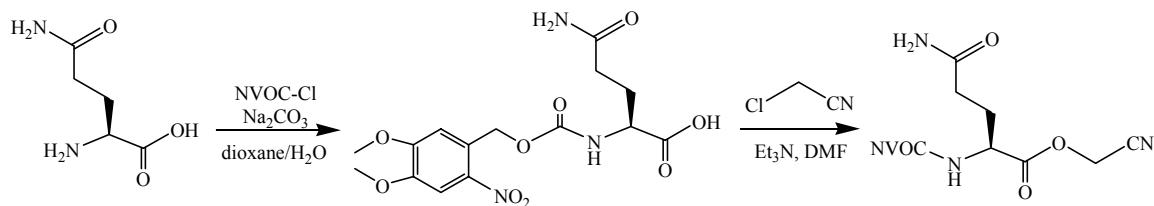
**2-((4,5-dimethoxy-2-nitrobenzyloxy)carbonylamino)-4-oxopentanoic acid (5a).** 180 mg of **4a** (0.45 mmol) in 2.3 ml of methanol and 125 mg of  $\text{K}_2\text{CO}_3$  (0.90 mmol) in 1.1 ml of  $\text{H}_2\text{O}$  were stirred at room temperature for 10 hours. The reaction was poured into 5.6 ml of  $\text{H}_2\text{O}$ , washed with ethyl ether (5 ml x 3). The aqueous layer was acidified with 6 N HCl until the product began to precipitate (pH around 2.0). The resulting cloudy solution was stored in the 4 °C frig overnight. After vacuum filtration, the solid was collected as one portion of the product; the filtered solution was extracted with ethyl acetate (15 ml x 3), and the combined organic layer was dried over  $\text{Na}_2\text{SO}_4$ , and rotary-evaporated to yield the other portion of the product. Altogether, 129 mg (78%) of the product was obtained as a pale-yellow powder.  $^1\text{H}$  NMR ( $\text{d}^6$ -DMSO)  $\delta$  = 2.10 (s, 3H), 2.87 (m, 2H), 3.85 (s, 3H), 3.90 (s, 3H), 4.37 (m, 1H), 5.34 (m, 2H), 7.13 (s, 1H), 7.69 (s, 1H), 7.78 (d, 1H). ESI-MS calcd for  $\text{C}_{15}\text{H}_{18}\text{N}_2\text{O}_9$ : 370.10. Found  $[\text{M}+\text{Na}]^+$ : 392.8,  $[\text{M}+\text{K}]^+$ : 408.8.

**2-((4,5-dimethoxy-2-nitrobenzyloxy)carbonylamino)-5-fluoro-4-oxopentanoic acid (5b).** Prepared as the procedure described above except using **4b** as the starting material. Yield: 78%.  $^1\text{H}$  NMR ( $\text{d}^6$ -DMSO)  $\delta$  = 2.10 (s, 3H), 2.86 (m, 2H), 3.85 (s, 3H), 3.90 (s, 3H), 4.39 (m, 1H), 5.04 (d, 2H,  $J$  = 46.8 Hz), 5.35 (m, 2H), 7.12 (s, 1H), 7.69 (s, 1H), 7.86 (d, 1H).  $^{19}\text{F}$  NMR ( $\text{d}^6$ -DMSO)  $\delta$  = 1.58 (t, 1F,  $J$  = 47.5 Hz). ESI-MS calcd for  $\text{C}_{15}\text{H}_{17}\text{FN}_2\text{O}_9$ : 388.09. Found  $[\text{M}+\text{Na}]^+$ : 411.0,  $[\text{M}+\text{K}]^+$ : 426.8,  $[\text{M}-\text{H}]^-$ : 387.0.

**Cyanomethyl 2-((4,5-dimethoxy-2-nitrobenzyloxy)carbonylamino)-4-oxopentanoate (6a).** 73 mg of **5a** (0.20 mmol) was dissolved in 5 ml of DMF. 380  $\mu$ l of chloroacetonitrile (6.0 mmol) and 105  $\mu$ l of triethylamine (0.75 mmol) were added. The mixture was stirred under argon at room temperature for 10 hours. The reaction was quenched with 10 ml of 0.1 M  $\text{KH}_2\text{PO}_4$  and 20 ml of  $\text{H}_2\text{O}$ , extracted with ethyl acetate (40 ml, 30 ml x 2). The combined organic layer was washed with 50 ml of  $\text{H}_2\text{O}$ , dried over  $\text{Na}_2\text{SO}_4$ , and rotary-evaporated. Flash chromatography (4:1 ethyl acetate / petroleum ether) gave 78 mg (90%) of product as a pale-yellow powder.  $^1\text{H}$  NMR ( $\text{CDCl}_3$ )  $\delta$  = 2.21 (s, 3H), 3.07 (dd, 1H), 3.30 (dd, 1H), 3.96 (s, 3H), 4.02 (s, 3H), 4.67 (m, 1H), 4.76 (s, 2H), 5.47 and 5.62 (AB, 2H), 5.83 (d, 1H), 7.02 (s, 1H), 7.72 (s, 1H). ESI-MS calcd for  $\text{C}_{17}\text{H}_{19}\text{N}_3\text{O}_9$ : 409.11. Found  $[\text{M}+\text{Na}]^+$ : 432.0,  $[\text{M}+\text{K}]^+$ : 447.8.

**Cyanomethyl 2-((4,5-dimethoxy-2-nitrobenzyloxy)carbonylamino)-5-fluoro-4-oxopentanoate (6b).** Prepared as the procedure described above except using **5b** as the starting material. Yield: 63%.  $^1\text{H}$  NMR ( $d^6$ -DMSO)  $\delta$  = 2.96 (m, 2H), 3.86 (s, 3H), 3.90 (s, 3H), 4.58 (m, 1H), 5.01 (s, 2H), 5.06 (d, 2H,  $J$  = 46.3 Hz), 5.36 (s, 2H), 7.13 (s, 1H), 7.69 (s, 1H), 8.09 (d, 1H).  $^{19}\text{F}$  NMR ( $d^6$ -DMSO)  $\delta$  = 1.22 (t, 1F,  $J$  = 45.5 Hz). ESI-MS calcd for  $\text{C}_{17}\text{H}_{18}\text{FN}_3\text{O}_9$ : 427.10. Found  $[\text{M}+\text{Na}]^+$ : 449.8,  $[\text{M}+\text{K}]^+$ : 465.8,  $[\text{M}+\text{Cl}]^-$ : 462.0.

#### 4.6.3.3 Synthesis of NVOC-Gln Cyanomethyl Ester



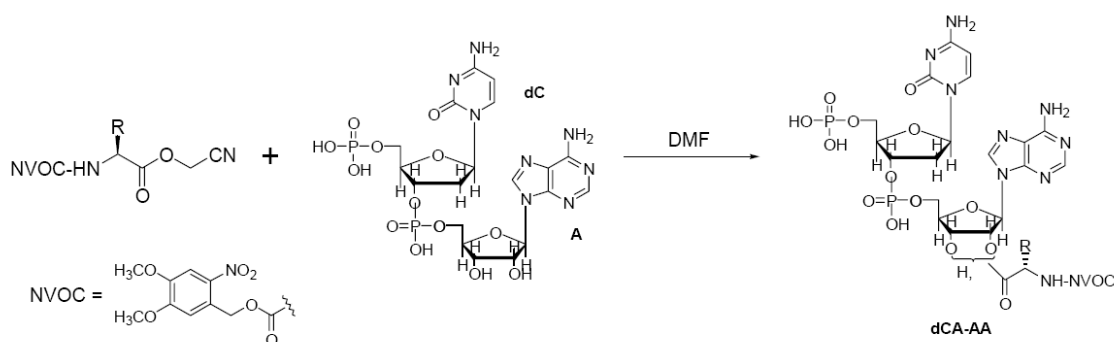
**Scheme 4.5** Synthesis of NVOC-Gln cyanomethyl ester.

**NVOC-Gln.** 219 mg (1.5 mmol) of glutamine in 15 ml of p-dioxane and 238 mg (2.25 mmol, 1.5 eq) of  $\text{Na}_2\text{CO}_3$  in 20 ml of water were stirred at room temperature. 413 mg (1.5 mmol) of NVOC-Cl in 15 ml of p-dioxane was added dropwise. The reaction was stirred at room temperature for 1 hour. The mixture was poured into 50 ml of  $\text{H}_2\text{O}$ , washed with ethyl ether (50 ml x 3). The aqueous layer was acidified with 6 N HCl until the product began to precipitate (pH around 2.0). The resulting cloudy solution was stored in the 4 °C refrigerator overnight. The crude crystals were collected by vacuum filtration, and afterward, recrystallized by using 1:1  $\text{H}_2\text{O}$  / MeOH. 486 mg (84%) of product was obtained as a pale-yellow crystal.  $^1\text{H}$  NMR ( $d^6$ -DMSO)  $\delta$  = 1.77 (m, 1H), 1.99 (m, 1H), 2.19 (t, 2H), 3.89 (s, 3H), 3.95 (s, 3H), 4.00 (m, 1H), 5.40 (m, 2H), 6.79 (s, 1H), 7.21 (s, 1H), 7.31 (s, 1H), 7.74 (s, 1H), 7.88 (d, 1H).

**NVOC-Gln cyanomethyl ester.** 83 mg of NVOC-Gln (0.22 mmol) was dissolved in 4 ml of DMF. 418  $\mu\text{l}$  of chloroacetonitrile (6.6 mmol) and 93  $\mu\text{l}$  of triethylamine (0.66 mmol) were added. The mixture was stirred under argon at room temperature for 10

hours. The reaction was quenched with 10 ml of 0.1 M  $\text{KH}_2\text{PO}_4$  and 15 ml of  $\text{H}_2\text{O}$ , extracted with ethyl acetate (30 ml x 2, 20 ml). The combined organic layer was washed with  $\text{H}_2\text{O}$  (30 ml x 2), dried over  $\text{Na}_2\text{SO}_4$ , and rotary-evaporated. Flash chromatography (pure ethyl acetate) gave 90 mg (93%) of product as a pale-yellow solid.  $^1\text{H}$  NMR ( $d^6$ -DMSO)  $\delta$  = 1.80 (m, 1H), 1.99 (m, 1H), 2.18 (t, 2H), 3.86 (s, 3H), 3.91 (s, 3H), 4.15 (m, 1H), 5.01 (s, 2H), 5.36 (m, 2H), 6.80 (s, 1H), 7.17 (s, 1H), 7.30 (s, 1H), 7.70 (s, 1H), 8.11 (d, 1H). ESI-MS calcd for  $\text{C}_{17}\text{H}_{20}\text{N}_4\text{O}_9$ : 424.12. Found  $[\text{M}+\text{H}]^+$ : 425.0,  $[\text{M}+\text{Na}]^+$ : 446.8,  $[\text{M}+\text{K}]^+$ : 462.8.

#### 4.6.3.4 General procedure for coupling of N- NVOC-protected amino acid cyanomethyl esters to dCA



**Scheme 4.6** General procedure for coupling of amino acids to dCA.

The N-protected amino acid cyanomethyl ester (~30  $\mu\text{mol}$ , 3 equivalents) was mixed with the tetrabutylammonium salt of the dCA dinucleotide (~10  $\mu\text{mol}$ , 1 equivalent) in 400  $\mu\text{l}$  of dry DMF. The reaction mixture was kept stirring for 3–5 hours under argon. The reaction was monitored by reverse-phase analytical HPLC with a gradient from 25 mM ammonium acetate (pH 4.5) to  $\text{CH}_3\text{CN}$ . The crude product was

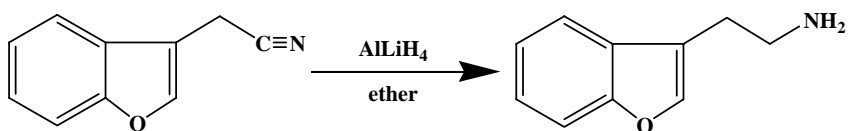
isolated using reverse-phase semi-preparative HPLC. The desired fractions containing the aminoacyl dinucleotide were combined, frozen, and lyophilized. The lyophilized solid was redissolved in 3:2 10 mM aqueous acetic acid / acetonitrile and lyophilized a second time to remove ammonium ions, which inhibit T4 RNA ligase in the ligation of dCA-amino acid to the tRNA. The products were characterized by mass spectrometry and quantified by UV / Vis spectra, assuming  $\epsilon_{350} \sim 6336$  per nitroveratryl group.

**dCA-NVOC-2-amino-4-oxopentanoic acid (7a).** Prepared as above using **6a** as the starting material. ESI-MS calcd for  $C_{34}H_{42}N_{10}O_{21}P_2$ : 988.20. Found  $[M-H]^-$ : 987.2,  $[M+Na-2H]^-$ : 1009.2,  $[M-NVOC]^-$ : 761.2.

**dCA-NVOC-2-amino-5-fluoro-4-oxopentanoic acid (7b).** Prepared as above using **6b** as the starting material. ESI-MS calcd for  $C_{34}H_{41}FN_{10}O_{21}P_2$ : 1006.19. Found  $[M-H]^-$ : 1005.2,  $[M-NVOC]^-$ : 775.2.

**dCA-NVOC-Gln (7b).** Prepared as above using NVOC-Gln cyanomethyl ester as the starting material. ESI-MS calcd for  $C_{34}H_{43}N_{11}O_{21}P_2$ : 1003.21. Found  $[M-H]^-$ : 1002.2.

#### 4.6.3.5 Synthesis of 2-(benzofuran-3-yl)ethylamine (BFEA)



**Scheme 4.7** Synthesis of 2-(benzofuran-3-yl)ethylamine.

**2-(benzofuran-3-yl)ethylamine.** 126 mg of LiAlH<sub>4</sub> (3.31 mmol, 1.3 eq) in 14 ml of anhydrous ether was stirred under argon at room temperature for 20 minutes. 400 mg of 2-(benzofuran-3-yl)acetonitrile (2.54 mmol, 1eq) in 5 ml of ether was added dropwise. The mixture was stirred under argon at room temperature for 10 hours. The reaction was quenched by the careful addition of 1 ml of saturated Na<sub>2</sub>SO<sub>4</sub> aqueous solution dropwise at 0 °C, decanted, and extracted with ether (10 ml, 4 ml x 5). The combined organic layer was dried over Na<sub>2</sub>SO<sub>4</sub>, and rotary-evaporated. Flash chromatography (15:85 to 50:50 methanol / ethyl acetate with 1% triethylamine) gave 226 mg (55%) of product as a yellow oil. <sup>1</sup>H NMR (CDCl<sub>3</sub>) δ = 2.89 (t, 2H), 3.09 (t, 2H), 7.30 (m, 2H), 7.50 (m, 2H), 7.59 (s, 1H). ESI-MS calcd for C<sub>10</sub>H<sub>11</sub>NO: 161.08. Found [M+H]<sup>+</sup>: 162.1.

#### 4.6.4 Computational Methods

All the calculations were performed in gas phase with the Gaussian 98 software.<sup>22</sup> The model system used was shown in Figure 4.7. Indole, and all the acetone analogues were optimized by AM1, HF/6-31G\*\*, and MP2/6-31G\*\*, respectively.

The hydrogen bond binding energy was calculated according to the following equation:

$$\text{Binding Energy} = E(\text{Indole}) + E(\text{Molecule}) - E(\text{Indole}\cdots\text{Molecule Complex})$$

The indole...acetone complex was optimized by HF/6-31G\*\* using seven different starting configurations, which varied the hydrogen bond angles and other related factors. The optimal indole...acetone structure was chosen from the one with the lowest

binding energy. All the other indole...molecule complexes were built based on the optimal indole...acetone structure and optimized by HF/6-31G\*\*. AM1 optimizations and MP2/6-31G\*\* single point energy calculations were performed on the HF/6-31G\*\* optimized indole...molecule complexes. The hydrogen bond binding energies were then obtained according to the above equation at the AM1, HF/6-31G\*\*, and MP2/6-31G\*\* levels.

#### 4.7 References

1. Dougherty, D. A., Unnatural amino acids as probes of protein structure and function. *Curr. Opin. Chem. Biol.* **2000**, 4, 645–652.
2. Miyazawa, A.; Fujiyoshi, Y.; Unwin, N., Structure and gating mechanism of the acetylcholine receptor pore. *Nature* **2003**, 423, 949–955.
3. Filatov, G. N.; White, M. M., The role of conserved leucines in the M2 domain of the acetylcholine-receptor in channel gating. *Mol. Pharmacol.* **1995**, 48, 379–384.
4. Labarca, C.; Nowak, M. W.; Zhang, H. Y.; Tang, L. X.; Deshpande, P.; Lester, H. A., Channel gating governed symmetrically by conserved leucine residues in the M2 domain of nicotinic receptors. *Nature* **1995**, 376, 514–516.
5. Notz, W.; Tanaka, F.; Barbas, C. F., Enamine-based organocatalysis with proline and diamines: The development of direct catalytic asymmetric Aldol, Mannich, Michael, and Diels-Alder reactions. *Accounts Chem. Res.* **2004**, 37, 580–591.
6. Cordova, A., The direct catalytic asymmetric Mannich reaction. *Accounts Chem. Res.* **2004**, 37, 102–112.
7. Cordova, A.; Notz, W.; Zhong, G. F.; Betancort, J. M.; Barbas, C. F., A highly enantioselective amino acid-catalyzed route to functionalized alpha-amino acids. *J. Am. Chem. Soc.* **2002**, 124, 1842–1843.
8. Suzuki, A.; Mae, M.; Amii, H.; Uneyama, K., Catalytic route to the synthesis of optically active beta,beta-difluoroglutamic acid and beta,beta-difluoroproline derivatives. *J. Org. Chem.* **2004**, 69, 5132–5134.

9. Jefford, C. W.; McNulty, J.; Lu, Z. H.; Wang, J. B., The enantioselective synthesis of beta-amino acids, their alpha-hydroxy derivatives, and the N-terminal components of bestatin and microginin. *Helv. Chim. Acta* **1996**, 79, 1203–1216.
10. Salomon, C. J.; Mata, E. G.; Mascaretti, O. A., Recent developments in chemical deprotection of ester functional-groups. *Tetrahedron* **1993**, 49, 3691–3734.
11. Kearney, P. C.; Nowak, M. W.; Zhong, W.; Silverman, S. K.; Lester, H. A.; Dougherty, D. A., Agonist binding site of the nicotinic acetylcholine receptor: Tests with novel side chains and with several agonists. *Mol. Pharmacol.* **1996**, 50, 1401–1412.
12. Chowdari, N. S.; Ramachary, D. B.; Barbas, C., Organocatalysis in ionic liquids: Highly efficient L-proline-catalyzed direct asymmetric Mannich reactions involving ketone and aldehyde nucleophiles. *Synlett* **2003**, 1906–1909.
13. Singh, R. P.; Cao, G. F.; Kirchmeier, R. L.; Shreeve, J. M., Cesium fluoride catalyzed trifluoromethylation of esters, aldehydes, and ketones with (trifluoromethyl)trimethylsilane. *J. Org. Chem.* **1999**, 64, 2873–2876.
14. Wiedemann, J.; Heiner, T.; Mloston, G.; Prakash, G. K. S.; Olah, G. A., Direct preparation of trifluoromethyl ketones from carboxylic esters: trifluoromethylation with (trifluoromethyl)trimethylsilane. *Angew. Chem.-Int. Edit.* **1998**, 37, 820–821.
15. Yokoyama, Y.; Mochida, K., Chemoselective trifluoromethylation of methyl esters using an Et<sub>3</sub>GeNa/C<sub>6</sub>H<sub>5</sub>SCF<sub>3</sub> combination: Efficient synthesis of trifluoromethyl ketones. *Synlett* **1997**, 907.
16. Boivin, J.; Elkaim, L.; Zard, S. Z., A new and efficient synthesis of trifluoromethyl ketones from carboxylic-acids.1. *Tetrahedron* **1995**, 51, 2573–2584.
17. Boivin, J.; Elkaim, L.; Zard, S. Z., An expedient access to trifluoromethyl ketones from carboxylic-acids. *Tetrahedron Lett.* **1992**, 33, 1285–1288.
18. Zacharie, B.; Connolly, T. P.; Penney, C. L., A simple one-step conversion of carboxylic-acids to esters using EEDQ. *J. Org. Chem.* **1995**, 60, 7072–7074.
19. Cashin, A. L.; Petersson, E. J.; Lester, H. A.; Dougherty, D. A., Using physical chemistry to differentiate nicotinic from cholinergic agonists at the nicotinic acetylcholine receptor. *J. Am. Chem. Soc.* **2005**, 127, 350–356.
20. Tolman, V.; Sedmera, P., Chemistry of 4-fluoroglutamic acid. Part 3. Preparation of the diastereomers of 4-fluoroglutamine and 4-fluoroisoglutamine. An enzymatic access to the antipodes of 4-amino-2-fluorobutyric acid. *J. Fluor. Chem.* **2000**, 101, 5–10.
21. Tsukamoto, T.; Coward, J. K., Facile synthesis of DL-4,4-difluoroornithine, DL-4,4-difluoroglutamine, and gamma-DL-4,4-difluoroglutamyl-containing peptides: Regiospecific addition of nucleophiles to N-Cbz-di-tert-butyl-DL-4,4-difluoroglutamate. *J. Org. Chem.* **1996**, 61, 2497–2500.

22. Frisch, M. J.; Trucks, G. W.; Schlegel, H. B.; Scuseria, G. E.; Robb, M. A.; Cheeseman, J. R.; Zakrzewski, V. G.; Montgomery, J. A. J.; Stratmann, R. E.; Burant, J. C.; Dapprich, S.; Millam, J. M.; Daniels, A. D.; Kudin, K. N.; Strain, M. C.; Farkas, O.; Tomasi, J.; Barone, V.; Cossi, M.; Cammi, R.; Mennucci, B.; Pomelli, C.; Adamo, C.; Clifford, S.; Ochterski, J.; Petersson, G. A.; Ayala, P. Y.; Cui, Q.; Morokuma, K.; Malick, D. K.; Rabuck, A. D.; Raghavachari, K.; Foresman, J. B.; Cioslowski, J.; Ortiz, J. V.; Baboul, A. G.; Stefanov, B. B.; Liu, G.; Liashenko, A.; Piskorz, P.; Komaromi, I.; Gomperts, R.; Martin, R. L.; Fox, D. J.; Keith, T.; Al-Laham, M. A.; Peng, C. Y.; Nanayakkara, A.; Gonzalez, C.; Challacombe, M.; Gill, P. M. W.; Johnson, B. G.; Chen, W.; Wong, M. W.; Andres, J. L.; Head-Gordon, M.; Replogle, E. S.; Pople, J. A., *Gaussian 98 (Revision A.9)*. Gaussian, Inc., Pittsburgh PA: 1998.

## **Chapter 5**

### **Tethered Agonist Approach to Map the Ligand-Binding**

#### **Site of MOD-1**

## 5.1 Introduction

Several tethered agonist strategies have been developed to probe the ligand-binding site in nAChR. The chemical modification of Cys residues was introduced by Karlin and co-workers, and further used by the Lester group and the Cohen lab.<sup>1-3</sup> However, this method depends on cysteine modification. If the Cys mutation is not functional or the modification reaction is not efficient, this method may not be a good choice. Another strategy to introduce tethered agonists is to directly incorporate the desired tethers at the site of interest using the powerful unnatural amino acid mutagenesis methodology.<sup>4</sup> Different tethers can be used to probe different sites, including those that are not accessible by external reagents. In the following, we will discuss the tethered agonist strategy by using the unnatural amino acid mutagenesis method.

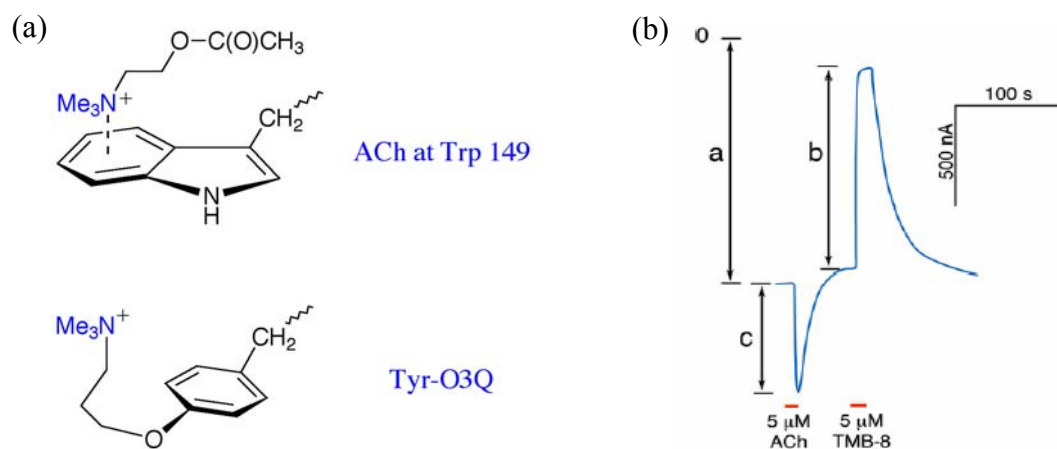


**Figure 5.1** The tethered agonist approach to map the acetylcholine (ACh) binding site in nAChR. (a) Incorporation of Tyr-O3Q at position 149 to mimic the natural agonist. (b) Spontaneously opening channel blocked by the open channel blocker TMB-8.

Tyrosine derived tethered agonists were used in nAChR.<sup>5,6</sup> As in Figure 5.1, the quaternary ammonium of acetylcholine (ACh) is positioned over the six-member ring of Trp 149. Incorporation of the unnatural amino acid Tyr-O3Q (see Figure 5.1 for the structure) at position 149 can deliver the quaternary ammonium to the same position as the natural agonist ACh. Therefore, Tyr-O3Q will mimic the behavior of ACh, produce a constitutively active receptor, and give standing currents without the addition of external agonists. The constitutively active channel can be blocked by the addition of a channel blocker, such as TMB-8. It should be pointed out that the tethered agonist can be viewed as a weak partial agonist. Therefore, the addition of acetylcholine can induce more current. The efficiency of the tethered agonists is expressed by the ratio of the constitutively opening current that is blocked by TMB-8 (labeled as **b** in Figure 5.1 (b)) to the ACh induced current (labeled as **c** in Figure 5.1 (b)). The larger the ratio of **b/c**, the more effective the tethered agonist. Several tethers with different lengths were incorporated into several positions near the binding site. Tyr-O3Q seemed to have the optimal length at position 149 and gave the highest efficiency. Later, the tethered agonist approach was applied to study the pH effect on the binding site in nAChR.<sup>7</sup>

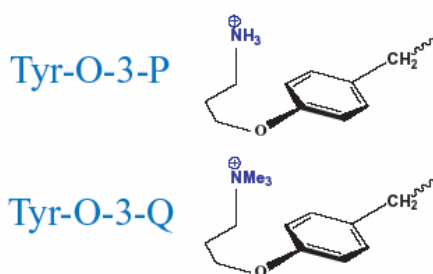


**Figure 5.2** Tethered agonists used in MOD-1.

In this chapter, we applied this strategy to further map the ligand-binding site of MOD-1. Serotonin has a primary ammonium instead of the quaternary ammonium of ACh. Therefore, we incorporated both Try-O3P to mimic the primary ammonium and Tyr-O3Q to mimic the quaternary ammonium at the sites of interest in MOD-1 (Figure 5.2). From previous studies we know that the primary ammonium of serotonin is positioned over the six-member ring of Trp 226 in MOD-1. Also Tyr 180 is near the binding site. These two sites were chosen for a detailed study. Other sites near the binding sites were also tried. The results show that the incorporation of Tyr-O3P at position 226 yields the highest efficiency, which is in agreement with our previous experiments.

## **5.2 Effect of the Channel Blocker Picrotoxin on MOD-1**

Before performing the tethered agonist experiments in the MOD-1 receptor, we need to have some knowledge on the following two aspects.

First, since the tethered agonist is a weak partial agonist, in order to observe the constitutively opening current after incorporation, the ion pore needs to be made to open more easily.

Second, we need to find a proper channel blocker. This blocker should not be near the agonist-binding site so that the incorporation of the tethered agonists will not affect the blockage behavior of this blocker.

To make the ion pore open more easily, from the study of nAChR, mutations at the Leu 9' position in the M2 region are good choices (Figure 5.3 (a)).<sup>8,9</sup> Therefore, we made the Val, Ala, Ser, and Thr mutations at the Leu 9' position in the M2 region of MOD-1. The results are shown in Table 2.1 and Figure 5.3 (b).

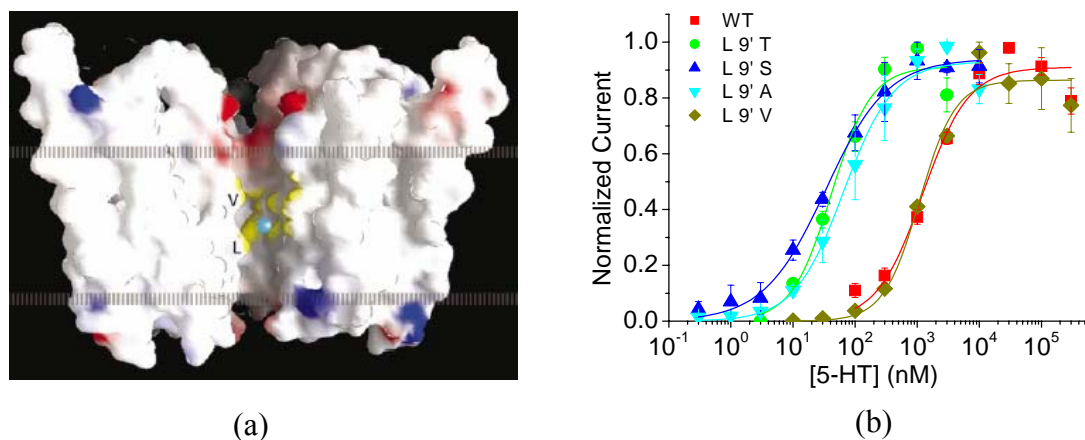


**Figure 5.3** The effect of L9' mutations on channel gating. (a) Structure of nAChR. Adapted from Ref<sup>8</sup>. (b) Dose-response curves of some L9' mutations in MOD-1.

**Table 5.1** EC<sub>50</sub> of L9' mutations in MOD-1 using serotonin.

	EC <sub>50</sub> (nM)	n <sub>Hill</sub>
WT	1220 ± 300	1.2 ± 0.3
L9'T	41 ± 9	1.4 ± 0.3
L9'S	33 ± 3	0.9 ± 0.1
L9'A	65 ± 11	1.1 ± 0.2
L9'V	1090 ± 200	1.5 ± 0.3

It can be seen that L9'T, L9'S, and L9'A mutants are much more sensitive to serotonin than wild type, while the L9'V mutant is similar to wild type. Therefore, L9'T, L9'S, and L9'A mutants were further tested for their blockage behaviors.

Some drugs were tested for their ability to block the wild type channel. These drugs included mianserin, an antagonist of MOD-1; picrotoxin, picrotoxinin, and penicillin G, the GABA<sub>A</sub> receptor blockers; and R(+)-IAA94, a potent chloride channel blocker. Penicillin G and R(+)-IAA94 did not block the channel; although mianserin blocked the channel efficiently, most possibly it acted as a competitive antagonist and did not meet our criteria for tethered agonist experiments; picrotoxinin had slightly lower blockage efficiency than picrotoxin. Therefore, we chose picrotoxin (IC<sub>50</sub> is about 500 μM with the application of 1 μM serotonin on wild type) as the channel blocker in the following experiments.

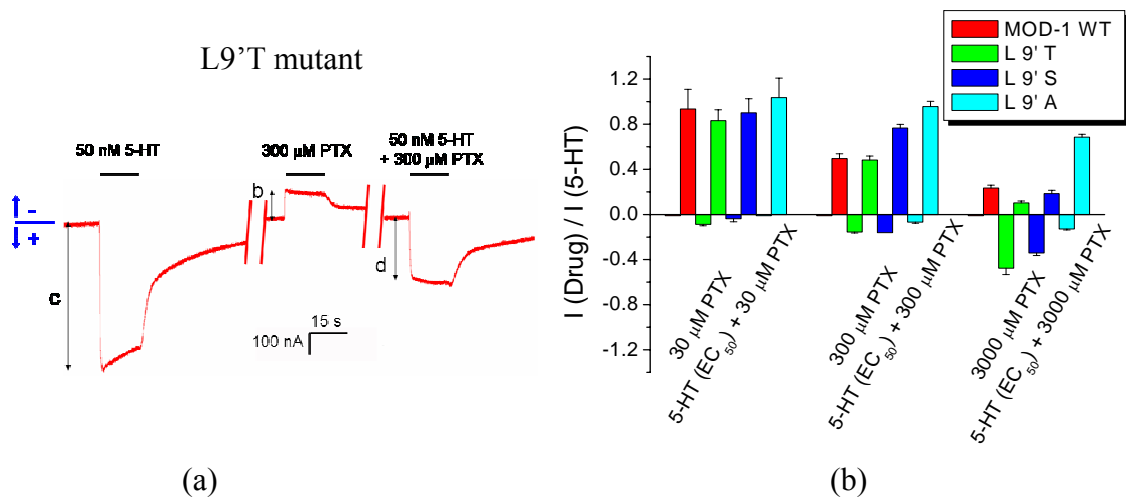


**Figure 5.4** Picrotoxin blockage effect on wild type and L9' mutant MOD-1s. (a) The typical experimental procedure and representative traces. (b) Summary of the picrotoxin blockage effect. The three data groups are for the application of picrotoxin at three different concentrations (30 μM, 300 μM, or 3000 μM). All the columns with positive values correspond to the **d/c** ratios; all the columns with negative values correspond to the **b/c** ratios.

We tested the picrotoxin effect on wild type and L9'T, L9'S and L9'A mutant

MOD-1s. The typical procedure and representative traces are shown in Figure 5.4 (a). First, 5-HT at the near  $EC_{50}$  concentration (1  $\mu$ M for wild type or 50 nM for all the mutants) was applied and the resulting inward current was recorded as a positive value **c**. Then picrotoxin (PTX) at different concentrations (30  $\mu$ M, 300  $\mu$ M, or 3000  $\mu$ M) was applied and the resulting outward current was recorded as a negative value **b**; this outward current occurs because the channel is spontaneously opening and thus is blocked by picrotoxin. Finally, 5-HT together with PTX was applied and the resulting inward current was recorded as a positive value **d**. The ratios of **b/c** and **d/c** at different picrotoxin concentrations for either wild type or the mutants are summarized in Figure 5.4 (b). There are three groups of data; each group corresponds to the application of picrotoxin at one concentration. All the columns with positive values correspond to the **d/c** ratios; all the columns with negative values correspond to the **b/c** ratios.

From Figure 5.4, we can see that picrotoxin at 300  $\mu$ M can efficiently block the wild type and L9'T mutant. However, all the mutants also produce spontaneously opening channels, and the constitutively opening current can be blocked by picrotoxin even before introduction of the tethered agonists (Figure 5.4). Therefore, we need to perform this control experiment when we incorporate the tethered agonists at the site of interest. Since the L9'T mutant can be blocked by picrotoxin efficiently, the tethered agonists would be incorporated at the sites of interest into this construct unless otherwise stated.

### **5.3 Tethered Agonist Experiments in MOD-1**

Using the construct with L9'T mutations in the M2 region, we tried to incorporate Tyr-O3P and Tyr-O3Q into the sites of Trp 226 in loop C and Try 180 in loop B. However, we did not find any spontaneously opening current even with the application of 3 mM picrotoxin.

Using the construct without L9'T mutations in the M2 region, we tried to put Try-O3P into the sites of Phe 83 in loop D, Try 180 and Trp 191 in loop B, and Try 221 and Trp 226 in loop C, and Try-O3Q into the sites of Try 180 in loop B, and Trp 226 in loop C. Again, we did not find any spontaneously opening current even with the application of 3 mM picrotoxin.

The above results seemed puzzling. However, we know that MOD-1 is a homopentamer. The incorporation of five Tyr-O3P or Tyr-O3Q into each receptor probably will not be successful or produce non-functional receptors. In order to incorporate less Try-O3P or Tyr-O3Q into each receptor, we could simultaneously incorporate some wild type amino acids at the site of interest. Therefore, we tried to inject tRNA mixtures and adjust their ratio. For example, to incorporate less Tyr-O3P into the site of Trp 226, we tried to inject both tRNA-Trp and tRNA-Tyr-O3P and vary their ratios. Our experiments showed that this strategy worked well. Constitutively active channels were found using the construct with L9'T mutations in the M2 region, which could be blocked by picrotoxin. The ratio of 1:1 tRNA mixtures yielded the optimal result (data not shown). Therefore, in the following experiments, we used tRNA mixtures with the ratio of 1:1 to incorporate corresponding tethered agonists unless otherwise noted.

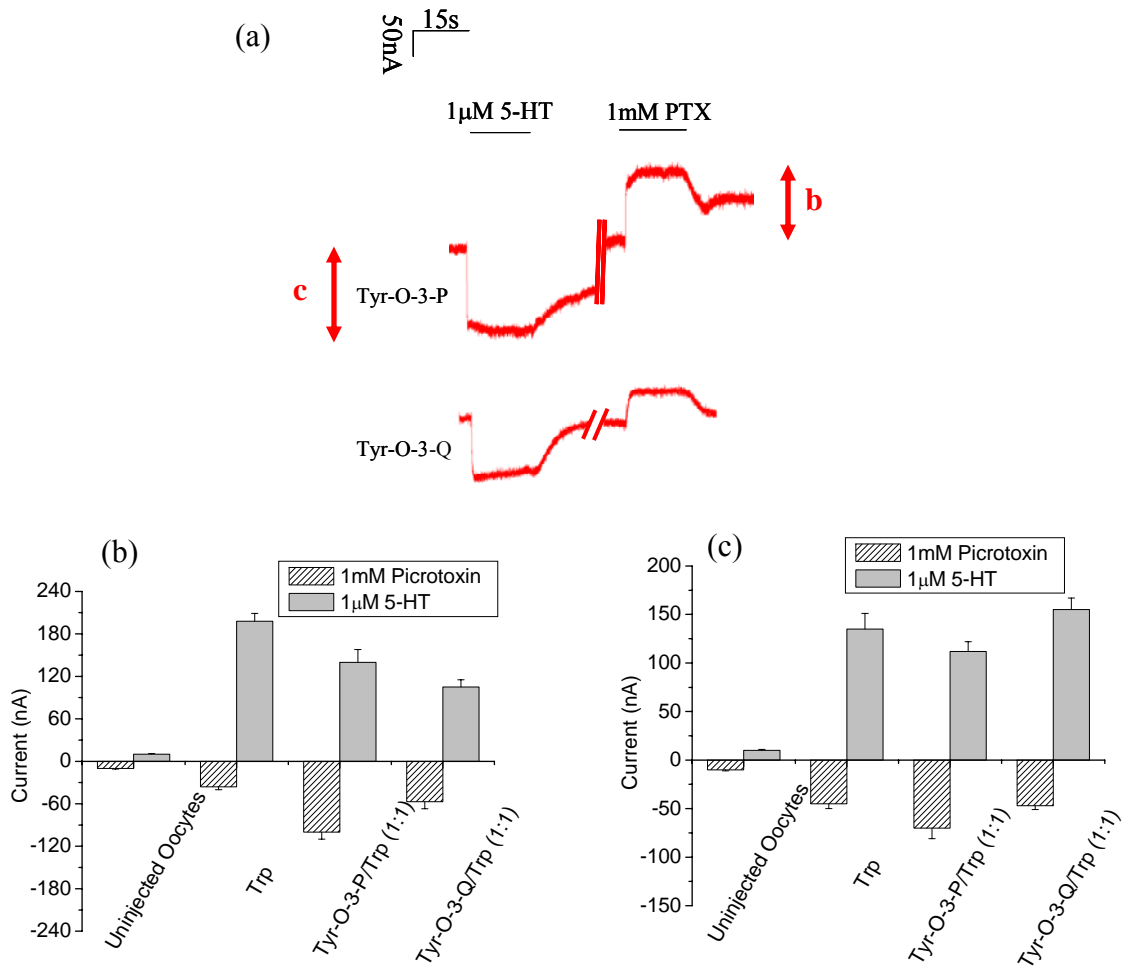


**Figure 5.5** Tethered agonist experiments at position 226 of MOD-1. (a) Representative electrophysiology recording traces. (b) Results from the recording with ND96 solution. (c) Results from the recording with Ca<sup>2+</sup>-free ND96 solution.

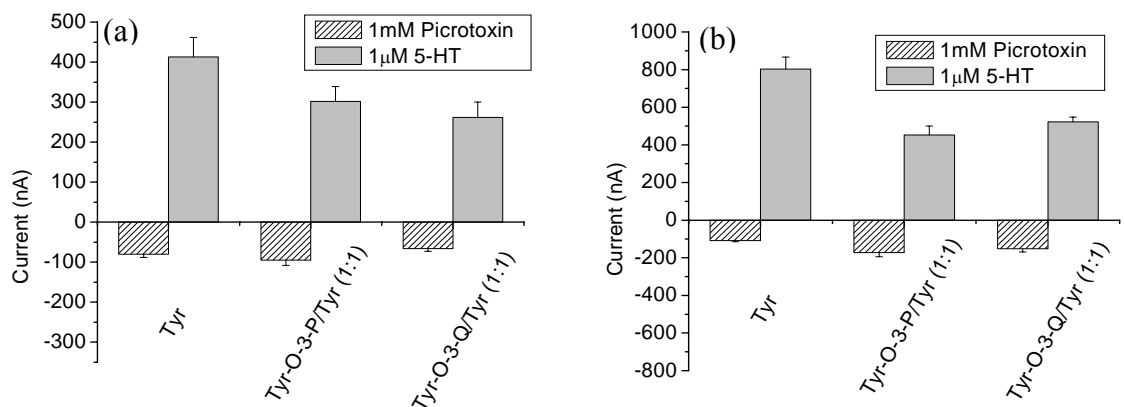


**Figure 5.6** Tethered agonist experiments at position 180 of MOD-1. (a) Results from the recording with ND96 solution. (b) Results with Ca<sup>2+</sup>-free ND96 solution recordings.

Using the 1:1 tRNA mixtures and the construct with L9'T mutations in the M2 region, again, we tried to incorporate Tyr-O3P and Tyr-O3Q into the sites of Trp 226 in loop C and Try 180 in loop B. The control experiments on uninjected oocytes and wild type with L9'T mutations were also conducted. The typical experimental procedure and electrophysiology recording traces are shown in Figure 5.6 (a). 5-HT (1  $\mu$ M) was applied and the resulting inward current was recorded as a positive number **c**; then picrotoxin (1 mM) was applied and the resulting outward current was recorded as a negative number **b**. Current amplitudes at position 226 and position 180 are summarized in Figure 5.6 and Figure 5.7, respectively. The effect of  $Ca^{2+}$  was also considered in the experiment. The efficiencies of the tethered agonists were measured using the absolute values of the **b/c** ratio. The results are summarized in Figure 5.8.

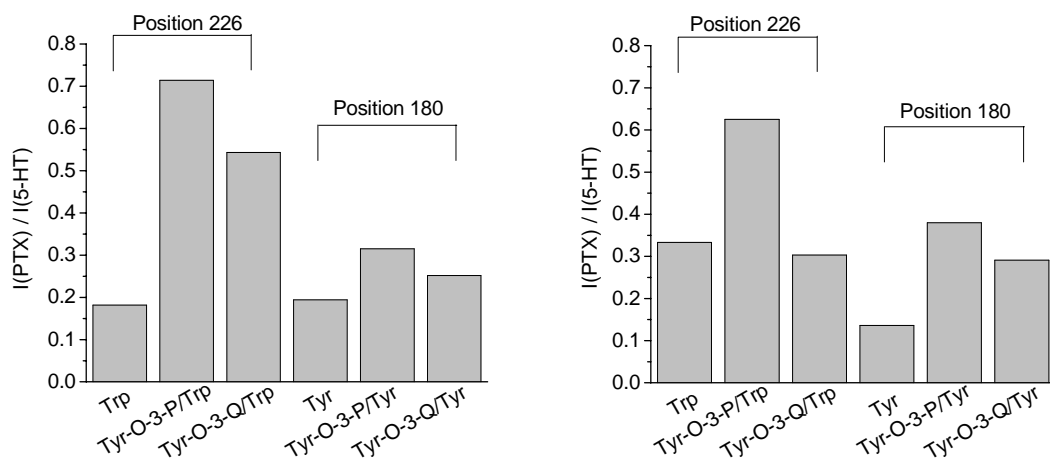


**Figure 5.7** Efficiencies of tethered agonists in MOD-1. (a) Recorded with ND96 solution. (b) Recorded with  $Ca^{2+}$ -free ND96 solution.

It can be seen that the results from the recordings with ND96 solution are similar to but better than those with  $\text{Ca}^{2+}$ -free ND96 solution (Figure 5.7). The tethered agonists Tyr-O3P and Tyr-O3Q both have higher efficiency at position 226 than at position 180. Tyr-O3P is more efficient than Try-O3Q at both position 226 and position 180. Since serotonin owns a primary ammonium that is above Trp 226 in MOD-1, it can be imagined that the incorporation of Tyr-O3P at position 226 gives the highest efficiency, which is the case in our tethered agonist experiments. However, the highest efficiency we obtained is about 0.7. If we considered that the application of Tyr-O-3Q at Trp 149 in nAChR could achieve an efficiency value of about 7, our current tethered agonist experiments in MOD-1 seemed to yield low efficiency.

#### **5.4 Conclusions**

We applied the tethered agonist approach to further map the ligand-binding site of MOD-1. Try-O3P and Tyr-O3Q were used to probe the sites of Trp 226 and Tyr 180. Current results agreed with our previous experiments.

However, the efficiency of the tethered agonists in MOD-1 was low. There are several possibilities for this low efficiency. First, the tethered agonists used here are not a perfect mimic of serotonin. From Chapter 4, we know that serotonin also contacts other residues by hydrogen bonds. But here, we just ignored those parts of serotonin. Not surprisingly, this should have some effect on binding. Second, since MOD-1 is a homopentamer, the incorporation of five tethered agonists into the specific position may be difficult. Although we used the tRNA mixtures to solve this problem, it is possible that

this solution is not optimal. To date only one subunit of MOD-1 has been found. If another subunit can be found to form stable heteropentamers with the current one, we can use the heteropentamer for the incorporation of the proper amount of tethered agonists into one receptor with more confidence. Third, picrotoxin may not be the best channel blocker used for this purpose because it is not very potent in MOD-1. The spontaneously opening currents may be underestimated by using picrotoxin. It may be possible to achieve higher efficiency by using other proper blockers.

The tethered agonist experiments have been successfully applied in mapping the nAChR binding site and yielded decent results in the MOD-1 receptor. By rational design of the tethered agonists in combination with the powerful unnatural amino acid mutagenesis methodology, the tethered agonist approach will be very useful in studying the ligand-binding sites. Understanding the details of the ligand-binding sites will provide guidance for drug designs.

## **5.5 Methods**

### **5.5.1 Electrophysiology**

Electrophysiological recordings were made 24–72 hours after injection. Whole-cell currents from stage VI oocytes of *Xenopus laevis* were measured in standard two-electrode voltage clamp mode using the OpusXpress<sup>TM</sup> 6000A (Axon Instruments, Union City, California). Microelectrodes were filled with 3M KCl and the resistances were between 0.5 and 2 M $\Omega$ . Oocytes were continuously perfused with calcium-free ND96 or ND96 bath solution at flow rates of 1 ml/min, 4 ml/min during drug application and 3

ml/ml during wash. The holding potential was -60 mV. Data were sampled at 125 Hz and filtered at 50 Hz. Drug applications were 15 s. Serotonin was purchased from Sigma/Aldrich and all drugs were prepared in calcium-free ND96 or ND96 solution. Dose-response data were obtained from 3 to 5 oocytes and data were reported as mean  $\pm$  standard error. Curves were fit to the Hill equation,  $I/I_{\max} = 1/[1 + (EC_{50}/[A])^{n_H}]$ , where  $I$  is the current for agonist concentration  $[A]$ ,  $I_{\max}$  is the maximum current,  $EC_{50}$  is the concentration to elicit a half-maximum response, and  $n_H$  is the Hill coefficient.

### **5.5.2 Incorporation of Unnatural Amino Acids by *in vivo* Nonsense Suppression**

#### **Methods**

For suppression experiments, 25 ng of tRNA and 10 ng of mRNA were co-injected in a total volume of 50 nL per oocyte. Immediately before the microinjection, the NVOC-aminoacyl-tRNA was deprotected by photolysis. The ligation of aminoacyl-dCA to tRNA and gene construction of suppressor tRNA have been described previously. The MOD-1 gene was subcloned into the plasmid pBlueScript. The MOD-1 TAG mutants were made by the Quickchange<sup>TM</sup> site-directed mutagenesis method and were monitored by DNA sequencing. Plasmid DNAs were linearized with *KpnI*, and mRNA was transcribed using the Ambion T3 mMESSAGE mMACHINE kit.

For wild type and conventional mutation experiments, only 5 ng mRNA was injected into oocytes in a 50 nL volume per cell with the same following procedure as described above.

The tethered agonists used in the experiments were obtained from Lintong Li and E. James Petersson. The preparations were described elsewhere.<sup>5-7</sup>

## 5.6 References

1. Sullivan, D. A.; Cohen, J. B., Mapping the agonist binding site of the nicotinic acetylcholine receptor: Orientation requirements for activation by covalent agonist. *J. Biol. Chem.* **2000**, *275*, 12651–12660.
2. Chabala, L. D.; Lester, H. A., Activation of acetylcholine-receptor channels by covalently bound agonists in cultured rat myoballs. *J. Physiol.-London* **1986**, *379*, 83–108.
3. Silman, I.; Karlin, A., Acetylcholine receptor: Covalent attachment of depolarizing groups at active site. *Science* **1969**, *164*, 1420–1422.
4. Dougherty, D. A., Unnatural amino acids as probes of protein structure and function. *Curr. Opin. Chem. Biol.* **2000**, *4*, 645–652.
5. Li, L. T.; Zhong, W. G.; Zacharias, N.; Gibbs, C.; Lester, H. A.; Dougherty, D. A., The tethered agonist approach to mapping ion channel proteins toward a structural model for the agonist binding site of the nicotinic acetylcholine receptor. *Chem. Biol.* **2001**, *8*, 47–58.
6. Zhong, W. G.; Gallivan, J. P.; Zhang, Y. O.; Li, L. T.; Lester, H. A.; Dougherty, D. A., From *ab initio* quantum mechanics to molecular neurobiology: A cation- $\pi$  binding site in the nicotinic receptor. *Proc. Natl. Acad. Sci. U. S. A.* **1998**, *95*, 12088–12093.
7. Petersson, E. J.; Choi, A.; Dahan, D. S.; Lester, H. A.; Dougherty, D. A., A perturbed pK(a) at the binding site of the nicotinic acetylcholine receptor: Implications for nicotine binding. *J. Am. Chem. Soc.* **2002**, *124*, 12662–12663.
8. Miyazawa, A.; Fujiyoshi, Y.; Unwin, N., Structure and gating mechanism of the acetylcholine receptor pore. *Nature* **2003**, *423*, 949–955.
9. Labarca, C.; Nowak, M. W.; Zhang, H. Y.; Tang, L. X.; Deshpande, P.; Lester, H. A., Channel gating governed symmetrically by conserved leucine residues in the M2 domain of nicotinic receptors. *Nature* **1995**, *376*, 514–516.